

## Abstract

### Studying Collagen with PyrATS: Pyrene-Appended Trimeric Systems

By

Jared Matthew Keever

July 2019

Director of Thesis: Dr. William E. Allen

Major Department: Chemistry

Collagens are a family of triple-helical structural proteins that are ubiquitous in vertebrates. Improper folding of collagen can lead to disorders such as osteogenesis imperfecta, or “brittle bone disease.” There is significant interest in understanding the factors that drive collagen folding and stability, but studying native collagens is difficult because they are hundreds of amino acids in length. This thesis describes a series of well-characterized (Pro-Hyp-Gly)<sub>7</sub> model peptides which have been tagged at their *N*-termini with the fluorophore pyrene. When in close contact, pyrene units can form excimers that emit low-energy light. This allows for the study of several fundamental questions in collagen research using fluorescence spectroscopy, including concentration dependence, folding directionality, and local fraying, upon solutions that are significantly more dilute than those customarily used in circular dichroism (CD) experiments. Notably, for most of the peptides studied, there is agreement between the melting temperatures ( $T_m$ ) obtained via fluorescence and CD techniques. In addition, the pyrene probes were found to provide a situational increase in thermal stability of triple helices.



# Studying Collagen with PyrATS: Pyrene-Appended Trimeric Systems

A Thesis

Presented to the Faculty of the Department of Chemistry

East Carolina University

In Partial Fulfillment of the Requirements for the Degree

Master of Science in Chemistry

By

Jared Matthew Keever

July 2019

© Jared Matthew Keever, 2019

# Studying Collagen with PyrATS: Pyrene-Appended Trimeric Systems

by

Jared Matthew Keever

APPROVED BY:

DIRECTOR OF

THESIS: \_\_\_\_\_

William E. Allen, PhD

COMMITTEE MEMBER: \_\_\_\_\_

Colin S. Burns, PhD

COMMITTEE MEMBER: \_\_\_\_\_

Nathan E. Hudson, PhD

COMMITTEE MEMBER: \_\_\_\_\_

Andrew L. Sargent, PhD

COMMITTEE MEMBER: \_\_\_\_\_

Anne M. Spuches, PhD

CHAIR OF THE DEPARTMENT

OF CHEMISTRY: \_\_\_\_\_

Andrew T. Morehead, PhD

DEAN OF THE

GRADUATE SCHOOL: \_\_\_\_\_

Paul J. Gemperline, PhD

*To those who have watched me grow and have guided me along the way. I love you all.*

## Acknowledgements

I could not be more grateful to the plethora of people who have gotten me to this point in my academic career. I would like to thank each and every one of them to the best of my ability.

Thank you to my committee for being patient with me and always answering my questions and making time for me. To Dr. Burns, thank you for your help on CD and for imparting in me a better knowledge of how proteins behave. To Dr. Hudson, thank you for generously agreeing to be part of my committee and for providing an invaluable outside insight. To Dr. Sargent, thank you for all the work you have done with Dr. Allen and I behind the scenes. Your generosity knows no bounds. And finally to Dr. Spuches, thank you for taking time to help me understand thermodynamics. You make physical chemistry not seem so scary.

To my parents, without you, I would never have had the confidence in my own abilities to even attempt graduate school or science in general. You have supported me for 24 years, and I know you will always be there for me. Mom and Dad, I love you both.

Thank you to my brother Seth for sparking my scientific curiosity at a young age. You have always been the coolest big brother I could ask for.

Thank you to my professors, advisors, and friends who have given incalculably impactful advice, love, and support thorough this project. Thank you to the members of the Allen lab in my time here: Patrick Banzon, Abby Hagwood, Jordan Stanley, Mufida Muhammad, Alexis Anderson, and Mikayla Stoudt. Without the friendships I've forged with all of you, I would have gotten more work done, but been considerably less happy. I am very grateful.

To future members of the Allen lab, good luck! Be more organized than I was. It will save you a ton of time when you are writing your own thesis. You are in a great place, and I can't wait to see what you accomplish!

Thank you to Dr. Allen for all of your advice. Thank you for the Christy's, frisbee golf, guitar lessons, and for your superhuman patience and care. You are a wise man, and invaluable mentor.

Thank you to my wonderful girlfriend Kate, who I love and adore. You have been very patient with me and for that I am greatly appreciative.

Lastly, thank you to my cats, Elsa and Sol, who I love despite their propensity for walking on my keyboardsasdf.



# TABLE OF CONTENTS

LIST OF TABLES .....	x
LIST OF FIGURES .....	xi
LIST OF EQUATIONS .....	xv
LIST OF ABBREVIATIONS .....	xvi
CHAPTER 1: BASIC COLLAGEN STRUCTURE AND FUNCTION .....	1
1.1 Introduction.....	1
1.2 Structure .....	1
1.3 Applications and diseases .....	4
1.4 Introduction to collagen modification.....	5
1.5 Modifications to the Yaa position .....	6
1.6 Modifications to the Xaa position .....	7
1.7 Backbone modifications .....	8
1.8 Basics of $\pi - \pi$ stacking .....	10
1.9 Stacking interactions in nature.....	12
1.10 Pyrene and its properties.....	12
1.11 Goals of this research .....	14
CHAPTER 2: SYNTHESIS AND PEPTIDE DESIGN .....	15
2.1 Introduction.....	15

2.2 Peptide design .....	15
2.3 Experimental conditions and solid phase peptide synthesis .....	25
2.4 Characterization of synthesized peptides .....	25
2.4.1 HPLC traces .....	25
2.4.2 Mass spectrometry .....	31
2.5 Circular dichroism studies .....	40
2.5.1 Determination of secondary structure .....	40
2.5.2 Thermal denaturation experiments .....	40
2.6 Fluorescence studies .....	41
2.6.1 Fluorescence spectra collection .....	41
2.6.2 Concentration dependent studies and folding kinetics .....	42
2.6.3 Thermal denaturation analyzed by fluorescence .....	43
CHAPTER 3: RESULTS .....	45
3.1 Collagen spectral data .....	45
3.2 Thermal denaturation experiments analyzed by CD spectroscopy .....	50
3.3 Exploration into concentration effects of fluorescence .....	54
3.4 Thermal denaturation experiments analyzed by fluorescence spectroscopy .....	58
CHAPTER 4: DISCUSSION .....	62
4.1 Collagen spectral data analysis .....	62
4.2 Discussion of thermal denaturation studies analyzed by CD spectroscopy .....	63

4.3 Discussion of concentration dependent pyrene fluorescence and kinetics studies ....	64
4.4 Discussion of thermal denaturation analyzed by fluorescence spectroscopy .....	66
4.5 Conclusion .....	70
REFERENCES .....	72

## LIST OF TABLES

<b>Table 2.1:</b> List of synthetic pyrene-labeled collagen systems with associated abbreviations.....	15
<b>Table 3.1:</b> Combined thermal denaturation data via circular dichroism. ....	53
<b>Table 3.2:</b> Combined thermal denaturation data via fluorescence. ....	61
<b>Table 4.1:</b> Difference between CD and fluorescence $T_m$ values. ....	67
<b>Table 4.2:</b> Difference between CD and fluorescence $\Delta H$ values. ....	68

## LIST OF FIGURES

<b>Figure 1.1:</b> Hydration structure of a collagen peptide .....	2
<b>Figure 1.2:</b> Depiction of the H-bonding framework in a collagen peptide. ....	3
<b>Figure 1.3:</b> Depiction of the triple helix in a collagen peptide. ....	4
<b>Figure 1.4:</b> Ring puckering of a proline like amino acid structure. ....	7
<b>Figure 1.5:</b> Aza-Glycine. ....	9
<b>Figure 1.6:</b> Sarcosine. ....	10
<b>Figure 1.7:</b> Depiction of theorized electrostatic interactions between aromatic systems. ....	11
<b>Figure 1.8:</b> Stereotypical pyrene fluorescence.....	13
<b>Figure 1.9:</b> Off-center face-to-face stacking of pyrene. ....	13
<b>Figure 2.1:</b> The Ac-KK system. ....	17
<b>Figure 2.2:</b> The Pyr(1)-KK system. ....	18
<b>Figure 2.3:</b> The Pyr(3)-KK system. ....	19
<b>Figure 2.4:</b> The Pyr(3)-KA system. ....	20
<b>Figure 2.5:</b> The Pyr(3)-AK system. ....	21
<b>Figure 2.6:</b> The Pyr(3)-EA system .....	22
<b>Figure 2.7:</b> The Pyr(3)-KSarK system. ....	23
<b>Figure 2.8:</b> The Pyr(3)-KSar <sub>3</sub> K system. ....	24
<b>Figure 2.9:</b> Representative chromatogram of Ac-KK, collected via HPLC. ....	26
<b>Figure 2.10:</b> Representative chromatogram of Pyr(1)-KK, collected via HPLC. ....	27

<b>Figure 2.11:</b> Representative chromatogram of Pyr(3)-KK, collected via HPLC.....	27
<b>Figure 2.12:</b> Representative chromatogram of Pyr(3)-KA, collected via HPLC.....	28
<b>Figure 2.13:</b> Representative chromatogram of Pyr(3)-AK, collected via HPLC.....	29
<b>Figure 2.14:</b> Representative chromatogram of Pyr(3)-EA, collected via HPLC. ....	29
<b>Figure 2.15:</b> Representative chromatogram of Pyr(3)-KSarK, collected via HPLC.....	30
<b>Figure 2.16:</b> Representative chromatogram of Pyr(3)-KSar <sub>3</sub> K, collected via HPLC. ....	31
<b>Figure 2.17:</b> Mass spectrometry of Ac-KK.....	32
<b>Figure 2.18:</b> Mass spectrometry of Pyr(1)-KK. ....	33
<b>Figure 2.19:</b> Mass spectrometry of Pyr(3)-KK. ....	34
<b>Figure 2.20:</b> Mass spectrometry of Pyr(3)-KA. ....	35
<b>Figure 2.21:</b> Mass spectrometry of Pyr(3)-AK. ....	36
<b>Figure 2.22:</b> Mass spectrometry of Pyr(3)-EA. ....	37
<b>Figure 2.23:</b> Mass spectrometry of Pyr(3)-KSarK.....	38
<b>Figure 2.24:</b> Mass spectrometry of Pyr(3)-KSar <sub>3</sub> K. ....	39
<b>Figure 3.1:</b> CD spectrum of the Ac-KK system.....	45
<b>Figure 3.2:</b> CD spectrum of the Pyr(1)-KK system. ....	46
<b>Figure 3.3:</b> CD spectrum of the Pyr(3)-KK system. ....	46
<b>Figure 3.4:</b> CD spectrum of the Pyr(3)-KA system. ....	47
<b>Figure 3.5:</b> CD spectrum of the Pyr(3)-AK system. ....	47
<b>Figure 3.6:</b> CD spectrum of the Pyr(3)-EA system.....	48

<b>Figure 3.7:</b> CD spectrum of the Pyr(3)-KSarK system. ....	48
<b>Figure 3.8:</b> CD spectrum of the Pyr(3)-KSar <sub>3</sub> K system.....	49
<b>Figure 3.9:</b> Overlaid CD Spectra of each measured collagen analog. ....	49
<b>Figure 3.10:</b> Thermal denaturation studies of Ac-KK. ....	50
<b>Figure 3.11:</b> Thermal denaturation studies of Pyr(1)-KK. ....	50
<b>Figure 3.12:</b> Thermal denaturation studies of Pyr(3)-KK. ....	51
<b>Figure 3.13:</b> Thermal denaturation studies of Pyr(3)-KA. ....	51
<b>Figure 3.14:</b> Thermal denaturation studies of Pyr(3)-AK. ....	52
<b>Figure 3.15:</b> Thermal denaturation studies of Pyr(3)-EA. ....	52
<b>Figure 3.16:</b> Thermal denaturation studies of Pyr(3)-KSarK. ....	53
<b>Figure 3.17:</b> Concentration dependence of Pyr(3)-KA.....	54
<b>Figure 3.18:</b> Concentration dependence of Pyr(3)-KSarK.....	55
<b>Figure 3.19:</b> Concentration dependence of Pyr(3)-KSar <sub>3</sub> K .....	56
<b>Figure 3.20:</b> Kinetics of folding/unfolding for Pyr(3)-KA. ....	57
<b>Figure 3.21:</b> Fluorescence melt of Pyr(3)-KK at low concentration.....	58
<b>Figure 3.22:</b> Fluorescence response of Pyr(1)-KK as a function of temperature.....	59
<b>Figure 3.23:</b> Fluorescence response of Pyr(3)-KK as a function of temperature.....	59
<b>Figure 3.24:</b> Fluorescence response of Pyr(3)-KA as a function of temperature.....	60
<b>Figure 3.25:</b> Fluorescence response of Pyr(3)-AK as a function of temperature.....	60
<b>Figure 3.26:</b> Fluorescence response of Pyr(3)-EA as a function of temperature. ....	61

**Figure 4.1:** Head-to-Head aggregation of triple helices..... 65



## LIST OF EQUATIONS

<b>Equation (1)</b> Thermal unfolding equation .....	41
<b>Equation (2)</b> Refolding kinetics equation .....	43
<b>Equation (3)</b> Water bath offset equation.....	43

## LIST OF ABBREVIATIONS

G	Glycine
Gly	Glycine
O	(2S,4R)-4-Hydroxyproline
Hyp	(2S,4R)-4-Hydroxyproline
P	Proline
Pro	Proline
K	Lysine
Lys	Lysine
E	Glutamic acid
Glu	Glutamic acid
A	Alanine
Ala	Alanine
Sar	Sarcosine
Xaa	Amino acid in the X position of an Xaa-Yaa-Gly repeat in a collagen system
Yaa	Amino acid in the Y position of an Xaa-Yaa-Gly repeat in a collagen system
SPPS	Solid phase peptide synthesis
HPLC	High performance liquid chromatography
Ac	Acetyl group
Pyr(1)	1-pyreneacetic acid

Pyr(3)	1-pyrenebutyric acid
CD	Circular dichroism
mL	milliliter
$\mu\text{L}$	microliter
$\mu\text{M}$	micromolar
mM	millimolar
s	second
A.U.	Arbitrary Units
H-bond	Hydrogen bond
$\Delta H$	Change in enthalpy
$\Delta\Delta H$	Change in the change in enthalpy
T	Temperature
$^{\circ}\text{C}$	Degrees celcius
$T_m$	Melting (unwinding) temperature

## **Chapter 1: Basic Collagen Structure and Function**

### **1.1 Introduction**

Collagen is an abundant protein in mammals, and is responsible for a plethora of biological processes. Collagen is perhaps most important as a structural protein, fulfilling roles as the primary scaffolding component of the extracellular matrix and of cartilage. Collagen is, in fact, so abundant in the human body that it accounts for one third of the total protein mass as well as accounting for three-quarters of the weight of human skin.<sup>1</sup>

### **1.2 Structure**

Natural collagen is not, in fact, a singular primary sequence of amino acids, but is instead a large class of proteins. In vertebrates alone, 28 types of collagenous proteins have been identified.<sup>1</sup> This defining motif consists of three staggered polypeptide strands coiled together in an overall right-handed helix of individual left-handed strands, these are known as polyproline type II helices. These structures are made possible by the XaaYaaGly repeats that make up each collagen strand, where Xaa and Yaa are the first two amino acids in each repeat. The amino acids in the Xaa and Yaa position can vary, but it is necessary in this structure that every third amino acid be a glycine residue for folding to be possible. This motif is less strictly followed in nonfibrillar collagens<sup>2</sup> but is necessary for the triple-helical structure to exist.

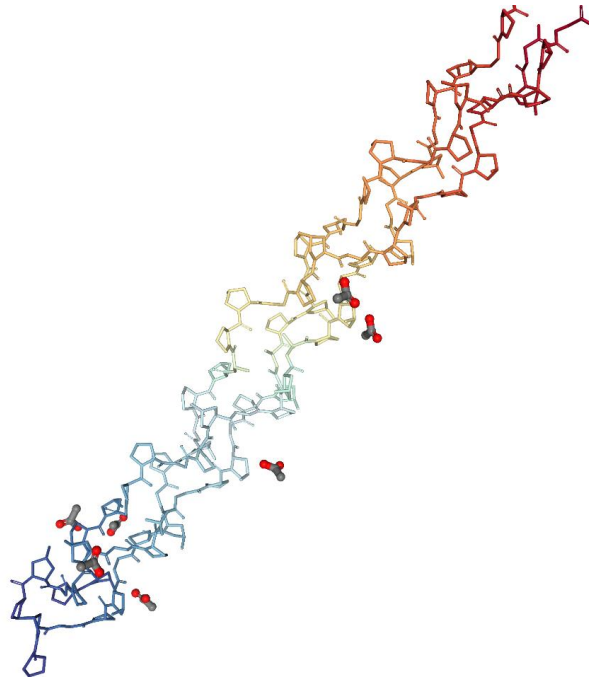


**Figure 1.1:** Hydration structure of a collagen peptide<sup>1</sup>

In addition to glycine, the other amino acids that form the triple-helix can be nearly any natural residue, however, the most common residues to take the Xaa and Yaa positions of natural collagen are proline (Pro) accounting for 28% of total amino acids, and (2S,4R)-4-hydroxyproline (Hyp) at 38%. The most common three amino acid repeat in collagen is ProHypGly or “POG”, accounting for 10.5% of triplet repeats. In nature, individual collagen helices (i.e. tropocollagen (TC)) aggregate to form complex hierarchical structures that fulfill the aforementioned biological roles.<sup>2</sup> The absence of ascorbic acid (Vitamin C) prevents the production of hydroxyproline, thus one of the symptoms of the illness scurvy involves the reduction in hydroxylation of proline.<sup>3</sup>

Glycine is not always conserved in natural collagen. In fibrillar collagen, any disruption of the XaaYaaGly sequence leads to disease states, however, in non-fibrillar collagen this motif is frequently broken.<sup>4</sup> In a study seeking to understand differences between these two states, peptides mimicking a natural G5G interruption (G-POALO-G) and a pathological Gly-to-Ala substitution (G-LOAPO-G) were

designed. The G5G peptide showed higher triple helicity and thermal stability than the Gly-to-Ala peptide. Replacement of Gly appears to always lead to disease states and lower stability, however, natural interruptions appear to increase stability and promote protein function in nature.<sup>5</sup>

The primary driving force for collagen triple helical formation is provided by the hydrogen bond. In natural collagen, a hydrogen bond forms between the N-H bond of each Gly residue, and the adjacent hydrogen bond acceptor in the form of the carbonyl C=O of an Xaa residue. Studies have shown that the strength of each hydrogen bond in a collagen triple helix is between  $\Delta G^0 = -1.8$  kcal/mol<sup>6</sup> and  $\Delta G^0 = -2$  kcal/mol<sup>7</sup> in model peptides, and closer to  $\Delta G^0 = -1.4$  kcal/mol in native collagen. These hydrogen bonds combine to form hyper-stable systems in nature on the backbone of this hydrogen bonding motif.

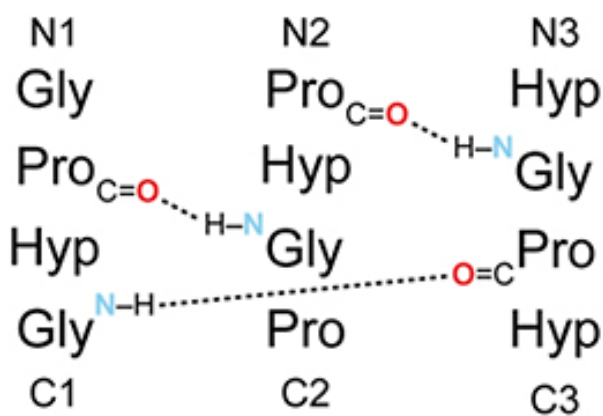


**Figure 1.2:** Depiction of the H-bonding framework in a collagen peptide. Hydrogen bonding takes place between the amide of the Gly residues with the carbonyl of an adjacent Xaa (depicted here as Proline). These strands have a one residue stagger.<sup>2</sup>

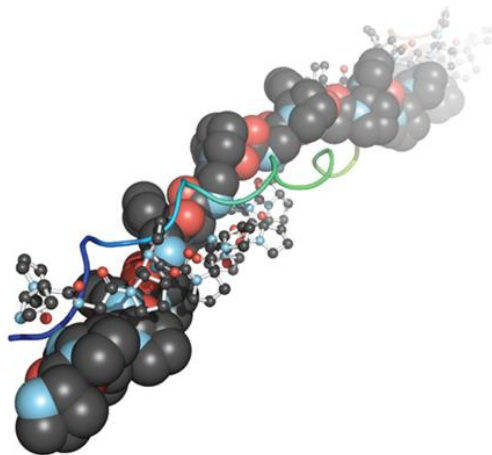


**Figure 1.3:** Depiction of triple helix in a collagen peptide. Individual strands are shown using ribbon, ball-and-stick, and space filling models, to allow for better visualization of the helix.<sup>2</sup>

The accepted literature hypothesis of collagen folding dictates that collagen folds from the C termini toward the N termini in a “zipper like” manner with a rate that is dependent on *cis/trans* isomerization of peptide bonds.<sup>8</sup> To determine the directionality and degree of fraying at the termini of a small collagen peptide based on a (POG)<sub>10</sub> system, sequential isotopic labeling of <sup>15</sup>N-Gly in 10 peptides was carried out in order to determine the extent of local fraying at positions along the collagen backbone. Several two-dimensional NMR techniques were utilized in order to probe both the fraying positions and the fraying temperature range. The study found that two POG triplets at each termini are necessary to ensure helical folding. Additionally, a great degree of disorder was found at the C-termini, with fraying extending 6 amino acids into the (POG)<sub>10</sub> sequence, this disorder being influenced by small sequence changes at the N-terminus.<sup>9</sup>

### 1.3 Applications and diseases

Collagen can be extracted from a variety of species, including bovine skin and tendons as well as porcine skin and intestines.<sup>10</sup> This natural collagen is used for a variety of applications, though comes

with the drawback of being less characterized than lab-grown collagen. Endogenous collagen displays a high degree of biocompatibility and biodegradability for biomedical applications in humans, however, exogenous collagen can elicit more complex and varied responses when degraded.<sup>10</sup> Collagen in a biomedical setting has been used for the creation of sponges for wound dressing, in films and membranes for reinforcement of compromised tissues, and as drug delivery mechanisms. Collagen has also been used to dress burns and ulcers, and as a replacement for skin.<sup>10</sup>

There are numerous diseases that have been discovered that are associated with malformed collagen, including osteogenesis imperfecta, in which mutations such as Gly-to-Ala substitutions in Type I collagen lead to potentially lethal structural irregularities.<sup>2</sup> As collagen plays a role in the healing of wounds and bone fractures, any perturbation to collagen formation will at least delay the healing process. Diseases associated with mutations in collagen structure can play a role in connective tissue disorders, basement membrane disorders, nervous system disorders, skin disorders, and many other disorders related to tissues.<sup>11</sup>

#### **1.4 Introduction to collagen modification**

Since its discovery and characterization, there have been many attempts to alter the primary structure of model collagen peptides to further understand the factors that contribute to collagen stability, as well as to learn important physical properties of the motif. The aforementioned studies to determine hydrogen bond strength utilized such studies.<sup>6,7</sup> Other studies have investigated replacing amino acids at specific positions in a small collagen peptide with synthetic amino acids, non-optimal amino acids, or more optimal amino acids to further determine the effects of the identities of the amino acids in the Xaa and Yaa positions on folding.



## 1.5 Modifications to the Yaa position

As stated previously, the most common amino acid in the Yaa position of collagen is the Hyp residue. This residue, formed from hydroxylation of a Pro residue by prolyl 4-hydroxylase (P4H), is understood to be essential for the stability of natural collagen.<sup>2</sup> For synthetic, small collagenous peptides, the sheer degree of stabilization from a Hyp residue in the Yaa position compared to a Pro residue can be seen when comparing melting (unfolding) temperatures of a (ProHypGly)<sub>7</sub> system with a (ProProGly)<sub>7</sub> system.<sup>12,13</sup> For the system containing the Hyp residue, 50% of triple helices are unfolded at a temperature ( $T_m$ ) of 36 °C. For the unhydroxylated system, however, a  $T_m$  value could not be obtained as all strands were unfolded at all temperatures. Arginine is also known to be stabilizing in the triple helix at the Yaa position and has similar stabilizing properties to Hyp.<sup>14</sup>

Many other experiments have been conducted in order to further understand the importance of the Hyp residue at the Yaa position. One such experiment replaced the (2S,4R)-4-hydroxyproline (Hyp) on a (ProHypGly)<sub>10</sub> system with the isomer (2S,4S)-4-hydroxyproline (hyp) and found no triple helix formation.<sup>15</sup>

Replacements of Hyp in the Yaa position with other residues have given further insight into the method of stabilization at this position. Replacement of Hyp with (2S,4R)-4-fluoroproline (Flp) at the Yaa position has been shown to yield increased stability in a (ProFlpGly)<sub>7</sub> system.<sup>12</sup> This stabilization, like the effects of the hyp residue, is lost when replaced with the enantiomer of Flp (2S,4S)-4-fluoroproline (flp).<sup>12</sup> This has led to the determination that the stereochemistry of the electronegative substituent at the 4-position of the Pro ring is of monumental importance in triple helical formation. This effect has been hypothesized to be a stereoelectronic effect due to the preference of stabilizing Yaa proline derivatives to adopt a C<sup>γ</sup>-exo ring pucker as opposed to a C<sup>γ</sup>-endo ring pucker (which is preferred by natural proline).<sup>12</sup> This isomer pre-organizes torsion angles along the main chain to be favorable to triple helix formation. The 4S versions of 4 position modifications to proline are counterproductive to this and cause a destabilizing effect.

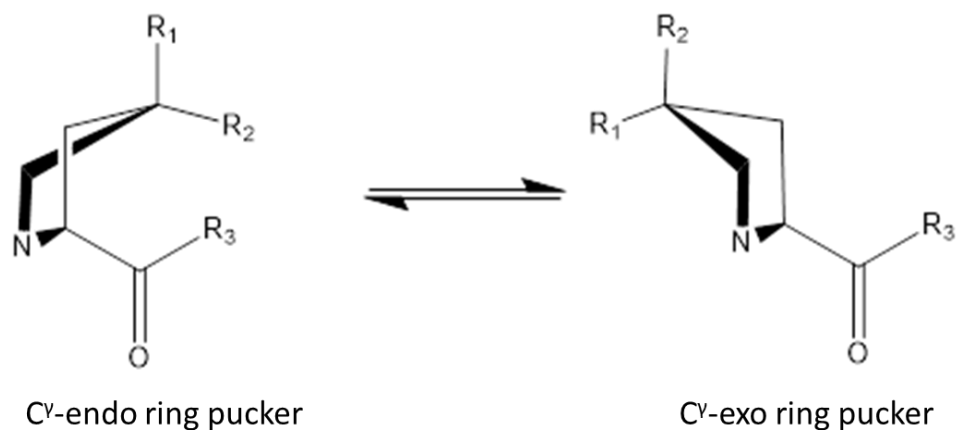


**Figure 1.4:** Ring Puckering of a proline like amino acid structure.

One interesting facet of stereoelectronic stabilization is that many groups can be beneficial to the triple helix when implemented as 4 position proline modifications. (2S,4R)-4-Methoxyproline (Mop) incorporated in the Yaa position was found to be stabilizing compared to controls,<sup>16</sup> as were (2S,4R)-4-chloroproline (Clp) residues.<sup>17</sup> Steric effects also play a role in stabilization at this position. For the residue (2S,4R)-4-methylproline (Mep)<sup>18</sup> and (2S,4R)-4-mercaptaproline (Mcp),<sup>19</sup> steric effects play a role in forcing the proline ring's pucker into a C $\gamma$ -exo conformation due to the attached group's steric bulk.

### 1.6 Modifications in the Xaa position

As enforcing a C $\gamma$ -exo ring pucker is important for stabilizing a proline derivative in the Yaa position, enforcing a C $\gamma$ -endo ring pucker is important for Xaa position stability.<sup>20</sup> Studies have shown that proline derivatives that are destabilizing in the Yaa position due to their stereochemistry, such as flp, clp, and mep, are all stabilizing in the Xaa position. In Type IV natural collagen, (2S,3S)-3-hydroxyproline, a proline derivative formed from a different post-translational modification of proline residues, is stabilizing in the Xaa position, as it preferentially adopts the C $\gamma$ -endo ring pucker.<sup>21</sup>

One interesting collagen modification focusing on Xaa modifications involves the introduction of large hydrophobic groups as substituents on proline rings in the center of the chain. Studies have shown

that the *cis/trans* isomerization of Xaa-Pro bonds is faster in organic solvents compared to aqueous solvents.<sup>22</sup> Fatty acids, a cholesterol derivative, and an aromatic molecule were attached to the 4-position of a proline ring on the central triplet of a (POG)<sub>7</sub> mimetic peptide. These modifications were shown to increase melting temperatures by up to ~ 27 °C compared to controls, as well as increase the kinetics of *cis/trans* isomerization among Xaa-Pro amide bonds. It is hypothesized that addition of a local hydrophobic environment through these hydrophobic chains can act as a “glue” to both hold the triple helix together, while providing the hydrophobic environment conducive to faster triple helical folding.<sup>23</sup>

### **1.7 Backbone modifications**

The vast majority of the research that has been done to date attempting to increase the stability of collagen peptides has relied on modifications of proline residues through synthetic modification. Relatively little work has been done on modifications that specifically seek to alter the peptide backbone of collagen systems, however, one modification has proved quite successful at stabilizing triple helices. That success is the introduction of an aza-glycine (azGly) residue in place of glycine. Replacement of Gly residues with azGly in a central repeat of a (POG)<sub>7</sub> analog increases the melting temperature by ~ 10 °C.<sup>24</sup> This increase in stability is further exaggerated when multiple azGly residues are incorporated, giving rise to triple helices even for short peptides of only twelve amino acids.<sup>25</sup> This stabilization is also somewhat dependent on position, providing additional stability in the center of the chain of a (POG)<sub>7</sub> analog compared to modifications at the N- or C- termini.<sup>25</sup> Studies of the resolved structures of these azGly-containing collagen systems reveal the additional hydrogen bond donor as within a reasonable molecular distance of nearby C=O groups for additional hydrogen bonding. Additionally, replacement of the  $\alpha$ -carbon of Gly with an N-H group pre-organizes the triple helical geometry to favor triple helices.<sup>26</sup> As hydrogen bonds are essential to the formation of the triple helix, and as pre-organizing geometries along the triple helix lessens the energetic cost of folding, the azGly residue appears to be the current best option for increasing collagen stability through backbone modifications.

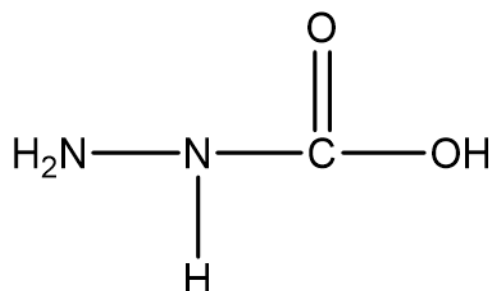
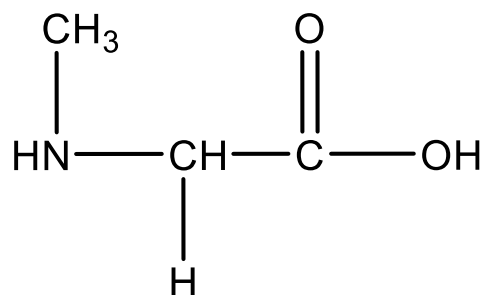


**Figure 1.5:** Aza Glycine

Other modifications focus on capping of a small collagen peptide with some anchoring group. Self-assembly of higher order triple helical structures have been made possible through modifications to the N- and C- termini of small collagen peptides through utilization of cation-pi interactions. Arginine (R) has a cationic sidechain at neutral pH, and phenylalanine (F) has an aromatic side chain. Electrostatic interactions between the electron clouds of phenylalanine and the positively charged sidechain of arginine are favorable and were hypothesized to promote aggregation of small collagen peptides in a RG(POG)<sub>10</sub>F peptide.<sup>27</sup> Investigating the role of capped termini versus uncapped charged collagen showed a destabilizing effect of uncapped charged collagen due to pH dependent electrostatic repulsion.<sup>28</sup> Experimentally, this system was shown to form higher order structures as well as possess a higher  $T_m$  than controls.<sup>27</sup> Incorporation of metal binding sites into collagenous peptides have also been shown to increase stability in a heterotrimer system of (POG)<sub>10</sub> cores anchored by C-terminal ProAlaHis, AlaHis, and His residues. His residues are well known to coordinate to transition metal ions in a predictable manner. Addition of Zn(II) and Cu(II) ions into this heterotrimeric system caused an increase in melting temperature of ~ 2.6 and 10.0 °C, respectively, compared to the same system in the absence of metal.<sup>29</sup>

In a comprehensive study performed by Horng et al.,<sup>30</sup> the effects on triple helical stability due to distortions using alanine,  $\beta$ -alanine, and sarcosine residues at different glycine positions in the triple helical network of (POG)<sub>8</sub> analogous systems provided insight into collagen folding and stability. It was found that distortions on the C-terminal end are more destabilizing than at the N-terminus, further supporting the hypothesis that folding propagates from the C-to-N termini. Additionally, this paper gives

insight into the destabilizing effects of a Gly-to-Sar replacement in the central position, destabilizing the helix considerably more than distortions at the C- or N-termini due to the interruption in the hydrogen bonding network.

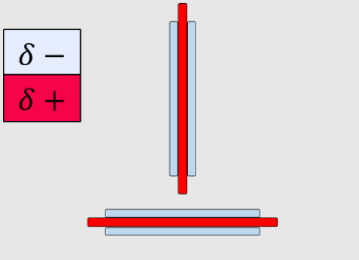
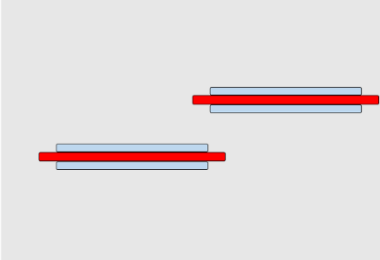
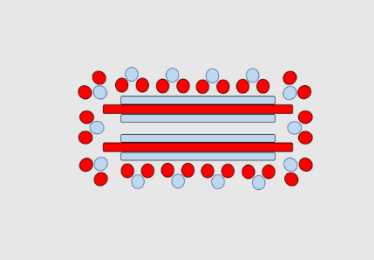


**Figure 1.6:** Sarcosine (Sar) residue. The methyl group replaces a hydrogen bond donor, destabilizing the triple helical network.

### 1.8 Basics of $\pi$ - $\pi$ stacking

The remainder of this thesis is focused on the effects of attaching large aromatic groups to the N-terminus of collagen strands. Thus, an introduction to so called “ $\pi$  -  $\pi$  stacking is warranted”. Of the many intermolecular and intramolecular interactions that are the basis for supramolecular chemistry, materials science, and biochemical aggregations, there are few interactions more divisive than that of  $\pi$  -  $\pi$  stacking or  $\pi$  -  $\pi$  interactions. These “stacking” interactions are thought to occur between the  $\pi$  systems of adjacent aromatic systems, which result in more stable aggregates. This model has, however, not held up in most computational modeling, and the favorable aggregates are instead thought to be a result of many interactions, including van der Waals interactions, electrostatic interactions, and solvent dependent interactions, such as the hydrophobic effect in aqueous solvents.<sup>31</sup>

While stacking interactions are certainly more complex than simple orbital overlap, this idea is often invoked whenever aromatic systems aggregate. Of the factors that are involved in stacking interactions, perhaps the most important is electrostatic. These interactions are depicted below.

T-Shaped	Off-Center Stacking	Face-to-face
Electrostatically favorable	Electrostatically Favorable	Only favorable in polar solvents due to the hydrophobic effect
		

**Figure 1.6:** Depiction of theorized electrostatic interactions between aromatic systems. The electron cloud is colored blue with the electropositive plane shown in red. For the face-to-face interaction, surrounding molecules are represented as acting as a hydration shell, with electropositive components in red and electronegative atoms in blue.

As would be expected, simple face to face aromatic interactions are not electrostatically favorable due to charge repulsion between electron clouds. Off-center and face-centered interactions, however, are electrostatically advantageous and could give rise to aggregation.<sup>31</sup>

Another component of stacking interactions that is often ignored is hydrophobic interactions in aqueous media. As aromatic species are more often than not non-polar, it is appropriate to assume that in a polar solvent (such as water) these non-polar components will aggregate. These interactions are driven largely by the entropic gain of reducing ordered “ice-like” water volume by minimizing exposed nonpolar surfaces, and by the enthalpic gain of allowing polar solvents to interact with each other in the solvation sphere.

Molecular distance additionally plays a major role in stacking interactions. For a stacking interaction, literature suggest that the aromatic systems need be within 3.4 – 3.8 Ångstroms of each other, or within an adequate van der Waals distance.<sup>32</sup>

## 1.9 Stacking interactions in nature

Previous work has shown that aromatic side chains of amino acids appear to aggregate in some protein structures, most notably in amyloid plaques or in the interior of proteins.<sup>32</sup> Numerous studies of both proteins and peptides have shown non-covalent interactions as being important when considering folding and stability, however, the contribution of “stacking” interactions as the driving force for these interactions is debated due to the high variance in the geometries and preferred conformations of these aggregates.<sup>31</sup> One area of stacking interactions in nature that is well understood are those interactions present in DNA. The structure of DNA has been known to incorporate stacking interactions between base pairs for some time. Interactions between base pairs and amino acids may also occur and have been supported by several different studies showing face-centered geometry of a phenylalanine-adenine interaction.<sup>31</sup>

## 1.10 Pyrene and its properties

Pyrene is a large flat aromatic compound that has been widely studied due to its remarkable fluorescence behavior.<sup>34</sup> Pyrene as a fluorophore emits light from 370-430 nm when excited in the UV region in its monomeric state. Pyrene, however, can form an excited state dimer or “excimer” when another chromophore is in close proximity. This excimer fluoresces at lower energy peaking at around 485 nm. Given its dependence on distance, the intensity of the excimer varies with concentration of the fluorophore. Local concentration can be increased by forcing the monomers into close proximity.<sup>35</sup> Luminophores containing pyrene fluorophores usually display high quantum yields and thermal stability.<sup>36</sup> The pyrene excimer is also known to be a result of face-to-face  $\pi$  stacking.<sup>36</sup> As  $\pi$ - $\pi$  stacking is of utmost importance for the formation of the pyrene excimer, excimer fluorescence can give information on the types of aggregation taking place in a solution containing pyrene fluorophores.

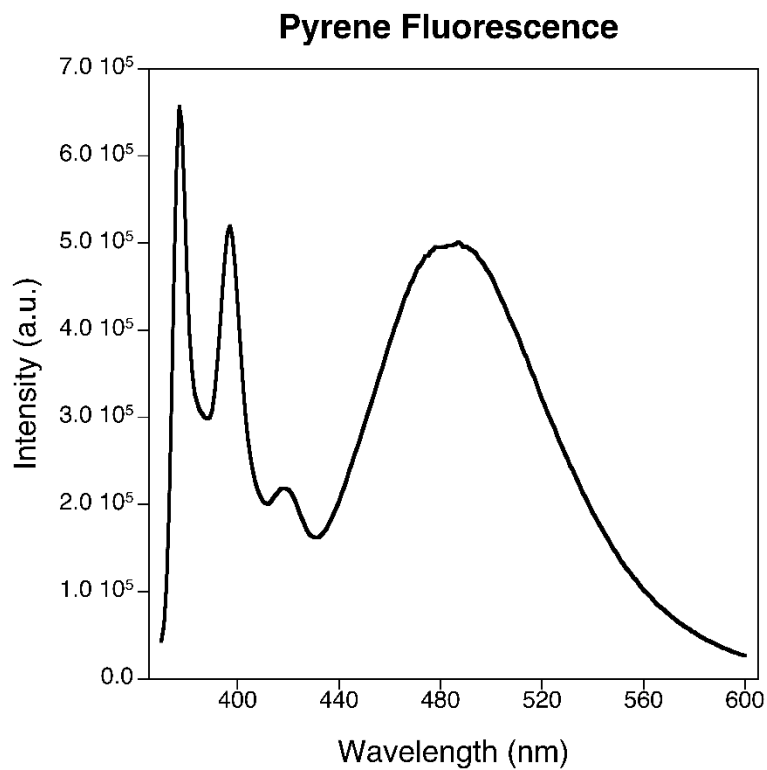


**Figure 1.7:** Stereotypical pyrene fluorescence. A stereotypical pyrene emission scan showing monomer fluorescence below 430 nm and excimer fluorescence appearing at lower energy.

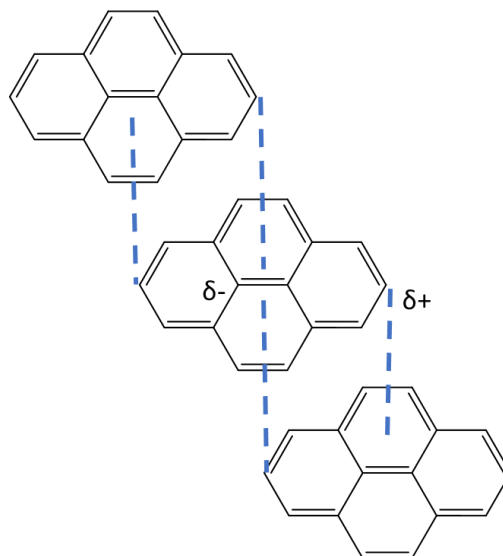


**Figure 1.8:** Off-center face-to-face stacking of pyrene. Visual representation of a stacking geometry of pyrene that would give rise to an excimer.



### **1.11 Goals of this research**

In the preceding sections, collagen structure and modification have been described in detail, with an eye toward stabilizing the triple helix. Additionally, the phenomenon of “ $\pi$ - $\pi$  stacking” was described briefly, in relation to the fluorophore pyrene. The following chapters of this thesis will seek to combine these topics toward the synthesis of a pyrene labeled collagen system, with the hypothesis that stacking interactions between pyrene fluorophores will allow for the analysis of thermal unwinding at low concentrations by fluorescence spectroscopy.

## Chapter 2: Synthesis and peptide design

### 2.1 Introduction

This chapter details the synthesis and characterization of pyrene-bearing collagenous peptides. Included are the design rationale of the peptide systems, synthesis and purification techniques, and characterization of each system.

### 2.2 Peptide design

N-Terminal pyrene-anchored collagenous peptides were synthesized in order to provide materials for testing by CD and fluorescence spectroscopies. Each system was synthesized using a XaaYaaGly core of ProHypGly for seven repeats with an additional amino acid flanking each end. The flanking amino acids were expected to impart differing degrees of fraying to the helix, which could then be probed by monitoring pyrene excimer emission. The following peptides were synthesized:

Formulae	Abbreviation
Ac-K(POG) <sub>7</sub> K-NH <sub>2</sub>	Ac-KK
Pyrene(CH <sub>2</sub> )CO-K(POG) <sub>7</sub> K-NH <sub>2</sub>	Pyr(1)-KK
Pyrene(CH <sub>2</sub> ) <sub>3</sub> CO-K(POG) <sub>7</sub> K-NH <sub>2</sub>	Pyr(3)-KK
Pyrene(CH <sub>2</sub> ) <sub>3</sub> CO-K(POG) <sub>7</sub> A-NH <sub>2</sub>	Pyr(3)-KA
Pyrene(CH <sub>2</sub> ) <sub>3</sub> CO-A(POG) <sub>7</sub> K-NH <sub>2</sub>	Pyr(3)-AK
Pyrene(CH <sub>2</sub> ) <sub>3</sub> CO-E(POG) <sub>7</sub> A-NH <sub>2</sub>	Pyr(3)-EA
Pyrene(CH <sub>2</sub> ) <sub>3</sub> CO-K(POG) <sub>3</sub> POSarcosine(POG) <sub>3</sub> K-NH <sub>2</sub>	Pyr(3)-KSarK
Pyrene(CH <sub>2</sub> ) <sub>3</sub> CO-KPOSarcosine(POG) <sub>2</sub> POSarcosine(POG) <sub>2</sub> POSarcosineK-NH <sub>2</sub>	Pyr(3)-KSar <sub>3</sub> K

**Table 2.1:** List of synthetic pyrene-labeled collagen systems, with associated abbreviations.

Abbreviations for each system will henceforward be used for clarity. Lys (K) was chosen to serve as the primary bracketing residue for several reasons. Lysine residues were expected to increase solubility in an aqueous buffer, while minimizing aggregation of adjacent triple-helical systems into higher-order structures through charge repulsion. The effects of these Lys residues at the terminal positions of the collagen core were further probed through replacement with either Ala to investigate the destabilizing effects of this Lys residue on the N- or C-termini, or Glu to investigate how replacement of a cationic amino acid with an anionic amino acid impacts stability on the N-terminus. Additional systems were synthesized with the amino acid sarcosine (Sar) in place of glycine at some positions. Replacement of glycine with sarcosine should prevent formation of triple helices due to distortion of the hydrogen bonding network.<sup>30,37</sup>

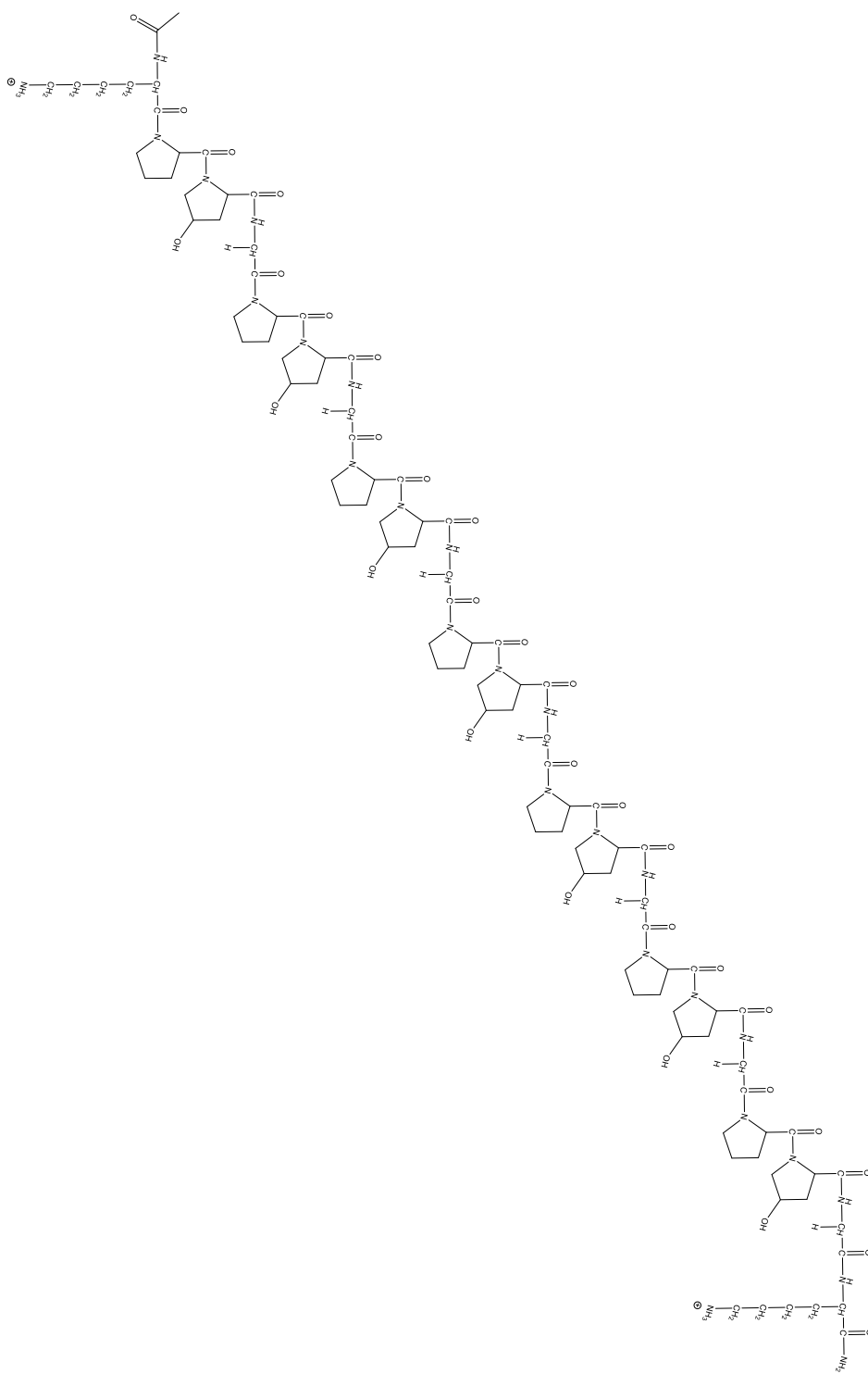


**Figure 2.1:** The Ac-KK system.

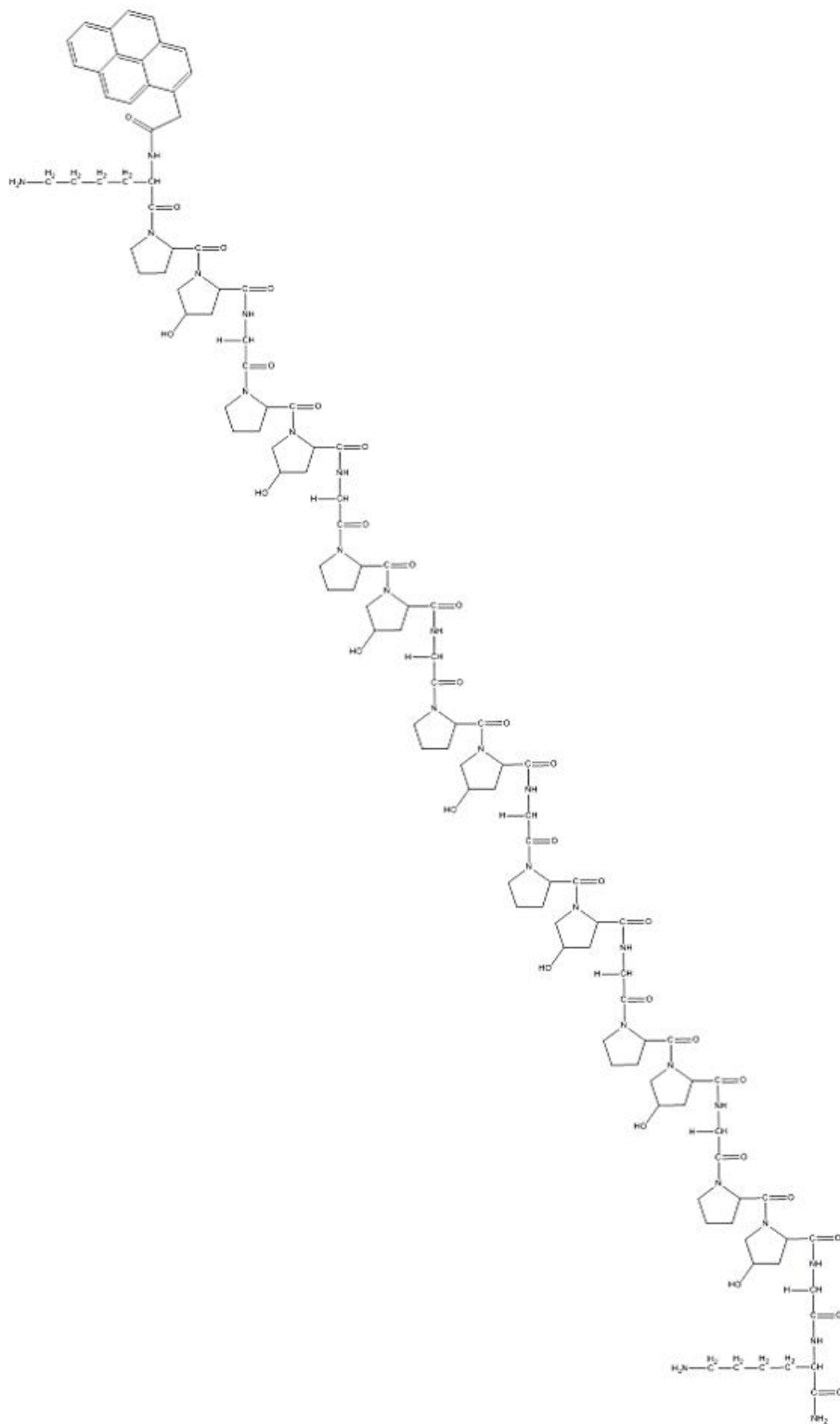


**Figure 2.2:** The Pyr(1)-KK system.

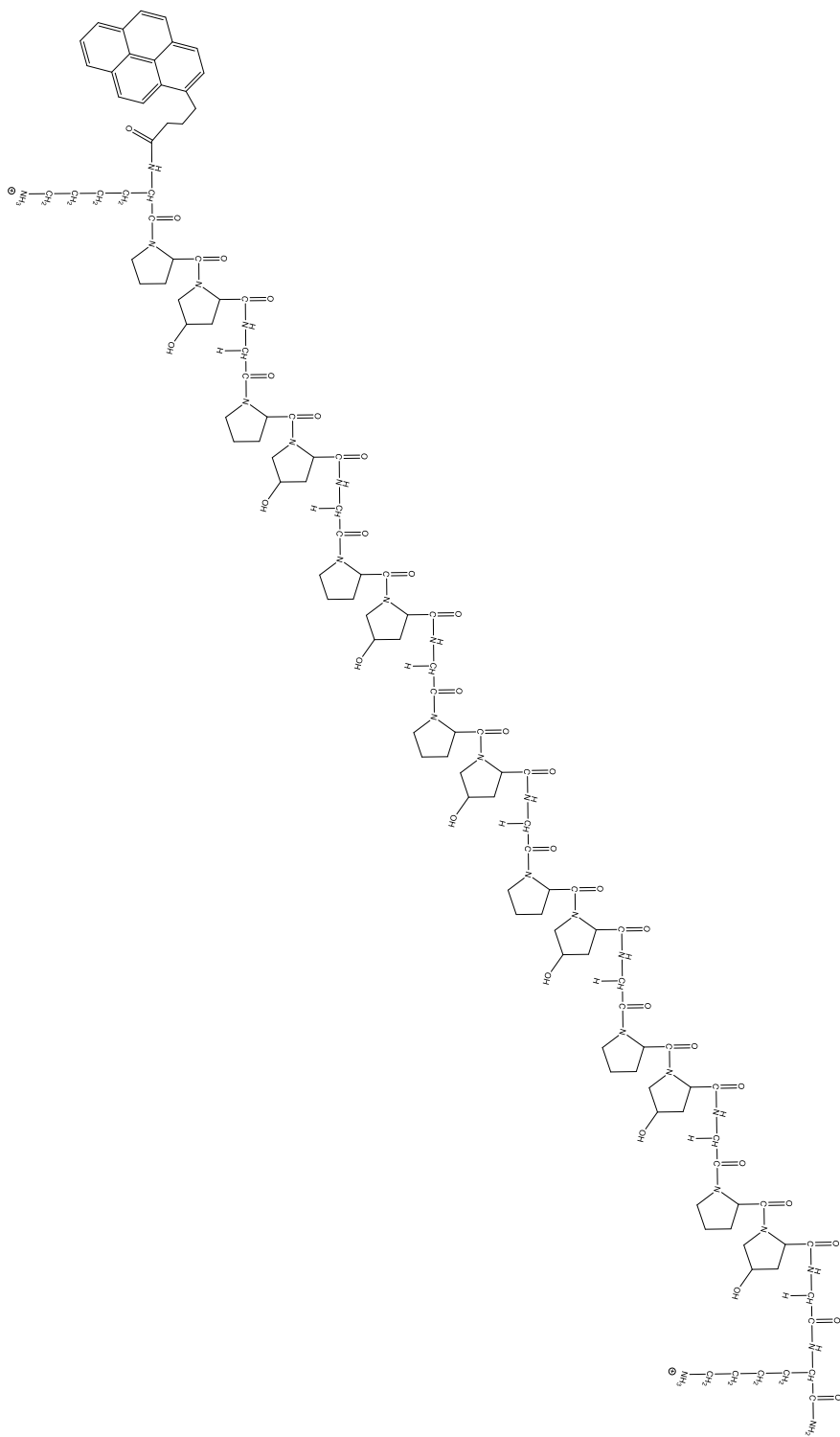


**Figure 2.3:** The Pyr(3)-KK system.

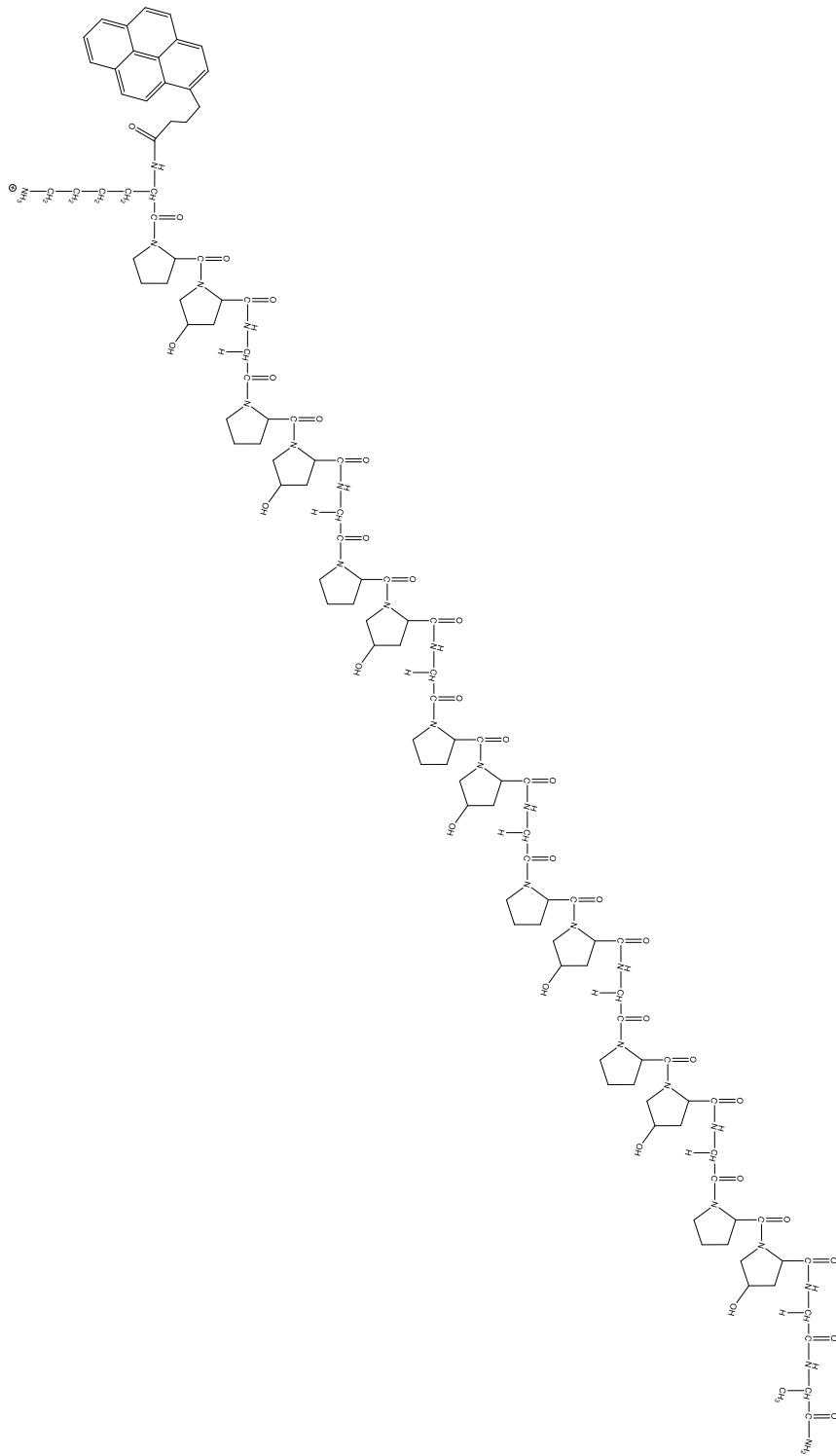


**Figure 2.4:** The Pyr(3)-KA system.

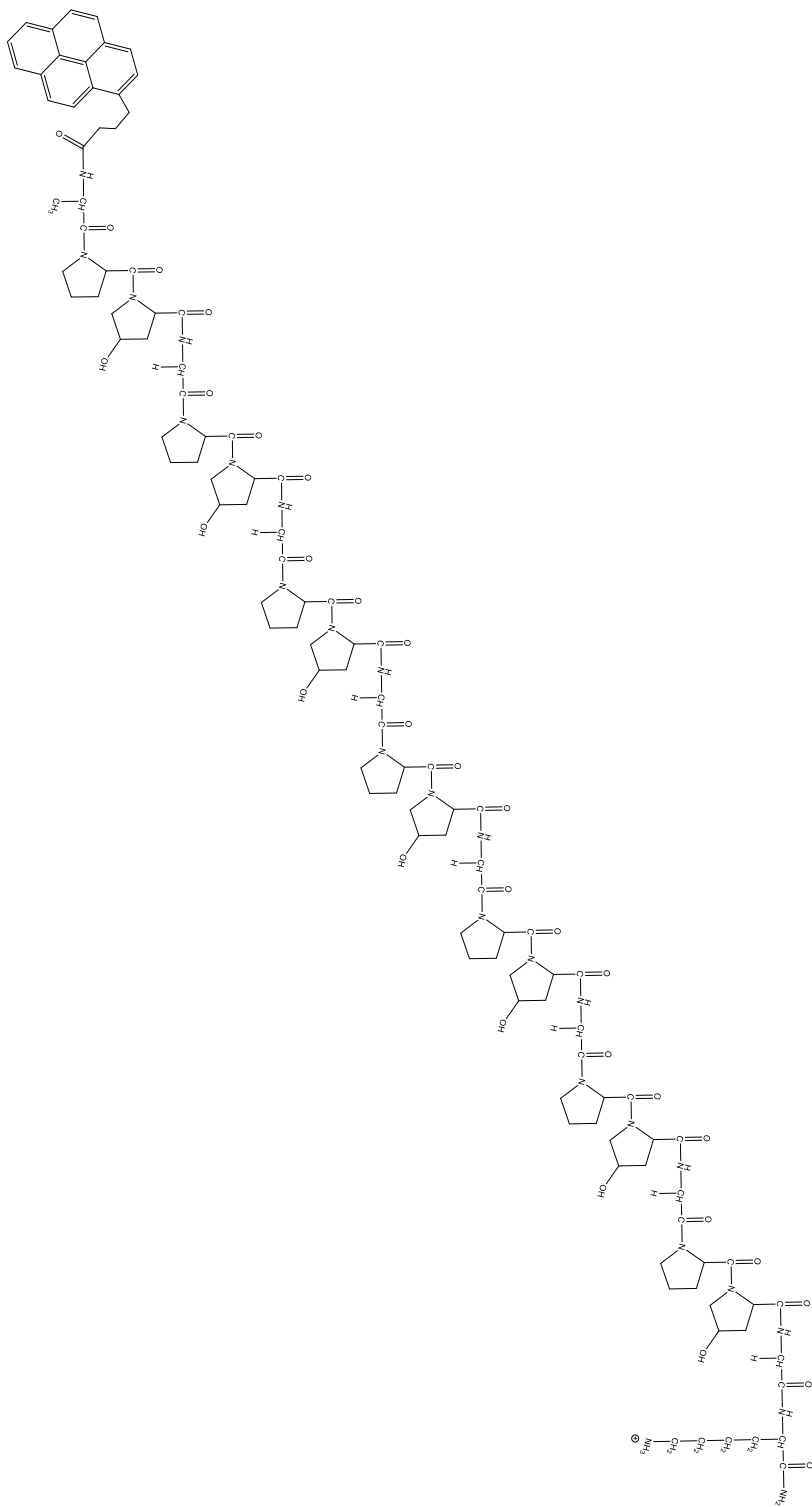


**Figure 2.5:** The Pyr(3)-AK system.



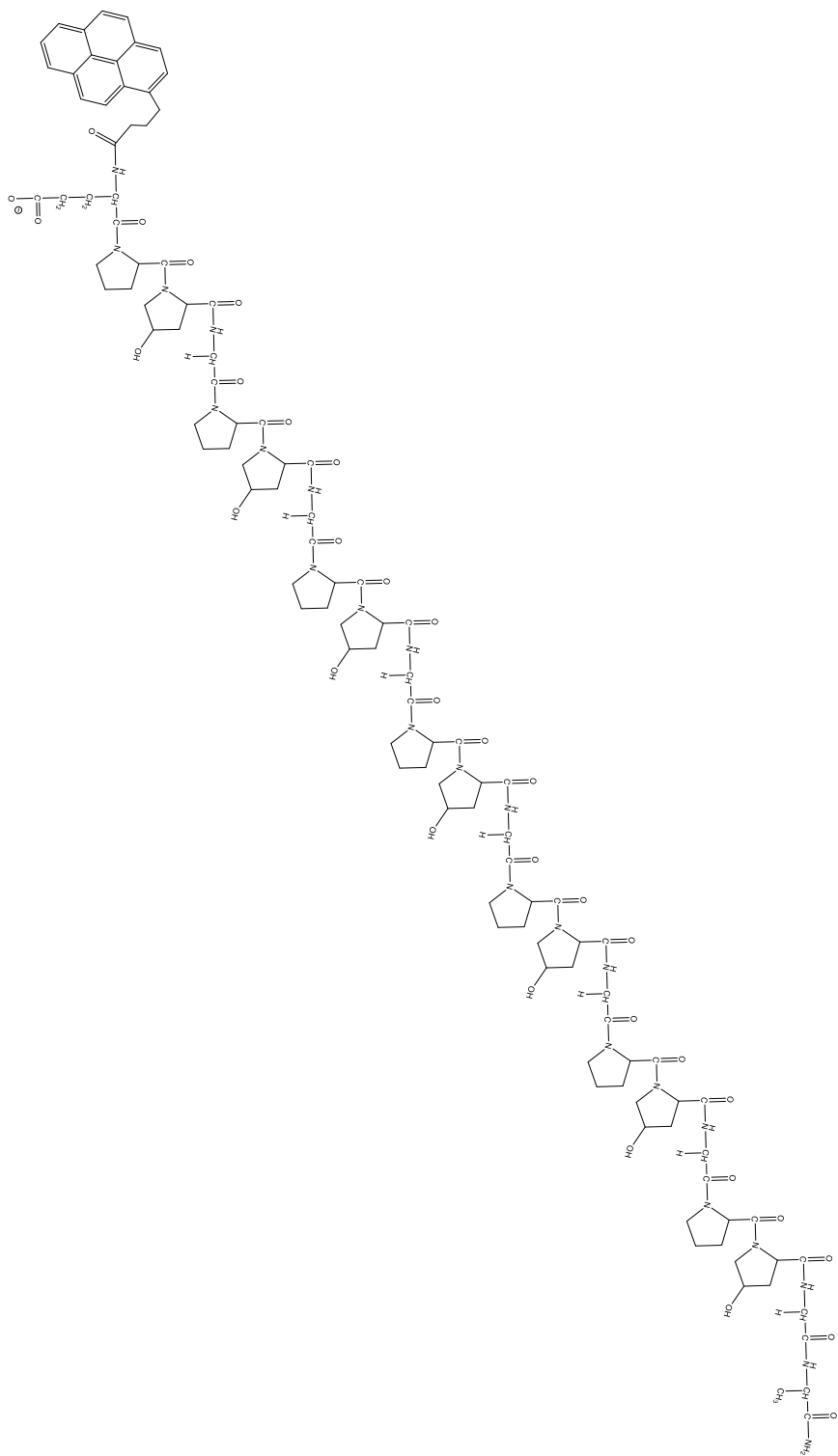


**Figure 2.6:** The Pyr(3)-EA system

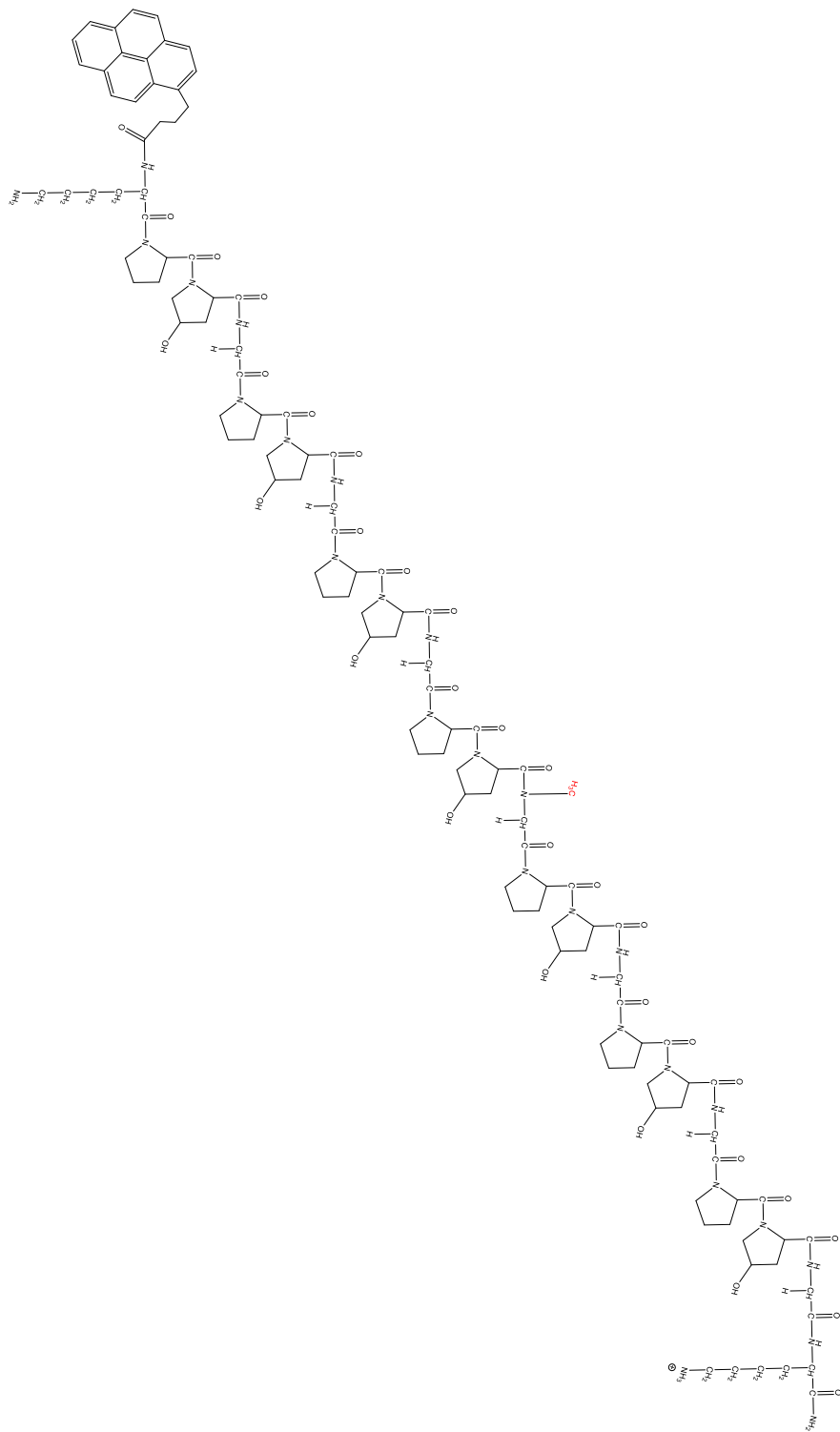


**Figure 2.7:** The Pyr(3)-KSarK system. Sarcosine residue is shown with the methyl group in red.

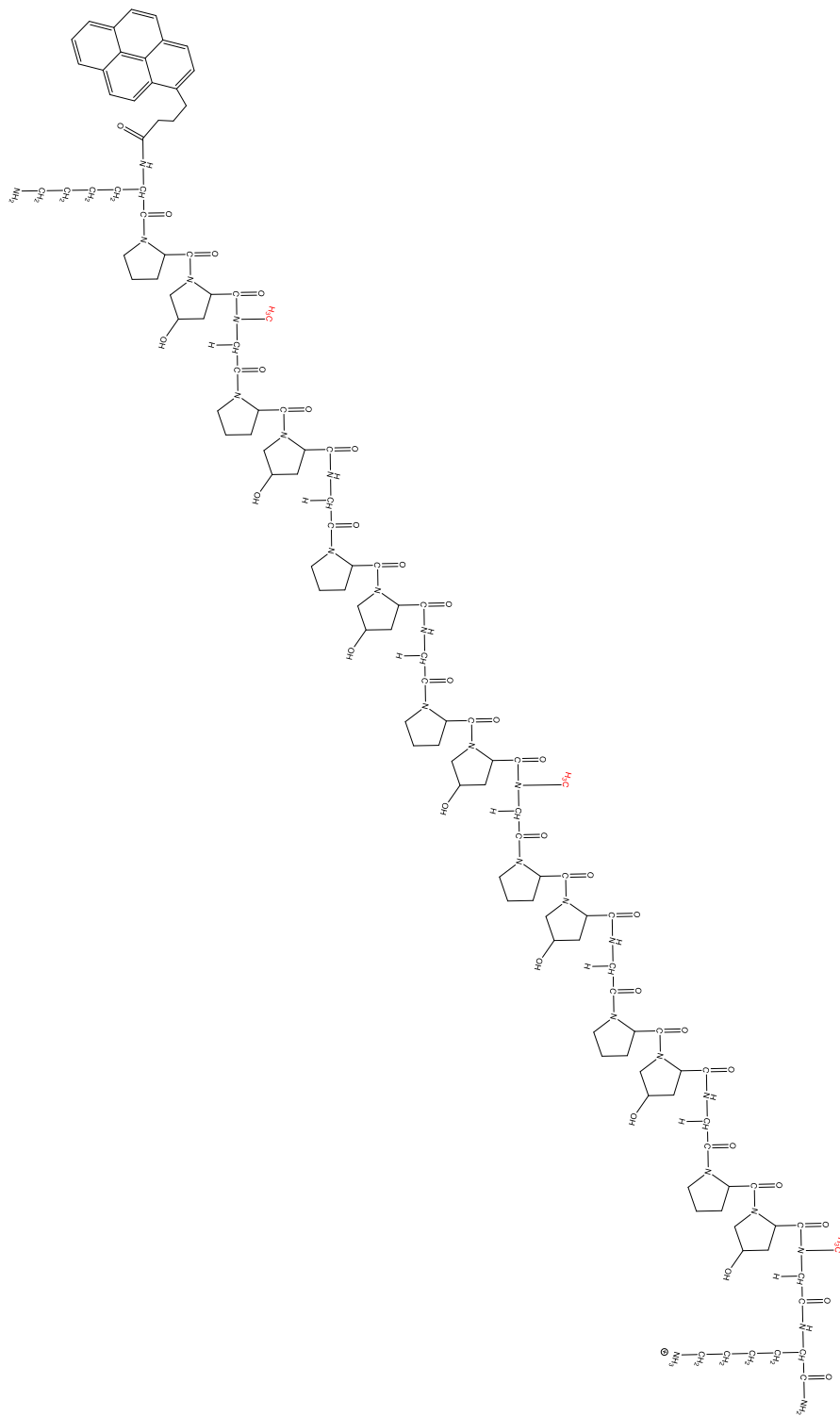


**Figure 2.8:** The Pyr(3)-KSar<sub>3</sub>K system. Sarcosine residues are shown with methyl groups in red.

## **2.3 Experimental conditions and solid phase peptide synthesis**

Peptides were synthesized using Fmoc-based solid-phase peptide synthesis (SPPS) on Rink amide low-loading resin. Amino acids were coupled in the presence of HBTU using N,N-dimethylformamide (DMF) as a solvent, 7% N,N-diisopropylethylamine (DIPEA) in DMF as an activant, and 20% 4-methylpiperidine in DMF as a deprotectant. For each pyrene containing system, a vial containing either pyrenebutyric acid “Pyr(3)” or pyreneacetic acid “Pyr(1)” was treated as an amino acid in the last synthesis step. Non pyrenated peptides were capped with an acetyl group using acetic anhydride. In the synthesis, each coupling step involving proline was programmed to occur twice without removal of the Fmoc protecting group from the first coupling step. This was done in order to maximize yield of pure peptide as Pro residues were presumed to be difficult coupling steps. Hyp residues were also “double coupled” in this manner for the last 5 Hyp residues added. The very first amino acid (at the C-terminus) was also double coupled.

Following synthesis, the resulting crude resin was washed over suction with glacial acetic acid, dichloromethane, and methanol. Following washing, the resin was dried under vacuum for > 3 hours before weighing to determine a crude yield. Following weighing, the resin was cleaved from the attached peptide with a mixture of 2 mL of trifluoroacetic acid, 100  $\mu$ L of triethylsilane, and 100  $\mu$ L of anisole, which was stirred for two hours. Following cleavage, the resin was filtered by suction and the filtrate was pipetted into a tube of ice cold diethyl ether and left to precipitate for >2 hours. Following equilibration, the peptide was filtered out of solution by suction. These crude peptides were then purified by HPLC for analysis.

## **2.4: Characterization of synthesized peptides**

### **2.4.1: HPLC traces**

High performance liquid chromatography was performed on each synthesized system in an attempt to purify the resultant crude peptide mixture from each SPPS operation. These experiments were

performed on a BioLogic Duo Flow HPLC using analytical and preparatory C – 18 columns to purify peptides. Eluents were distilled water and acetonitrile, each containing 1% trifluoroacetic acid in order to discourage aggregation. Each run was completed over varying time periods and flow rates depending on the composition of each crude peptide mixture, and the wavelengths 214 nm, 254 nm, 280 nm, and 355 nm were each monitored over the course of the experiments to allow for determination of retention times. Species could then be analyzed by mass spectrometry to determine the success of each synthesis.

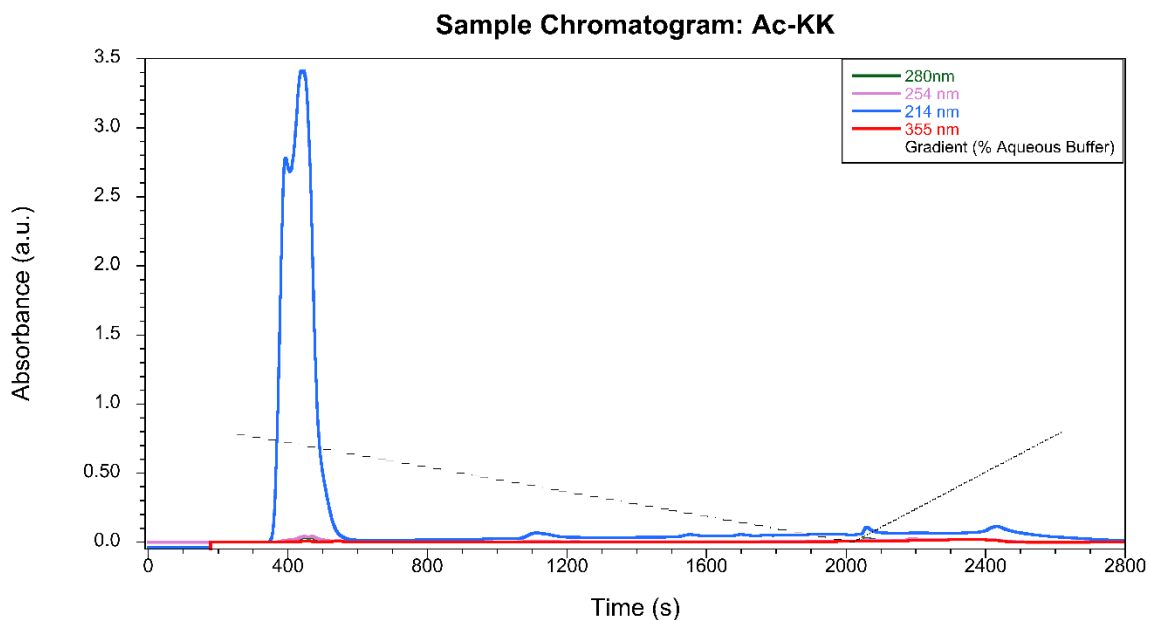


**Figure 2.9:** Representative chromatogram of Ac-KK, collected via HPLC. The peak with retention time of approximately 8 minutes was found to be the correct peptide. \*This chromatogram was collected from previously purified Ac-KK, as the original chromatogram following synthesis was lost due to a hard drive error.

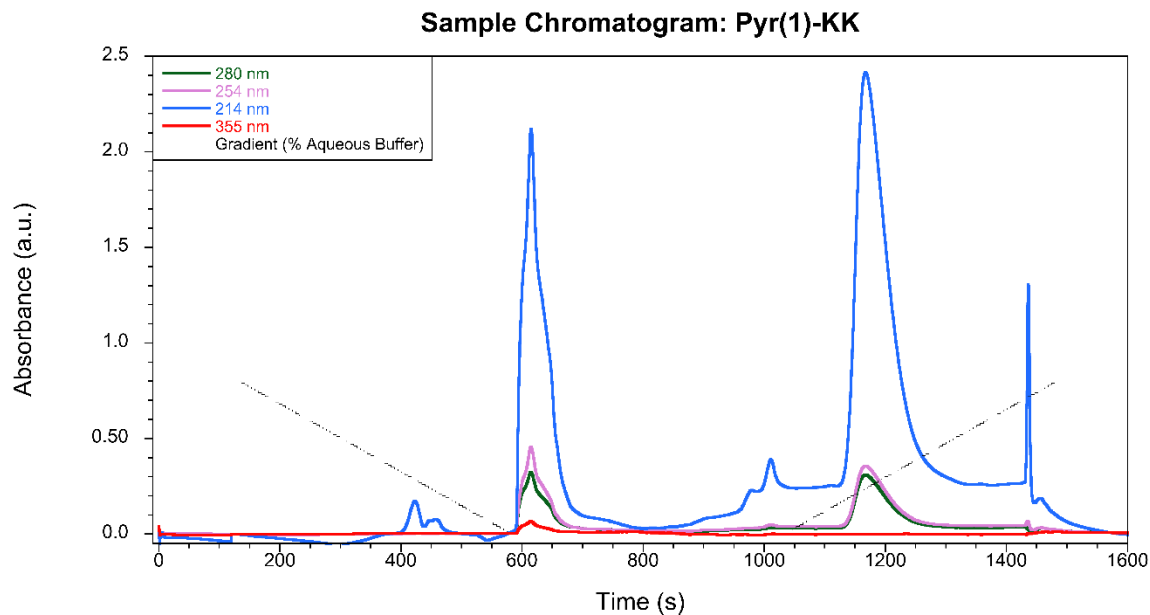


**Figure 2.10:** Representative chromatogram of Pyr(1)-KK, collected via HPLC. Wavelengths monitored are indicated in the legend on the graph. A fraction was collected at ~ 10 minutes (600 seconds) to be analyzed by mass spectrometry. \* This chromatogram is of an attempt to re-purify the original pure peptide after use. The original chromatogram following synthesis was lost due to a hard drive error.

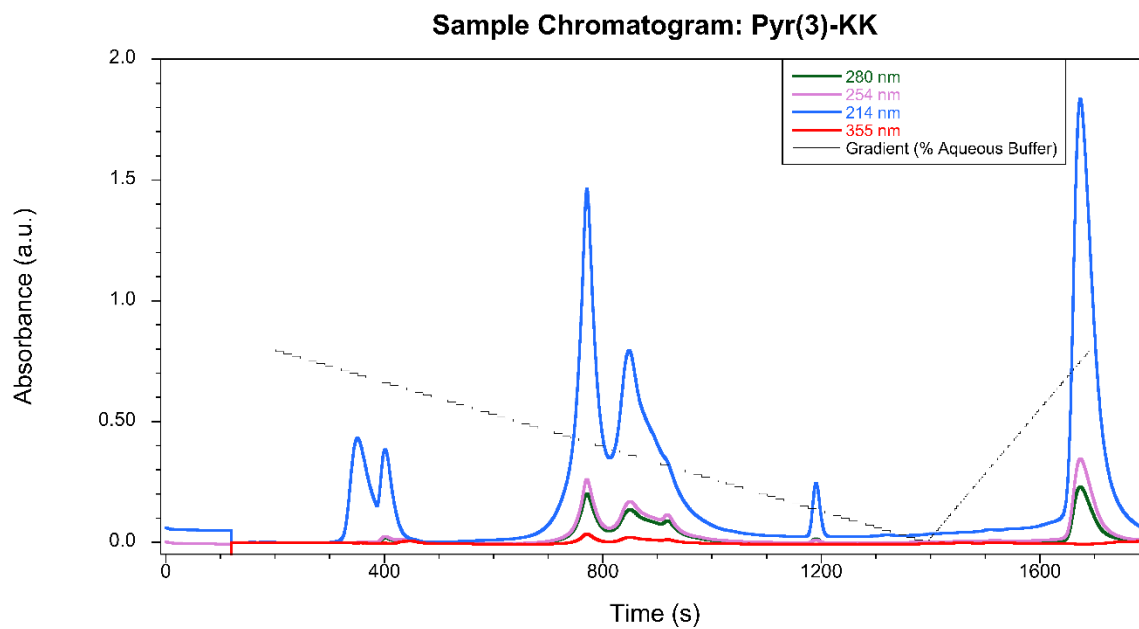


**Figure 2.11:** Representative chromatogram of Pyr(3)-KK collected via HPLC. Monitored wavelengths are indicated in the legend on the graph. The peak with a retention time of 11 minutes was shown to be the correct species.

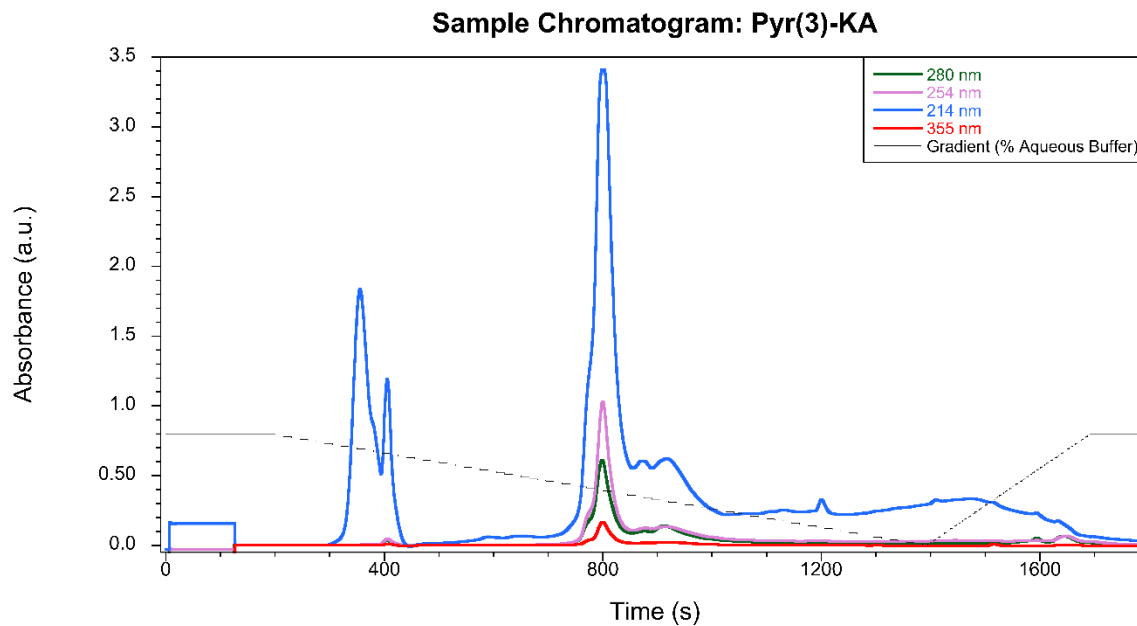


**Figure 2.12:** Representative chromatogram of Pyr(3)-KA, collected via HPLC. Monitored wavelengths are indicated in the legend on the graph. The peak with a retention time of 13 minutes was shown to be the correct peptide.

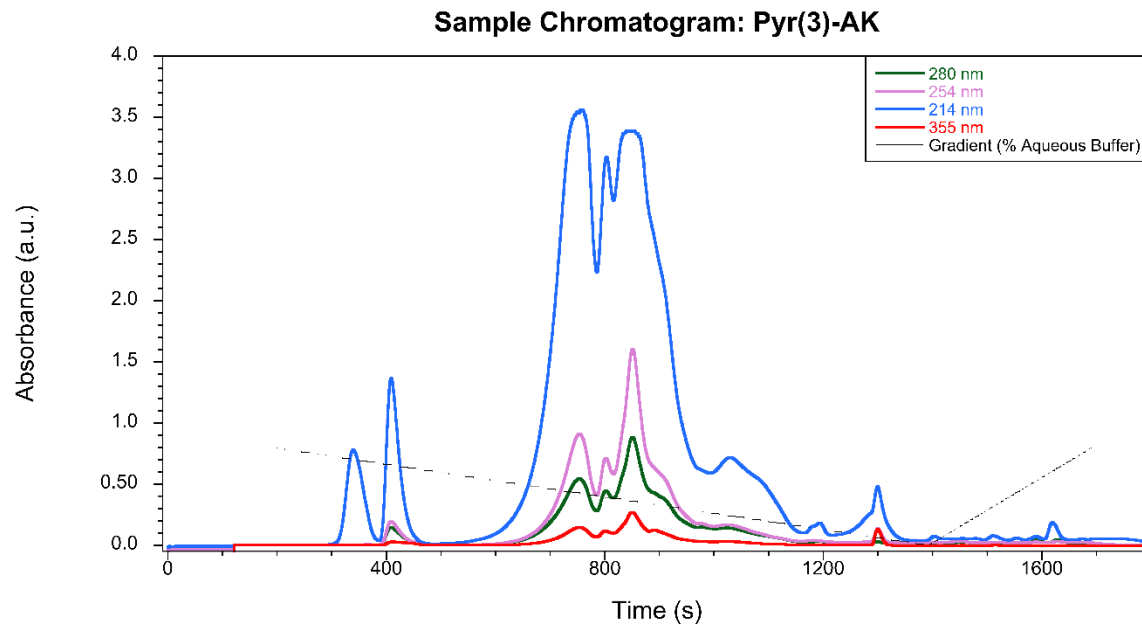


**Figure 2.13:** Representative chromatogram of Pyr(3)-AK, collected via HPLC. Monitored wavelengths are indicated in the legend on the graph. The peak at approximately 14 minutes was found to be the correct peptide.

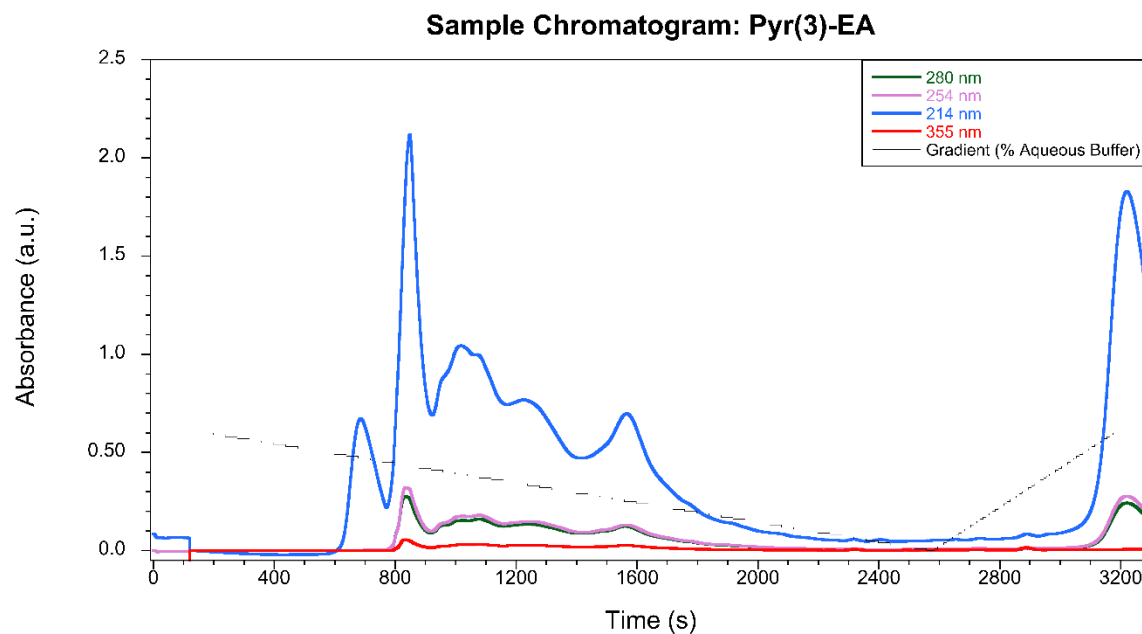




**Figure 2.14:** Representative chromatogram of Pyr(3)-EA collected via HPLC. Wavelengths measured are indicated in the legend on the graph. The peak with a retention time of approximately 13 minutes was found to be the correct peptide.

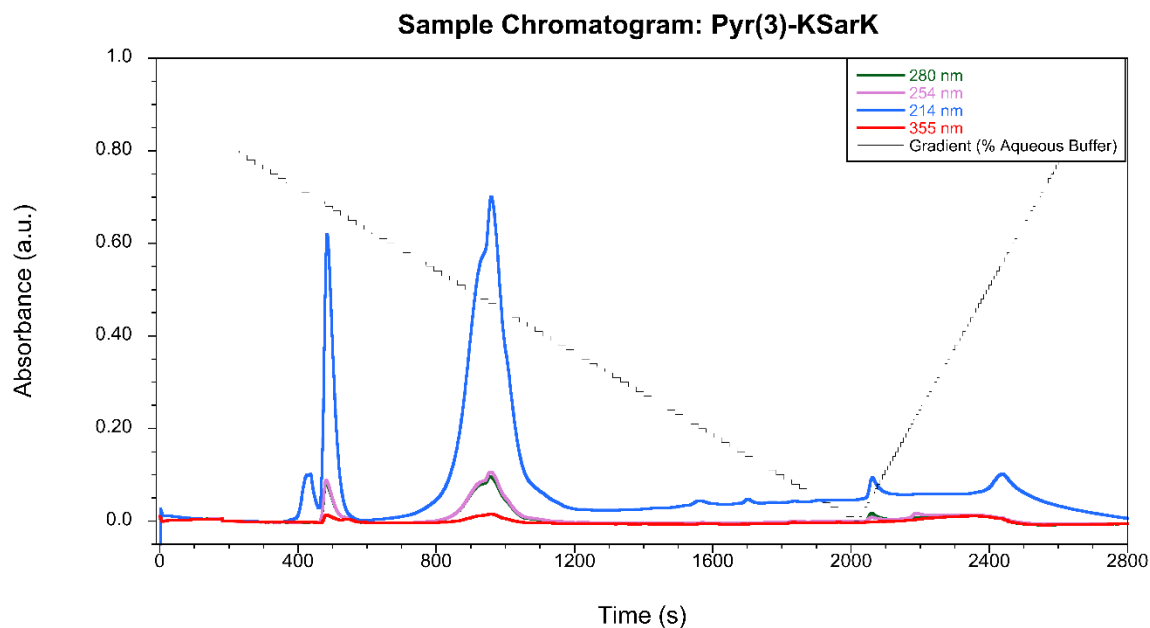


**Figure 2.15:** Representative chromatogram of Pyr(3)-KSarK, collected via HPLC. Monitored wavelengths are indicated in the legend on the graph. The peak with a retention time of approximately 15 minutes was found to be correct peptide. \* This chromatogram is of an attempt to re-purify the original pure peptide after use. The original chromatogram following synthesis was lost due to a hard drive error.

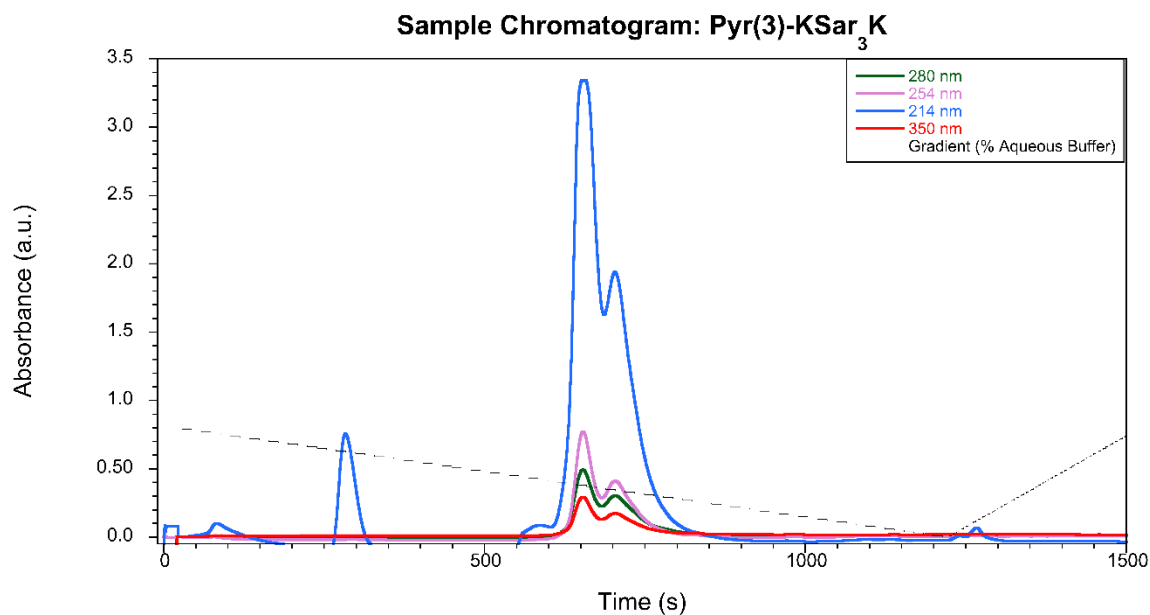


**Figure 2.16:** Representative chromatogram of Pyr(3)KSar<sub>3</sub>K, collected via HPLC. Monitored wavelengths are indicated in the legend on the graph. The peak with a retention time of 11 minutes was shown to be the correct peptide by mass spectrometry.

#### 2.4.2: Mass spectrometry

Prominent peaks from above were tested by mass spectrometry using either Quadrupole time-of-flight (Q-tof) or Matrix Assisted Laser Desorption Ionization time-of-flight (MALDI-tof) instruments in order to determine the identity of these peaks as desired product. MALDI was used for the Pyr(3)-KA and Pyr(3)-EA systems, as the Q-tof was unavailable. Once the identities of each system were confirmed, the peaks in question from HPLC were isolated for further experiments.

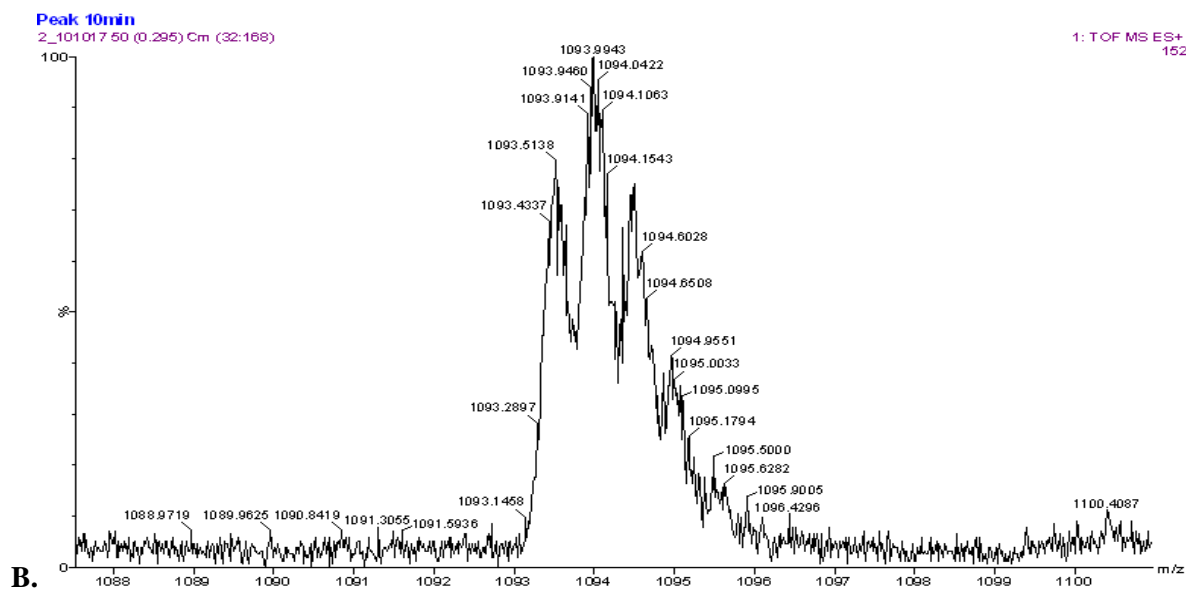
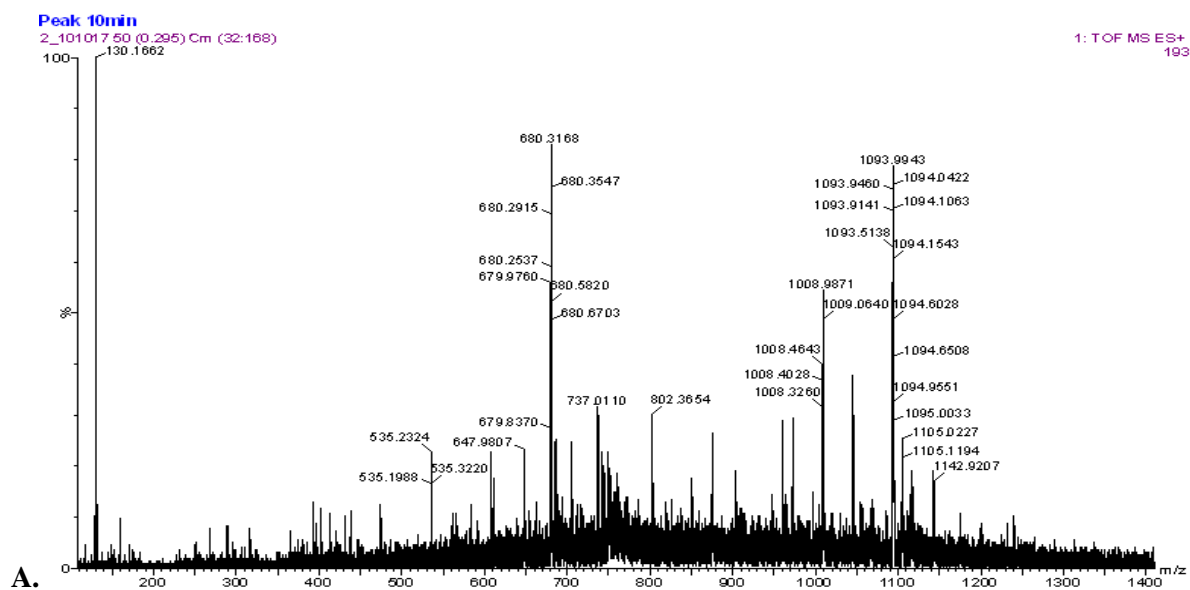


**Figure 2.17:** Mass spectrometry of Ac-KK. A.) Full collected spectrum. B.) Expansion of the region at ~1093 amu confirming the peptide's identity. Calculated for  $(M+2H)^{2+}$   $m/z = 1093.55$  amu.

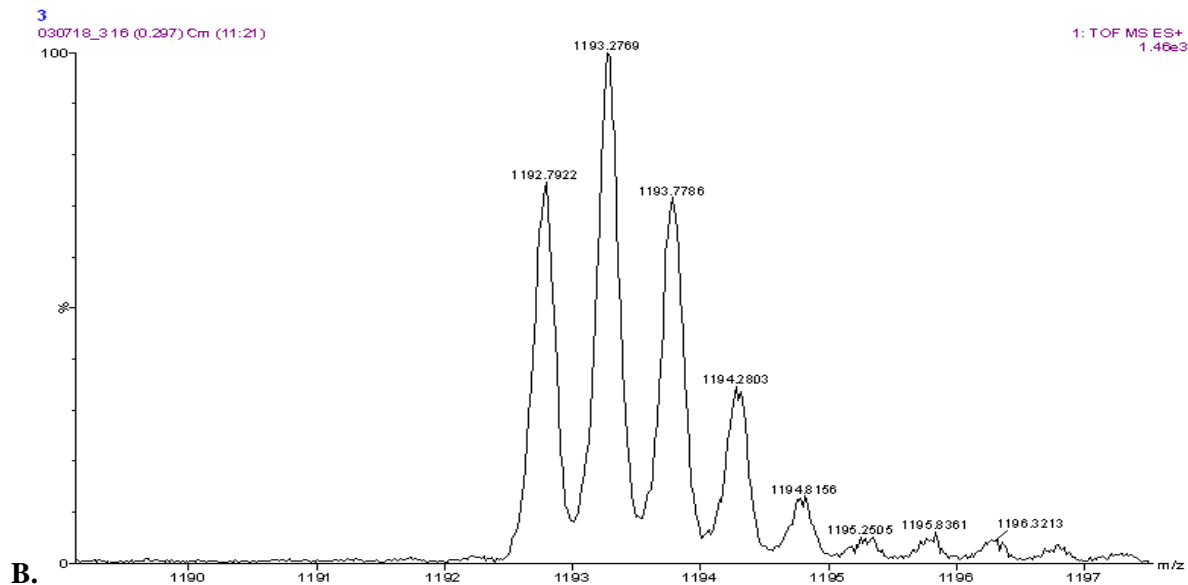
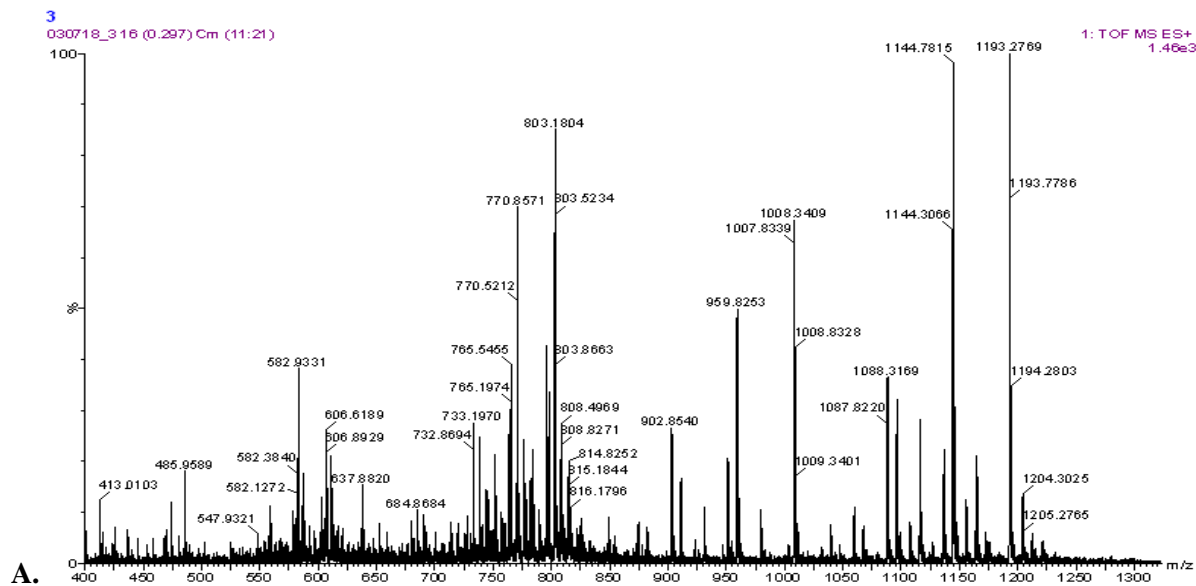


**Figure 2.18:** Mass spectrometry of Pyr(1)-KK. A.) Full collected spectrum. B.) Expansion of the region at ~ 1193 amu indicative of the desired peptide. Calculated for  $(M+2H)^{2+}$   $m/z = 1193.58$  amu.

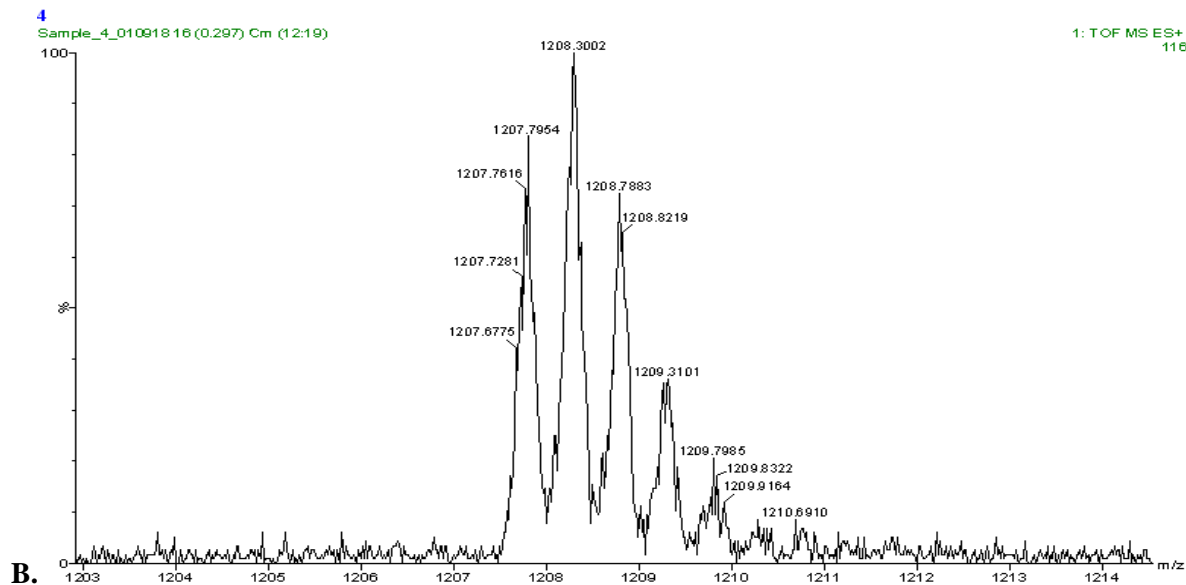
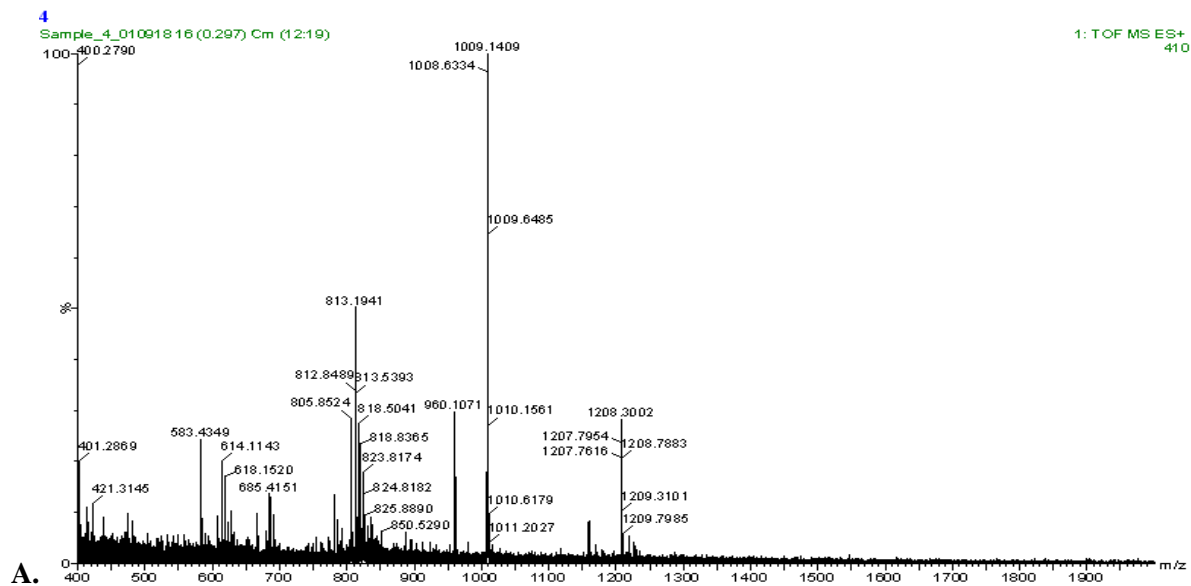


**Figure 2.19:** Mass spectrometry of Pyr(3)-KK. A.) Full collected spectrum. B.) Expansion of the region at ~ 1208 amu indicative of the desired peptide. Calculated for  $(M+2H)^{2+}$   $m/z = 1207.60$  amu.

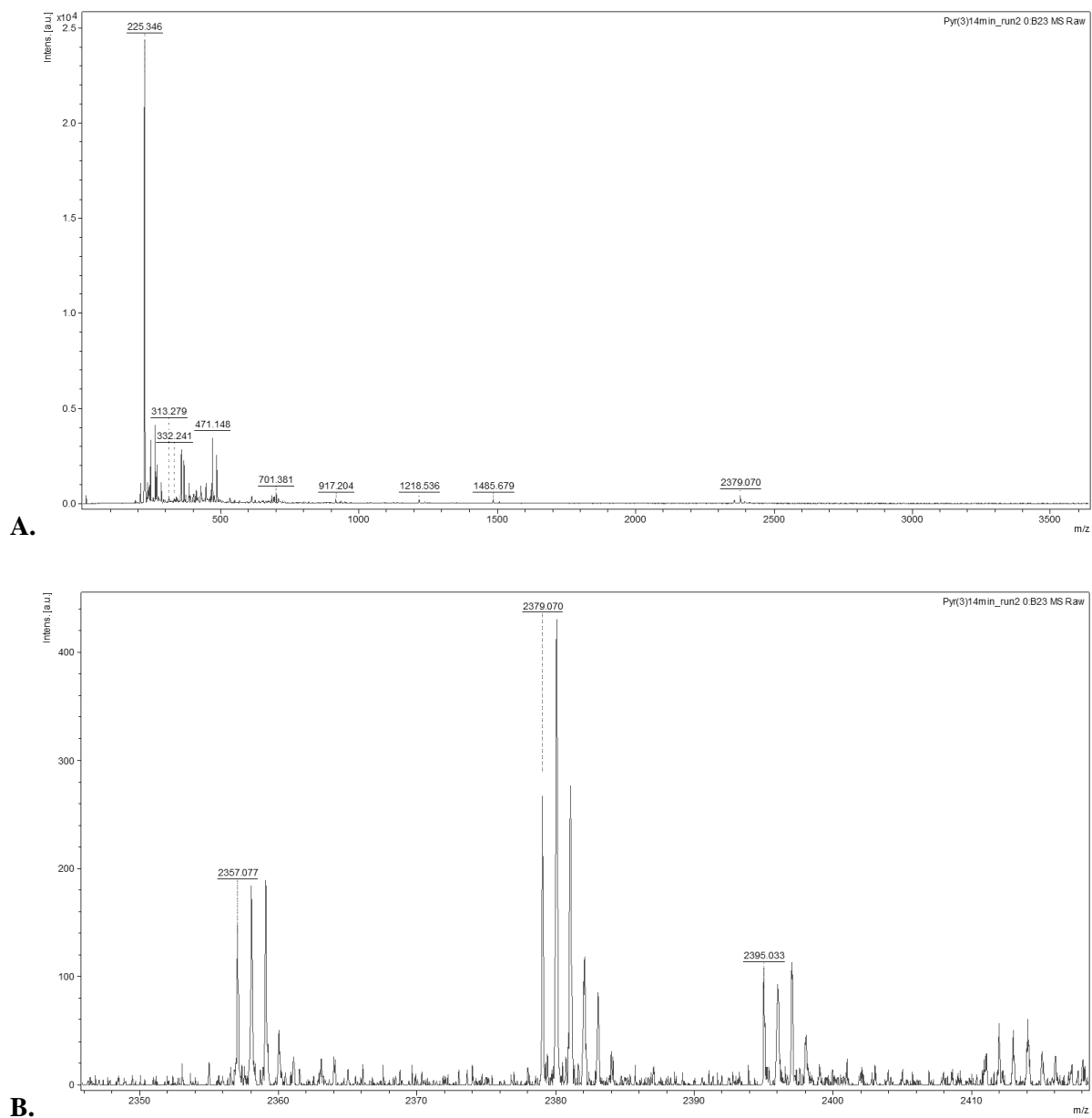


**Figure 2.20:** Mass spectrometry of Pyr(3)-KA. A.) Full spectrum collected via MALDI-tof. B.) Expansion of the region at ~2379 amu indicative of the desired peptide with an attached sodium. Calculated for  $(M+2H)^{2+}$   $m/z = 2357.12$  amu.

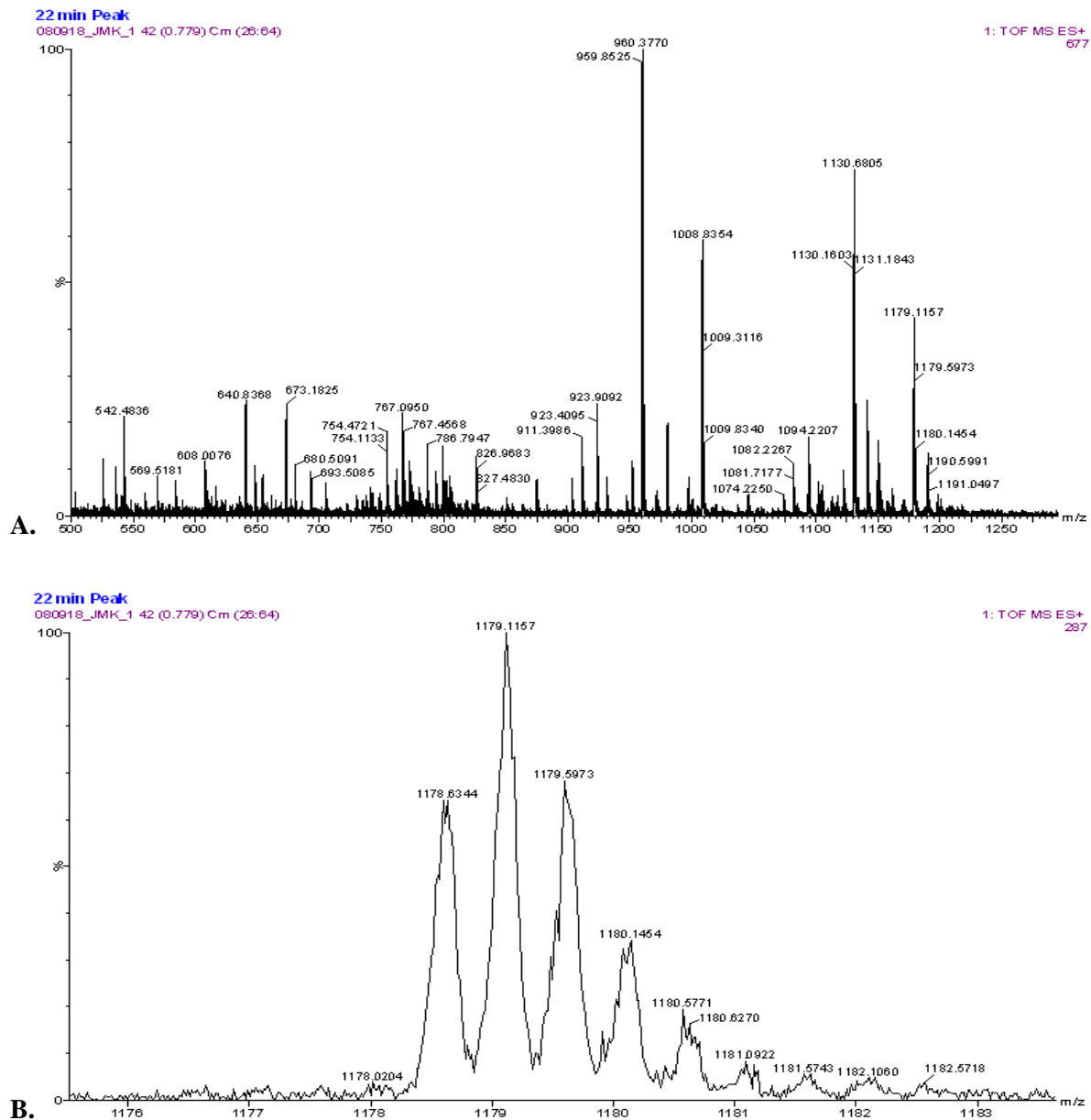


**Figure 2.21:** Mass spectrometry of Pyr(3)-AK. A.) Full collected spectrum. B.) Expansion of the region at ~ 1179 amu indicative of the desired peptide. Calculated for  $(M+2H)^{2+}$   $m/z = 1178.56$  amu.

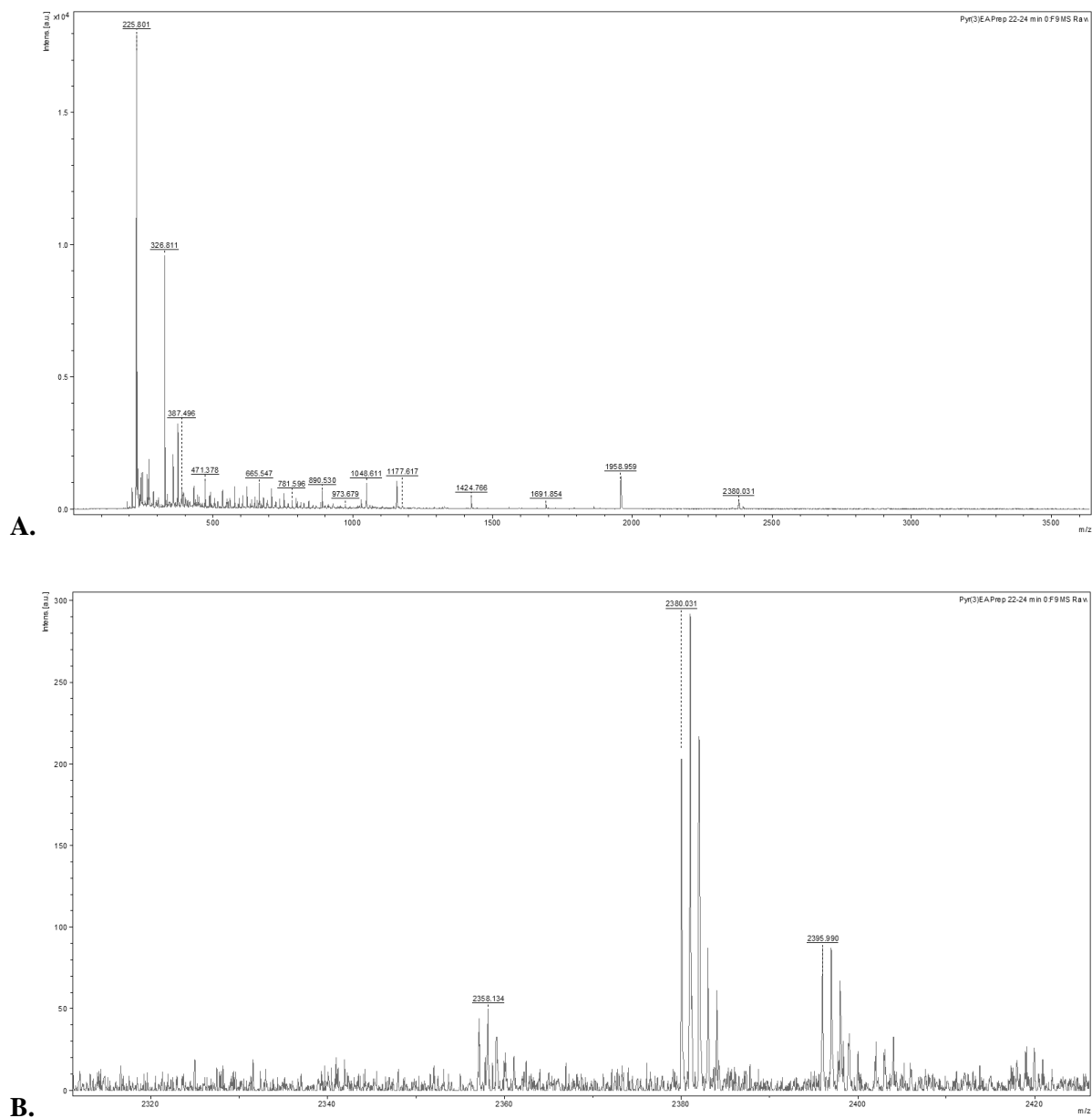


**Figure 2.22:** Mass spectrometry of Pyr(3)-EA. A.) Full collected spectrum collected via MALDI-tof. B.) Expansion of the region at ~2380 amu indicative of the desired peptide with the addition of a sodium ion. Calculated for  $(M+2H)^{2+}$   $m/z = 2357.06$  amu.



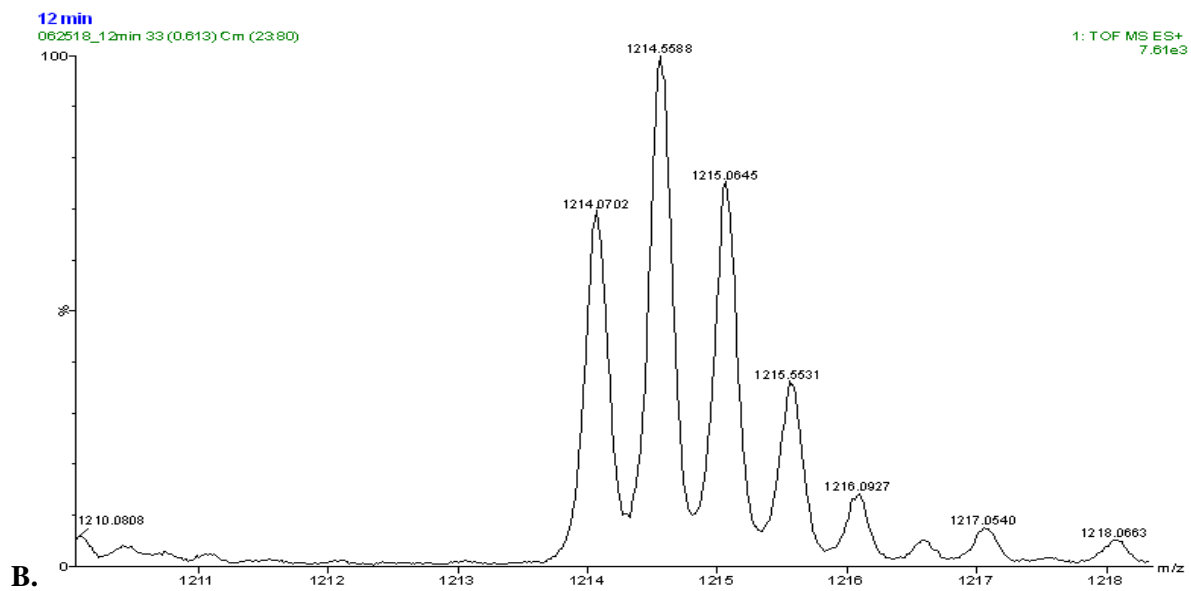
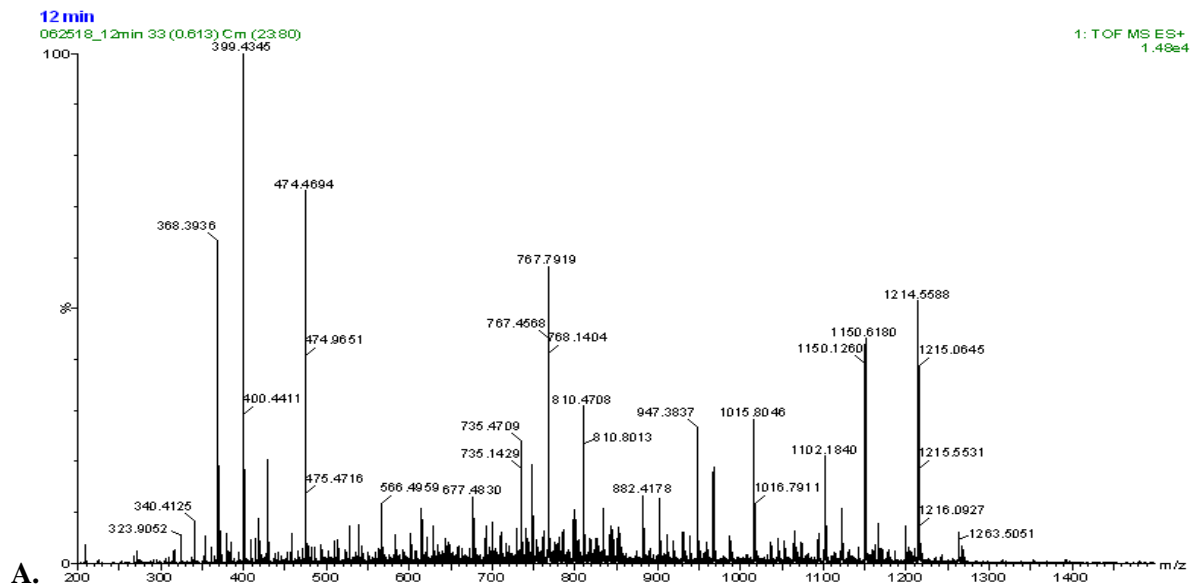


**Figure 2.23:** Mass spectrometry of Pyr(3)-KSarK. A.) Full collected spectrum. B.) Expansion of the region at ~ 1214 amu indicative of the desired peptide. Calculated for  $(M+2H)^{2+}$   $m/z = 1214.60$  amu.

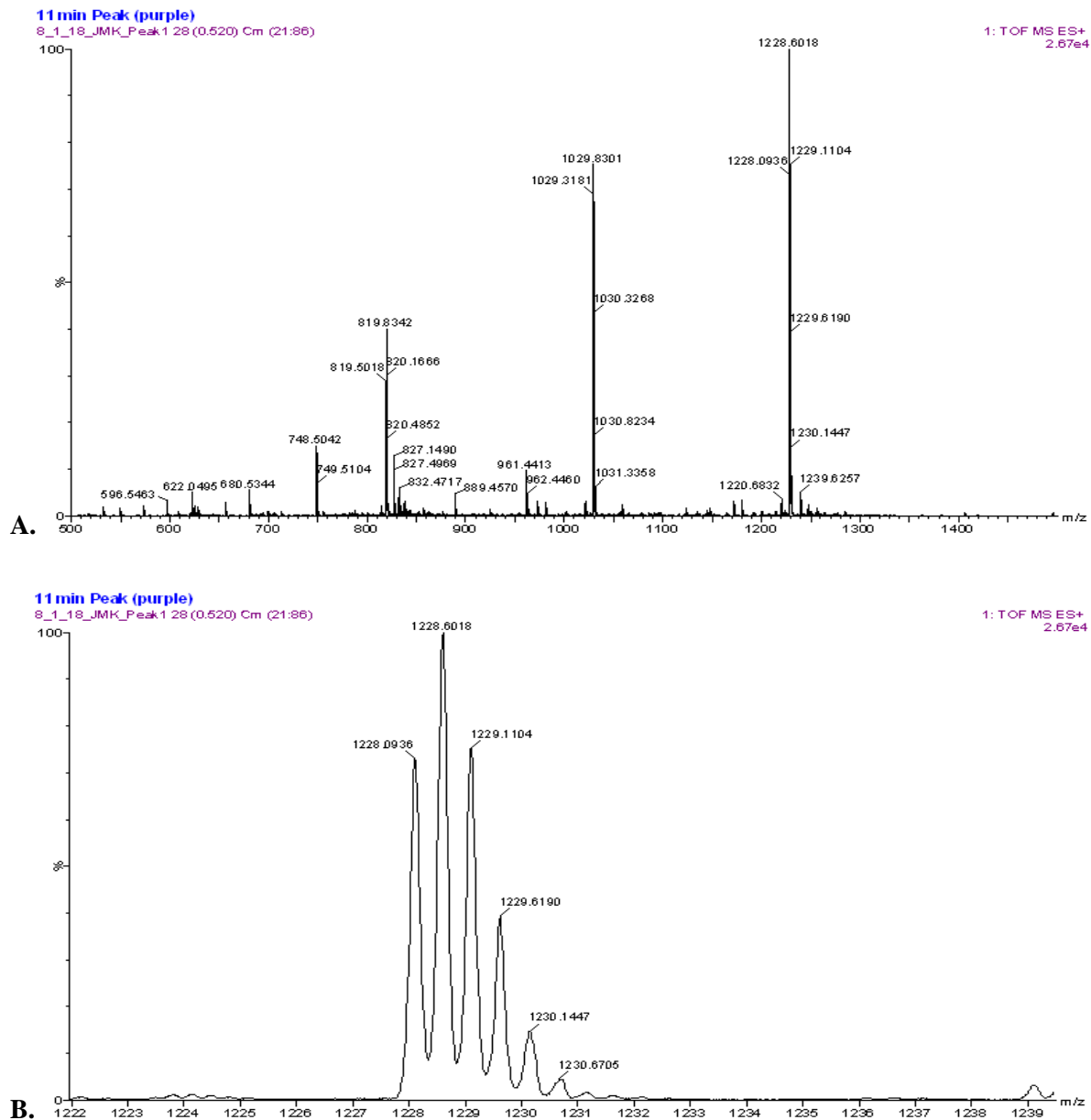


**Figure 2.24:** Mass spectrometry of Pyr(3)-KSar<sub>3</sub>K. A.) Full collected spectrum. B.) Expansion of the region at ~ 1228 amu indicative of the desired peptide. Calculated for  $(M+2H)^{2+}$   $m/z = 1228.62$  amu.

## 2.5 Circular dichroism studies

### 2.5.1: Determination of secondary structure

Each system, following verification by mass spectrometry, was analyzed using a Jasco CD Spectrometer to determine the triple helicity and thermal stability in a pH 7.4, 0.10 M phosphate buffered saline (PBS) solution. Samples were dissolved in buffer to a concentration of approximately 0.2 mM and allowed to stand overnight at 4 °C in the dark to equilibrate before measurement. Spectra were acquired at 20 °C (293.15 K) measuring the differential absorbance from 190 – 240 nm. A local maximum at ~ 224 nm in the CD spectrum indicative of a polyproline helix was utilized to quantify collagen secondary structure; loss of intensity of this peak during denaturation studies was taken as evidence for unfolding. Additionally, deviations in spectra from the baseline Ac-KK spectrum were used to qualitatively indicate differences in secondary structure through further modifications, i.e. the incorporation of pyrene.<sup>39</sup>

### 2.5.2: Thermal denaturation experiments

Following determination of a “collagen like” secondary structure for each system, the systems were subjected to thermal denaturation studies in order to determine the unwinding temperature ( $T_m$ ) of each system. Systems were heated from 10 – 60 °C at 12 °C/hour, measuring the change in ellipticity at 224 nm. It is important to note that the Pyr(3)AK system was measured from 10 – 80 °C, as full thermal denaturation had not occurred by 60 °C and therefore the resultant  $T_m$  values to this temperature were inaccurate. All thermal denaturation experiments were performed in triplicate to ensure repeatability. Thermally denatured peptide was not reused for additional CD thermal denaturation experiments to ensure no biases were introduced by re-use.

Following measurement, the thermal denaturation data were fitted to a two-state model as described by previous studies, where  $X_n$  is the fraction of the native folding state at temperature  $T$ , and  $T_m$  is the melting temperature of the peptide.<sup>39</sup>

$$X_n = 1/[1 + \exp\left(-\Delta H^\circ \frac{1-\frac{T}{T_m}}{RT}\right)] \quad (1)$$

**Equation 2.1:** Thermal unfolding equation

This equation allowed for the determination of melting temperature values as well as enthalpies of unfolding ( $\Delta H$ ). Thermal denaturation data were also used to support qualitative CD spectral measurements, as cooperative unfolding of a system is indicative of triple helical denaturation and in turn, the identity of the species as triple helical collagen.

## 2.6 Fluorescence studies

### 2.6.1: Fluorescence spectra collection

Fluorescence experiments on each pyrene containing peptide were performed on a Photon Technologies International (PTI) fluorometer. Emission data were acquired from 370-600 nm for each system and concentration unless otherwise noted. A point on the shoulder of pyrene's absorbance spectrum (365 nm) was used as the excitation wavelength, as at that wavelength all sample solutions had optical density < 0.1. This allowed higher concentrations than are typically used in fluorescence studies to be tested. All measurements were done with an integration time of 0.25 seconds, two averages, and a slit width of 1 mm. PBS was used as the solvent for each measurement, and a 1.0 cm quartz cuvette was used for sample collection.

For the purposes of determining triple helicity via fluorescence, the pyrene excimer was examined. Loss of excimer character in the fluorescence spectra was attributed to a decrease in triple helicity, while any increase in excimer was attributed to increased triple helical character. After inspection of several emission scans, 428 – 429 nm was chosen as the cutoff for excimer character for the purposes of peak integration, where the peak area at 428 nm and below was attributed to monomer

fluorescence and any peak intensity over 429 nm was attributed to triple helix or some other type of aggregation.

It is hypothesized that presence of excimer fluorescence will be indicative of triple helix formation due to the distance limit of stacking interactions.<sup>32</sup> Loss of that excimer fluorescence due to the changing of a variable should then be indicative of unwinding of the triple helix.

### **2.6.2: Concentration dependent studies and folding kinetics**

In order to determine the effective concentration to perform fluorescence experiments on triple helical collagen, several studies were performed on pyrene containing systems to determine the effect of concentration on excimer intensity. The integrated intensity of excimer fluorescence was compared to monomer fluorescence over a range of concentrations from ~ 5 – 55  $\mu\text{M}$ . These studies were performed through the use of a series of separate solutions brought to known concentrations from a stock solution of ~ 0.6 mM. PBS buffer (2.00 mL) was added to each of ten vials, with aliquots of stock peptide solution added in volumes ranging from 20 – 200  $\mu\text{L}$  using an appropriate pipettor. These solutions were then left overnight in a refrigerator at 4  $^{\circ}\text{C}$  to equilibrate before measurement. Initial attempts using a simple titration of stock peptide solution followed by data acquisition did not allow adequate time for equilibration to occur between measurements. This determination was made following a kinetic experiment that utilized 30  $\mu\text{M}$  solutions of Pyr(3)-KA. Two solutions were made of this peptide solution, one being allowed to equilibrate overnight at 4  $^{\circ}\text{C}$  with the other heated beyond the determined CD melting temperature to 50  $^{\circ}\text{C}$  for 20 minutes prior to measurement. Both solutions were then analyzed by fluorescence spectroscopy at 15 min time intervals to measure growth or loss of integrated excimer intensity. The results were fitted to the equation described in the next section (Equation 2.2). This equation allowed for the determination of both rate constants ( $k$ ) for folding and unfolding of the peptide in question as well as a half-life of folding ( $t_{1/2}$ ). The results of this study necessitated the method for

concentration dependent measurements described above, as peptides were found to take hours before reaching equilibrium.

$$\alpha = t / \left[ \frac{1}{k_1 c_0} + \frac{nt}{2} \right] \quad (2)$$

**Equation 2.2:** Refolding kinetics equation.<sup>38</sup>

Here,  $\alpha$  is the fraction folded at time  $t$ ,  $k_1$  is the rate constant,  $c_0$  is the initial concentration, and  $n$  is the order of the reaction. The value for  $t_{1/2}$  can be interpolated from the results of the equation fit to a set of data for an estimated reaction order. For rate of unfolding, the inverse of the excimer/monomer ratio was used as the y-axis in order to fit the data with the equation.

### 2.6.3: Thermal denaturation analyzed by fluorescence

Thermal denaturation experiments were performed using an attached water bath to modulate the temperature. Due to loss of heat between the external water bath and the cuvette containing the peptide solution, an offset equation was first determined by comparing the actual temperature in a cuvette with the set temperature on the water bath in order to ensure the validity of temperature variables. This was done via manually determining the temperature in a water filled cuvette housed in the cell holder of the fluorometer over a temperature range using a thermometer. The results were fitted to a graph finding an offset equation of:

$$T = 0.87(T_o) + 3.1 \quad (3)$$

**Equation 2.3:** Water bath offset equation.  $T$  represents the actual temperature in the cuvette with  $T_o$  being the set temperature on the attached water bath.

Solutions used for thermal denaturation experiments were set to 50  $\mu$ M in PBS in order to promote triple helical formation. Studies on less concentrated solutions suggested that at concentrations

below  $\sim 30 \mu\text{M}$  systems were not triple helical as judged by the absence of excimer formation. Fluorescence spectra were taken at  $5^\circ\text{C}$  increments from  $10 - 60^\circ\text{C}$  and the resulting data was fit to the same equation used to fit CD melting curves.<sup>38</sup> Monomer fluorescence was determined to be calculated from  $370 - 428 \text{ nm}$  and excimer fluorescence from  $429 - 600 \text{ nm}$ . These cutoffs correspond to an iso-emissive point found in the spectra of temperature dependent studies of Pyr(3)-KA. The integrated intensity of the monomer region of the graph was set as ratios between zero and one in order to fit equation (2), with zero being the least intense measurement and one being the most intense. This decision was made due to the lack of consistency between fluorescence in the excimer region between systems, as fitting the data with this region yielded results that were highly suspect. Fitting in this manner yielded “fraction unfolded” curves. All thermal denaturation studies via fluorescence were performed in duplicate.

## Chapter 3: Results of circular dichroism and fluorescence experiments

### 3.1 Collagen spectral data

Circular dichroism spectroscopy was used to probe the triple helicity of each system. Spectral results are shown in the following section of both individual spectra and overlaid spectra.

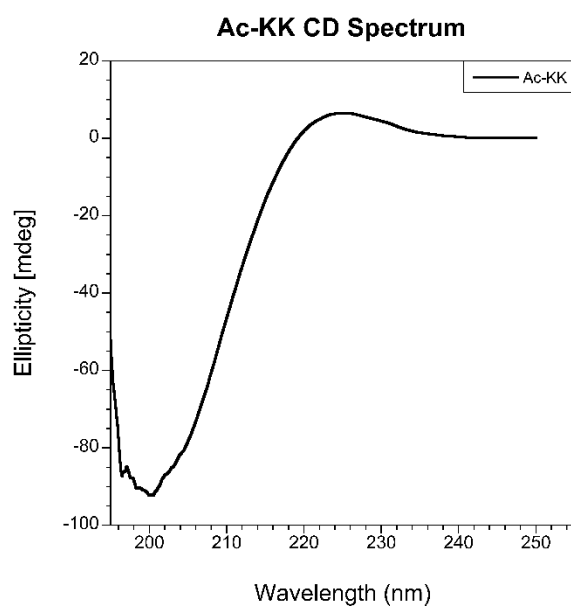


**Figure 3.1:** CD spectrum of the Ac-KK system. Spectrum displays characteristic  $\lambda_{\max}$  of  $\sim 224$  nm indicative of triple helical structure.



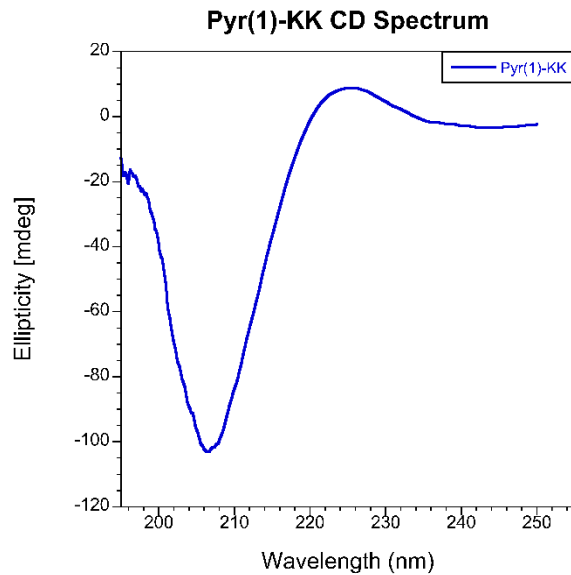


**Figure 3.2:** CD spectrum of the Pyr(1)-KK system. Spectrum displays characteristic  $\lambda_{\text{max}}$  of  $\sim 224$  nm indicative of triple helical structure.

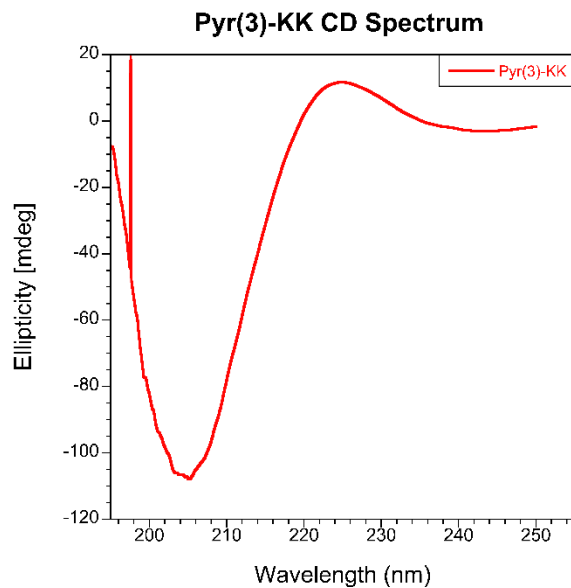


**Figure 3.3:** CD spectrum of the Pyr(3)-KK system. Spectrum displays characteristic  $\lambda_{\text{max}}$  of  $\sim 224$  nm indicative of triple helical structure.

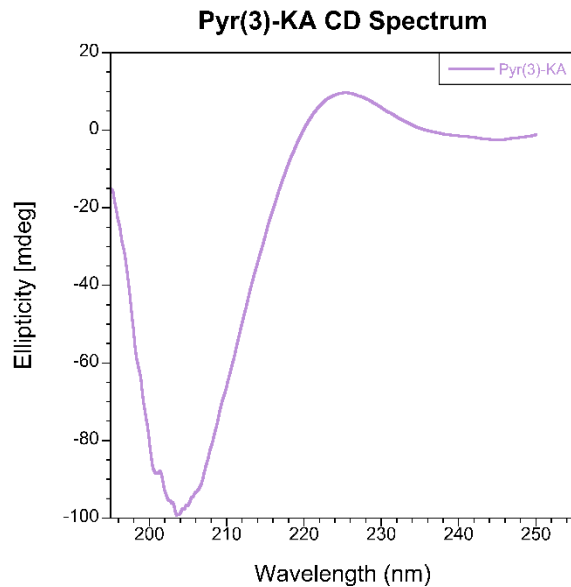


**Figure 3.4:** CD spectrum of the Pyr(3)-KA system. Spectrum displays characteristic  $\lambda_{\text{max}}$  of  $\sim 224$  nm indicative of triple helical structure.

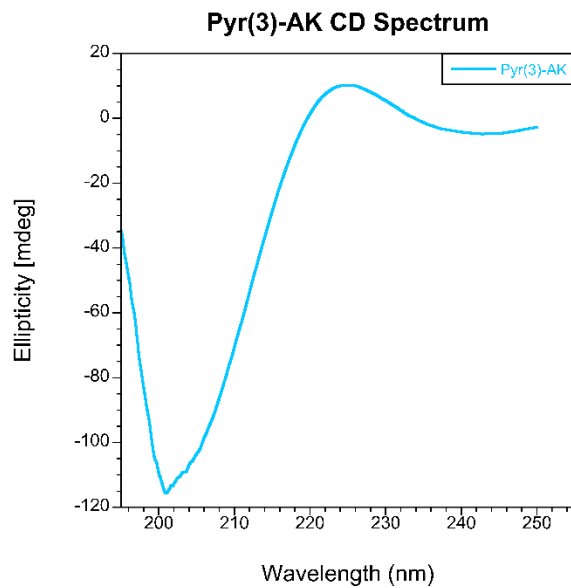


**Figure 3.5:** CD spectrum of the Pyr(3)-AK system. Spectrum displays characteristic  $\lambda_{\text{max}}$  of  $\sim 224$  nm indicative of triple helical structure.

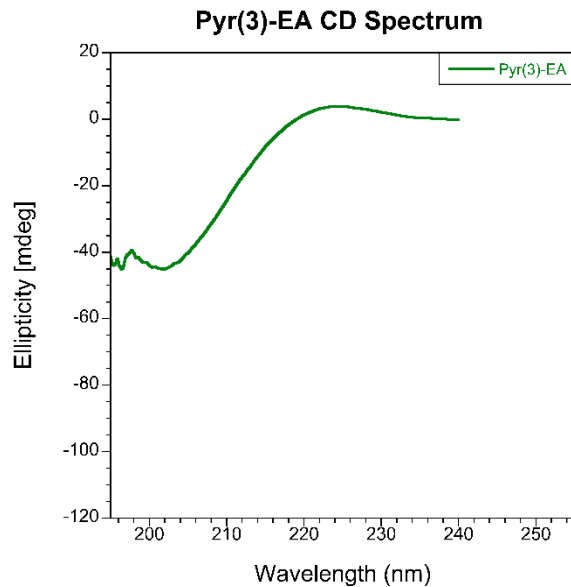


**Figure 3.6:** CD spectrum of the Pyr(3)-EA system. The maximum absorbance is slightly blue-shifted away from ~224 nm. In addition, the signal at ~ 200 nm is less intense than the other peptides in this study.

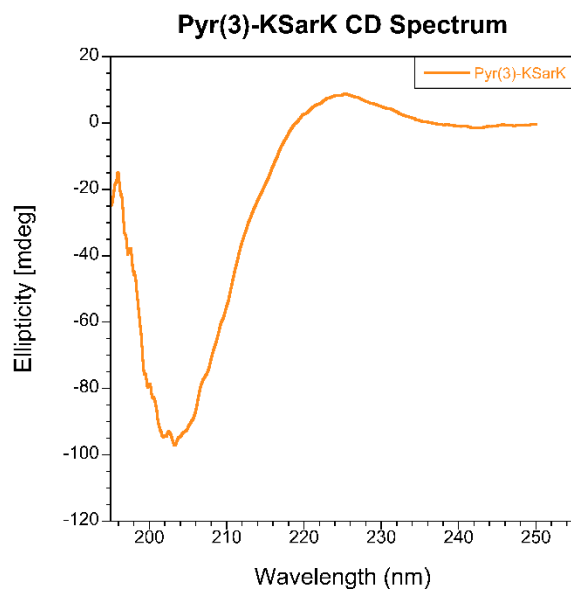


**Figure 3.7:** CD spectrum of the Pyr(3)-KSarK system. Spectrum displays characteristic  $\lambda_{\text{max}}$  of ~224 nm indicative of triple helical structure.

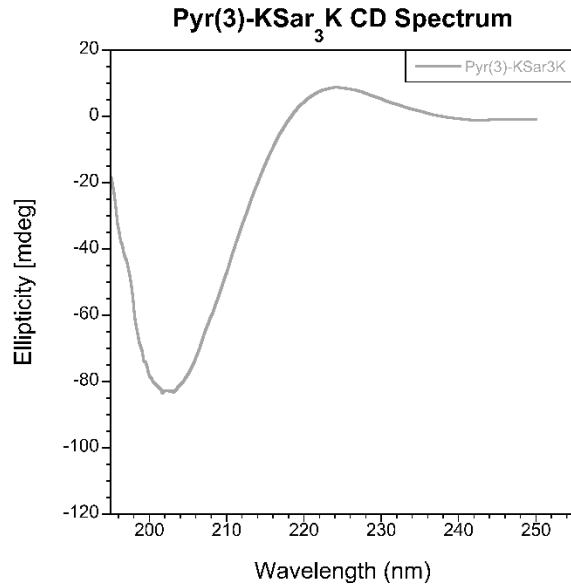


**Figure 3.8:** CD spectrum of the Pyr(3)-KSar<sub>3</sub>K system. Spectrum displays a slightly blue shifted  $\lambda_{\max}$  of ~222 nm possibly indicating some structure other than a triple helix.

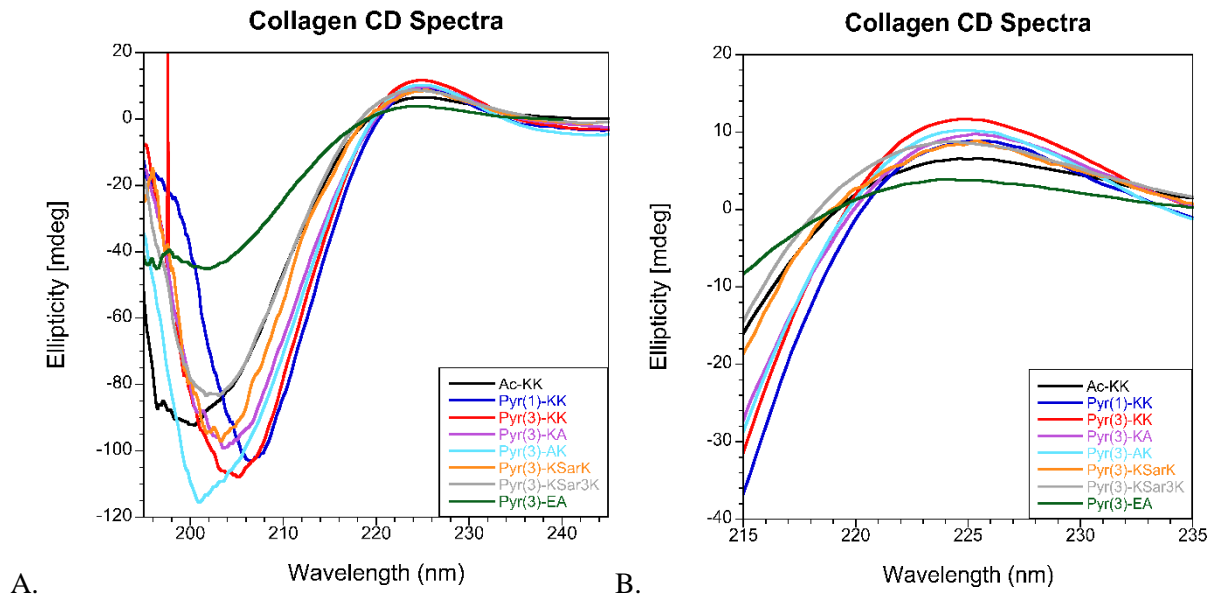


**Figure 3.9:** Overlaid CD Spectra of each measured collagen analogue. A.) Full spectra of each show perturbation of collagen structure with various modifications to the Ac-KK control species. B.) Expanded view highlights blue shifts in the Pyr(3)-KSar<sub>3</sub>K and the Pyr(3)-EA systems.

### 3.2 Thermal denaturation experiments analyzed by CD spectroscopy

Thermal denaturation experiments using CD were performed using the method described in Chapter 2, with data fit to a two-state equation.<sup>39</sup> The following are the results.

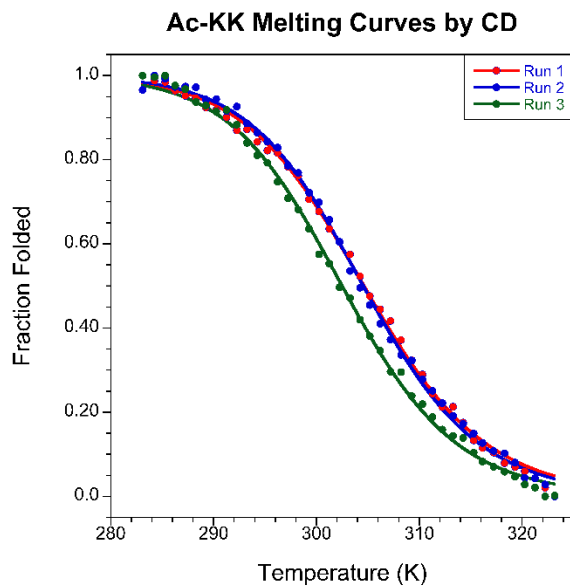


**Figure 3.10:** Thermal denaturation studies of Ac-KK. Each trial is shown to indicate repeatability.

Thermodynamic parameters can be found in Table 3.1.

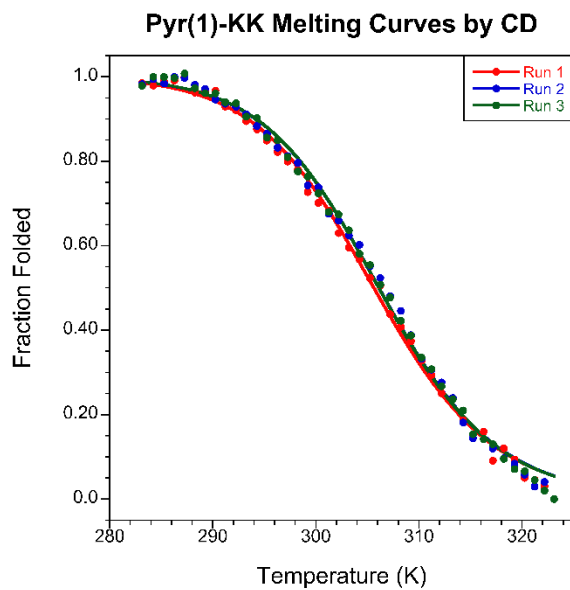


**Figure 3.11:** Thermal denaturation studies of Pyr(1)-KK. Each trial is shown to indicate repeatability.

Thermodynamic parameters can be found in Table 3.1.

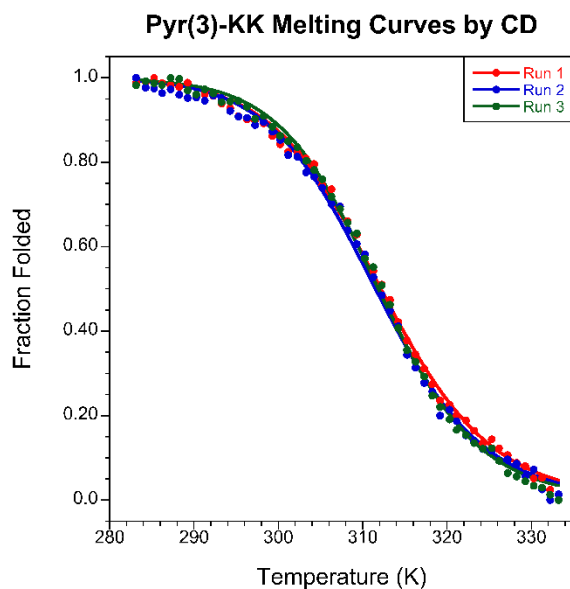


**Figure 3.12:** Thermal denaturation studies of Pyr(3)-KK. Each trial is shown to indicate repeatability.

Thermodynamic parameters can be found in Table 3.1.

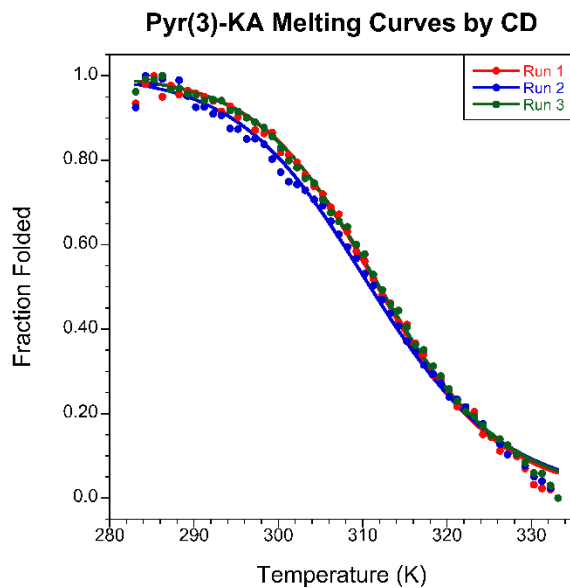


**Figure 3.13:** Thermal denaturation studies of Pyr(3)-KA. Each trial is shown to indicate repeatability.

Thermodynamic parameters can be found in Table 3.1.

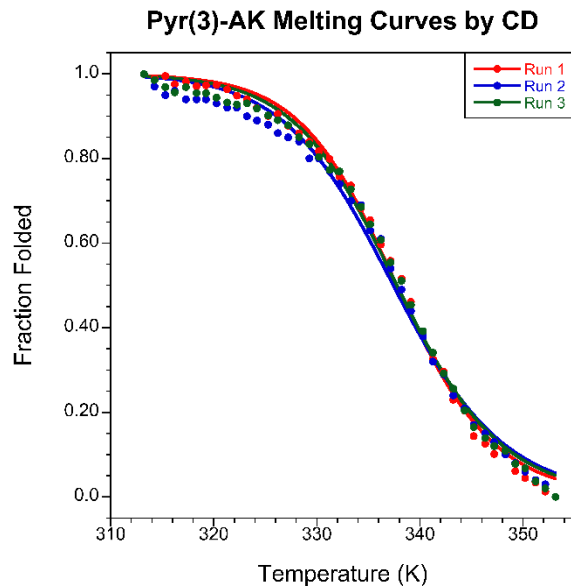


**Figure 3.14:** Thermal denaturation studies of Pyr(3)-AK. Each trial is shown to indicate repeatability. Thermodynamic parameters can be found in Table 3.1.

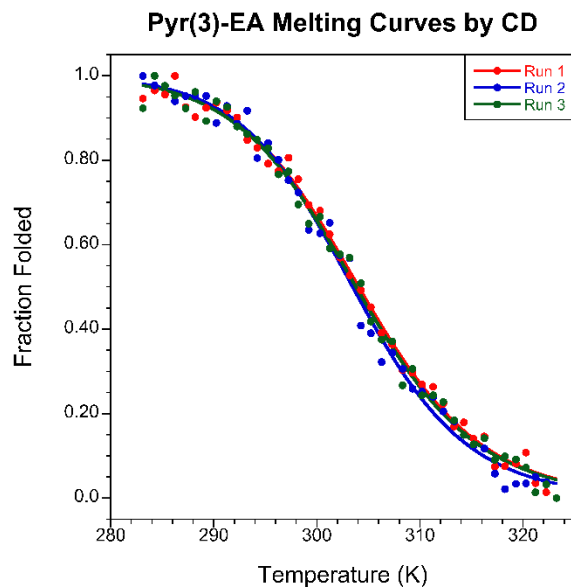


**Figure 3.15:** Thermal denaturation studies of Pyr(3)-EA. Each trial is shown to indicate repeatability. Thermodynamic parameters can be found in Table 3.1.

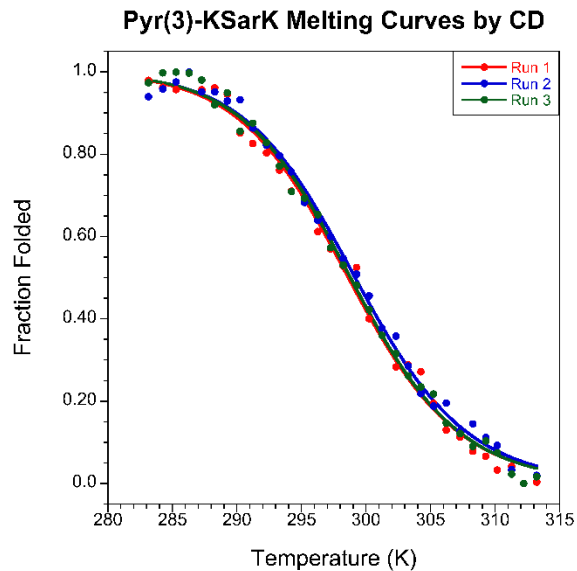


**Figure 3.16:** Thermal denaturation studies of Pyr(3)-KSarK. Each trial is shown to indicate repeatability.

Thermodynamic parameters can be found in Table 3.1.

System	Average $T_m$ °C	Average $\Delta H$ (kcal/mol)
Ac-KK	$30.9 \pm 1.3$	$32.4 \pm 0.9$
Pyr(1)-KK	$32.8 \pm 0.3$	$32.4 \pm 0.5$
Pyr(3)-KK	$38.7 \pm 0.3$	$30.7 \pm 1.5$
Pyr(3)-KA	$38.4 \pm 0.6$	$25.8 \pm 1.3$
Pyr(3)-AK	$64.5 \pm 0.2$	$45.2 \pm 2.6$
Pyr(3)-EA	$30.6 \pm 0.3$	$31.7 \pm 1.3$
Pyr(3)-KSarK	$25.7 \pm 0.3$	$41.6 \pm 0.4$
Pyr(3)-KSar <sub>3</sub> K	N.A.	N.A.

**Table 3.1: Combined thermal denaturation data via circular dichroism.** Temperatures and unfolding enthalpies shown are averages of the three trials with the standard deviations shown.



### 3.3: Exploration into concentration effects of fluorescence

Fluorescence studies posed more of a challenge than originally anticipated due to the behavior of collagen systems at the relatively low concentrations that are more typical for emission spectroscopy. Therefore, before thermal denaturation experiments were completed, several experiments were performed in order to ensure that the conditions for thermal denaturation would yield valid results. These results are highlighted in the following section.

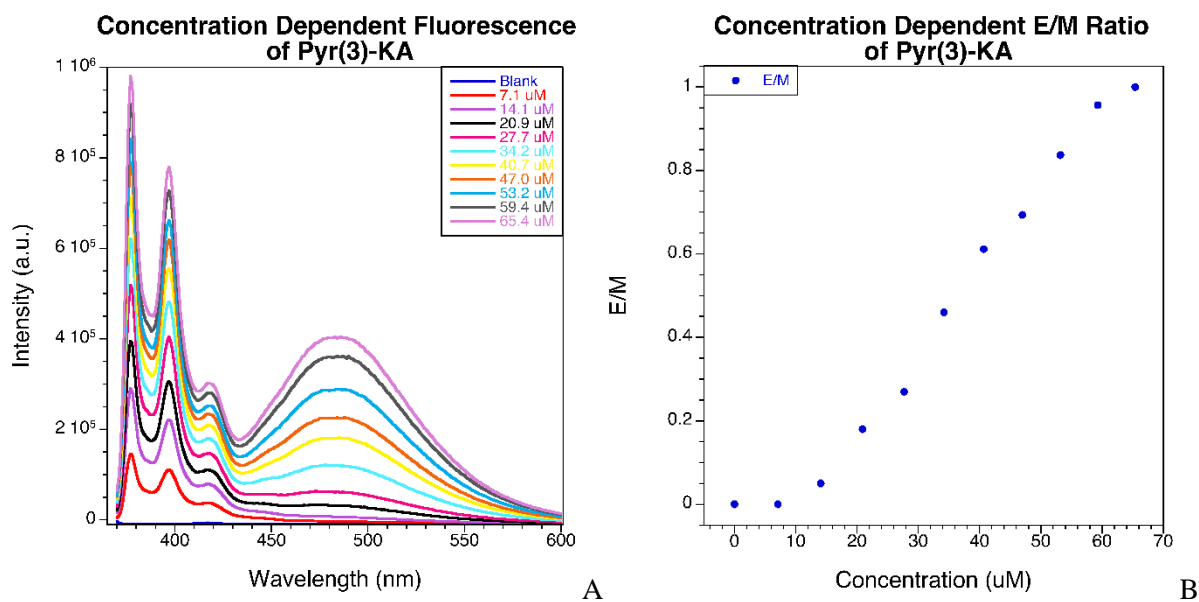


**Figure 3.17:** Concentration dependence of Pyr(3)-KA. A.) Several solutions of known concentration were studied to determine the effect of concentration on excimer fluorescence. B.) An increase in the ratio of integrated intensity of excimer fluorescence (429 – 600 nm) compared to the intensity of the monomer (370 – 428 nm) can be observed. It follows an approximately linear relationship within the concentration range 10 – 60  $\mu\text{M}$ .

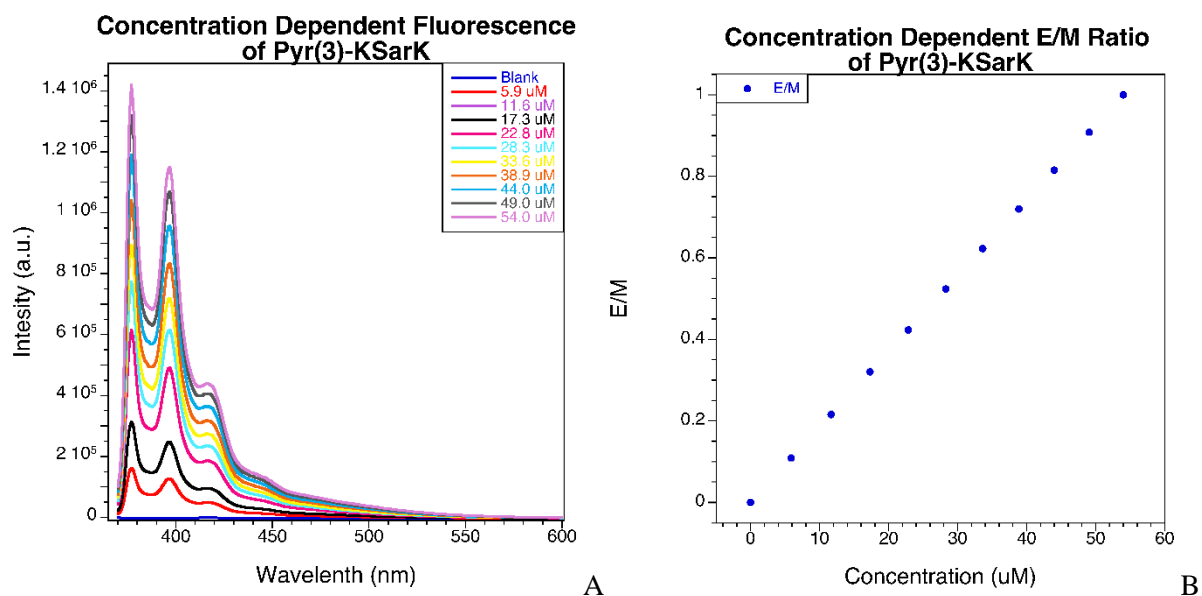


**Figure 3.18:** Concentration dependence of Pyr(3)-KSarK. A.) Several solutions of known concentration were studied to determine the effect of concentration on excimer fluorescence. B.) An increase in the ratio of integrated intensity of excimer fluorescence (429 – 600 nm) compared to the intensity of the monomer (370 – 428 nm) can be observed. It follows a strictly linear relationship across all concentrations.

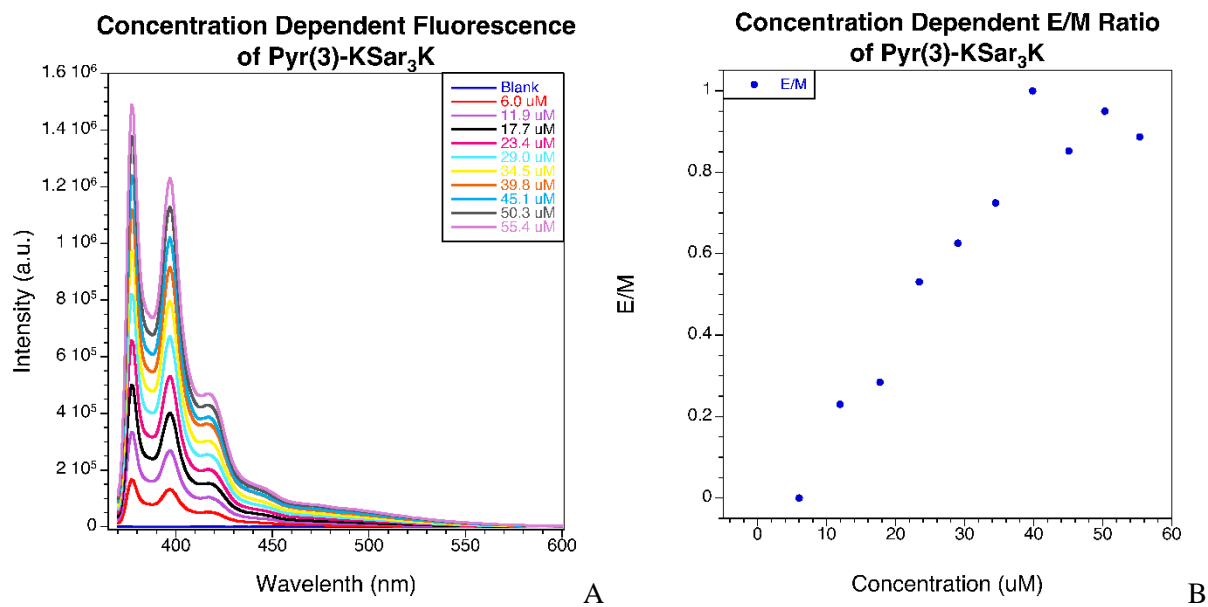


**Figure 3.19:** Concentration dependence of Pyr(3)-KSar<sub>3</sub>K. A.) Several solutions of known concentration were studied to determine the effect of concentration on excimer fluorescence. B.) An increase in the ratio of integrated intensity of excimer fluorescence (429 – 600 nm) to the intensity of the monomer (370 – 428 nm) can be observed, however, there is no well-defined linear relationship compared to triple helical systems.

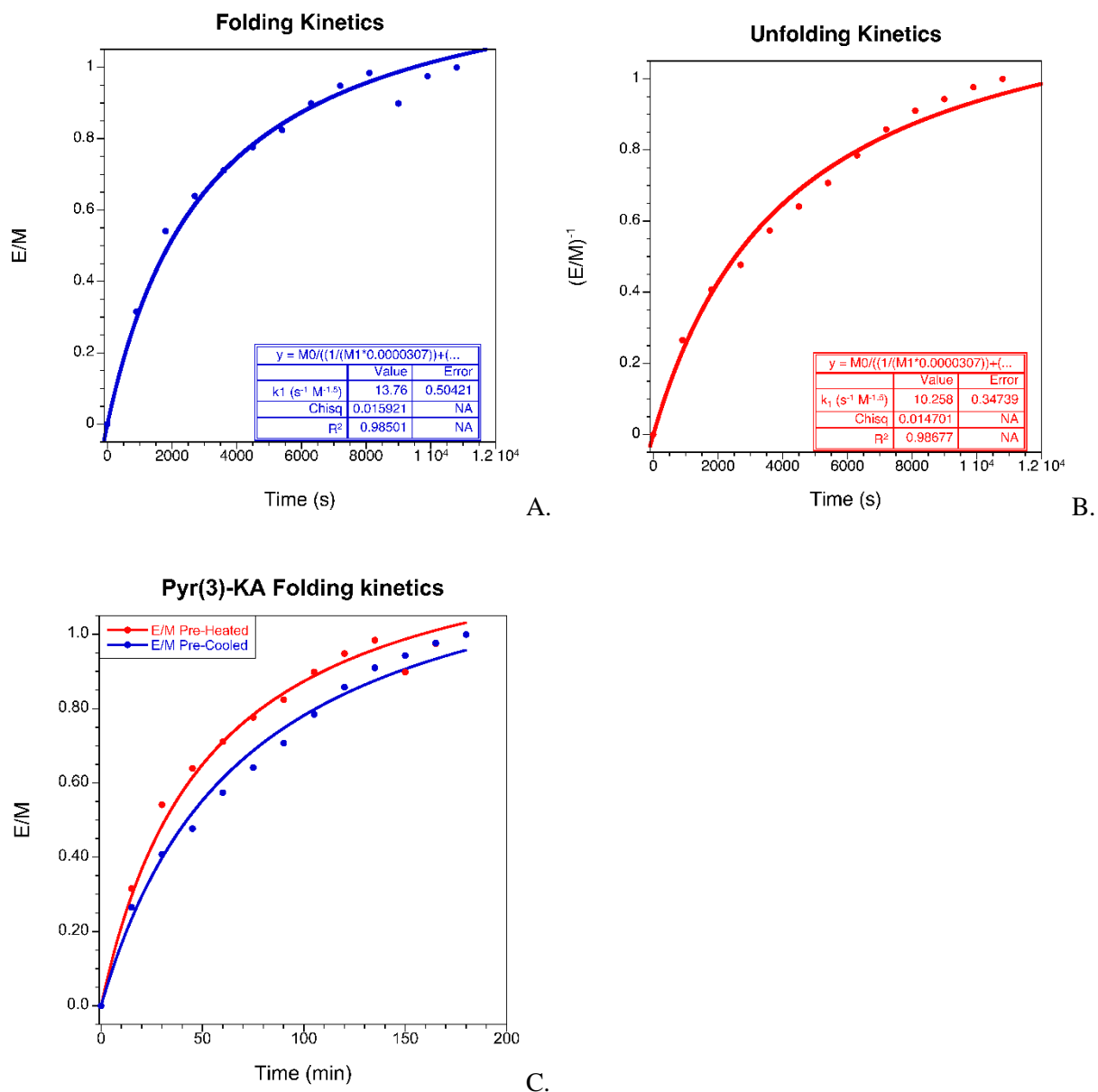


**Figure 3.20:** Kinetics of folding/unfolding for Pyr(3)-KA. A 30  $\mu\text{M}$  solution of Pyr(3)-KA was either A.) pre-heated allowing for determination of refolding kinetics, or B.) Pre-cooled, allowing for determination of unfolding kinetics at room temperature. Half-life ( $t_{1/2}$ ) values were extracted from the fit line. C.) Depicts both folding and unfolding curves, with folding appearing to be a faster process.

### 3.4: Thermal denaturation experiments analyzed by fluorescence spectroscopy

To determine the applicability of utilizing fluorescence to determine the triple helicity of collagen model systems, thermal denaturation experiments were performed in a manner similar to the previously described circular dichroism experiments. Following preliminary thermal denaturation experiments at low  $< 5 \mu\text{M}$  concentrations (Figure 3.21), concentration dependent fluorescence studies highlighted in section 3.3 were conducted to ensure that solutions were concentrated enough for a significant amount of aggregation to occur. A concentration of  $\sim 50 \mu\text{M}$  was chosen as the most optimal for performing thermal denaturation studies via fluorescence spectroscopy. The results of these studies are highlighted in the following section.

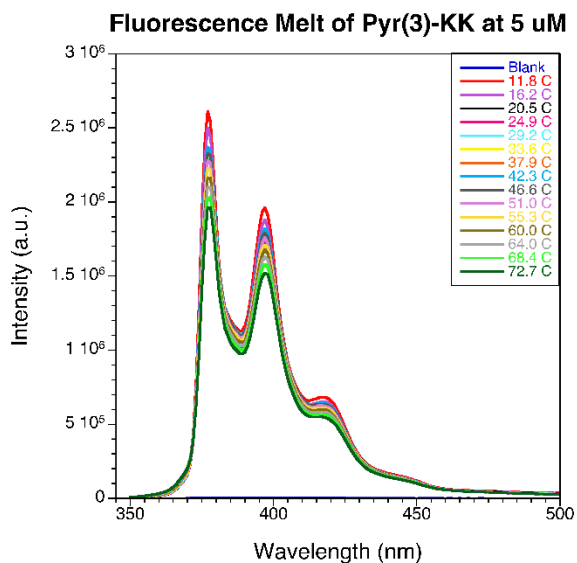


**Figure 3.21:** Fluorescence melt of Pyr(3)-KK at low concentration. At concentrations of  $\sim 5 \mu\text{M}$  Pyr(3)-KK does not appear to be triple helical, as judged by absence of excimer fluorescence. Due to this, concentration studies described in the previous section were conducted to ensure that solutions were concentrated enough for a significant amount of aggregation to occur.

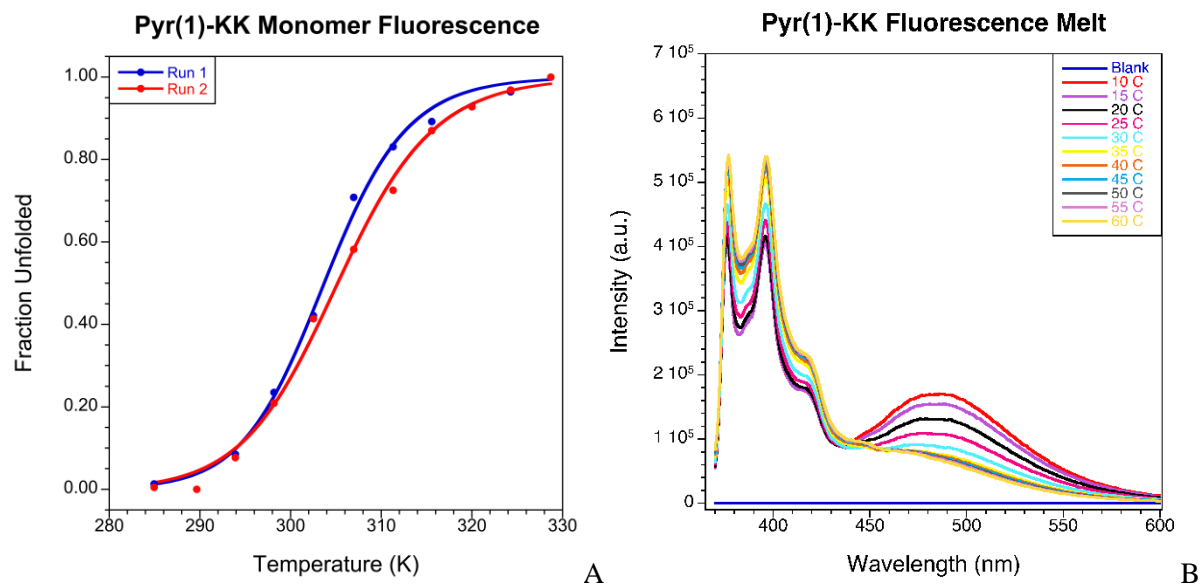


**Figure 3.22:** Fluorescence response of Pyr(1)-KK as a function of temperature. A.) Change in the normalized monomer integrated intensity, a proxy for the fraction of peptide in a folded state. B.) Raw spectra.

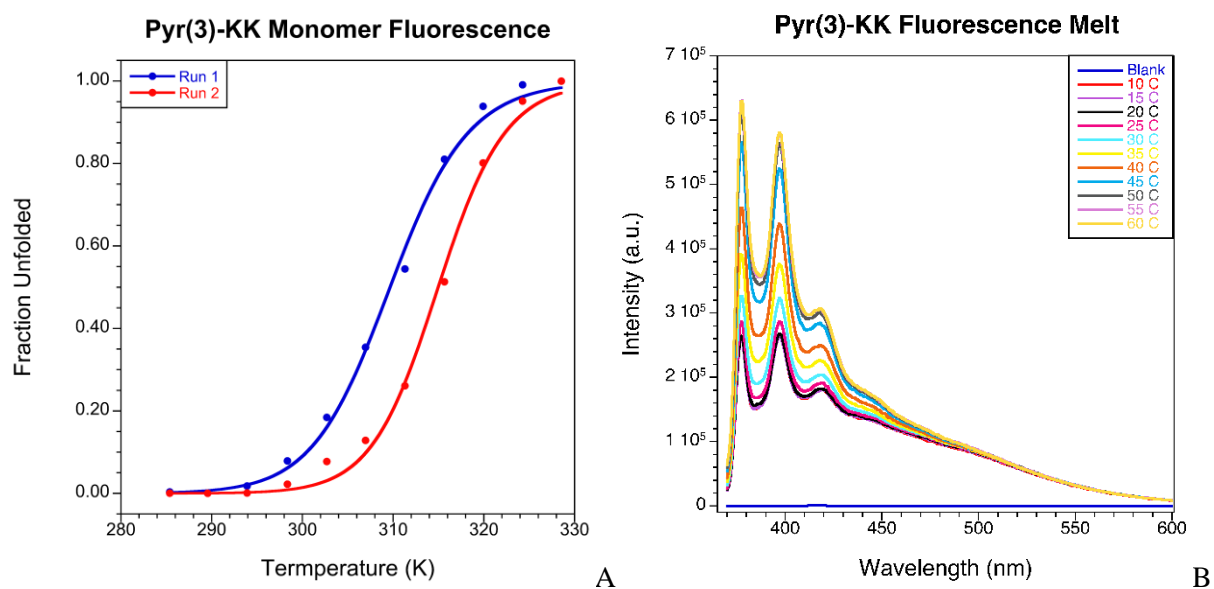


**Figure 3.23:** Fluorescence response of Pyr(3)-KK as a function of temperature. A.) Change in the normalized monomer integrated intensity, a proxy for the fraction of peptide in a folded state. B.) Raw spectra.

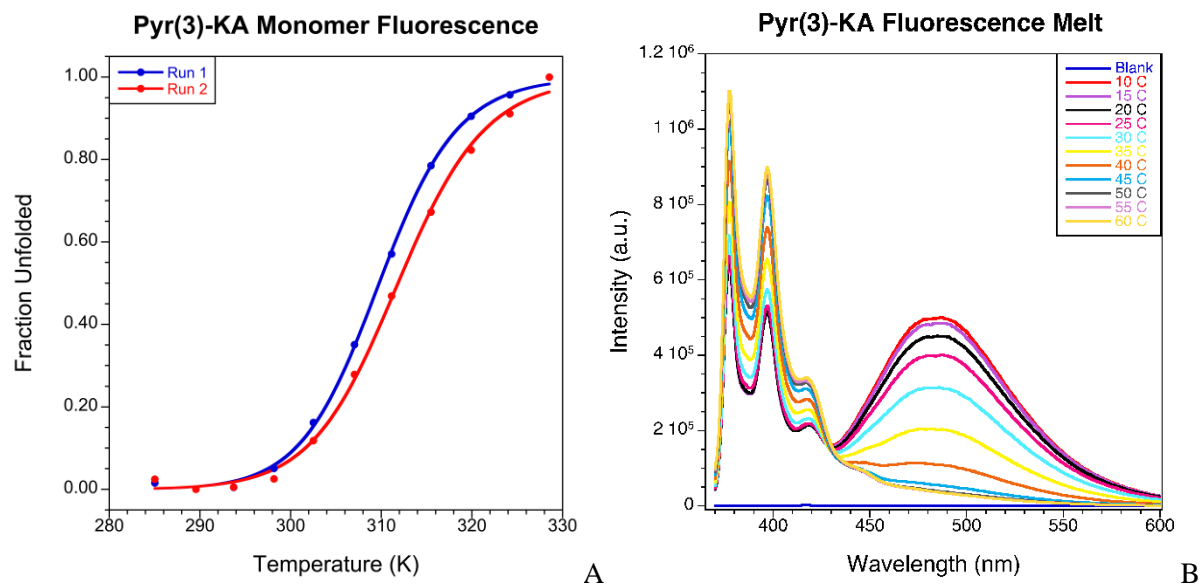


**Figure 3.24:** Fluorescence response of Pyr(3)-KA as a function of temperature. A.) Change in the normalized monomer integrated intensity ratio, a proxy for the fraction of peptide in a folded state. B.) Raw spectra.

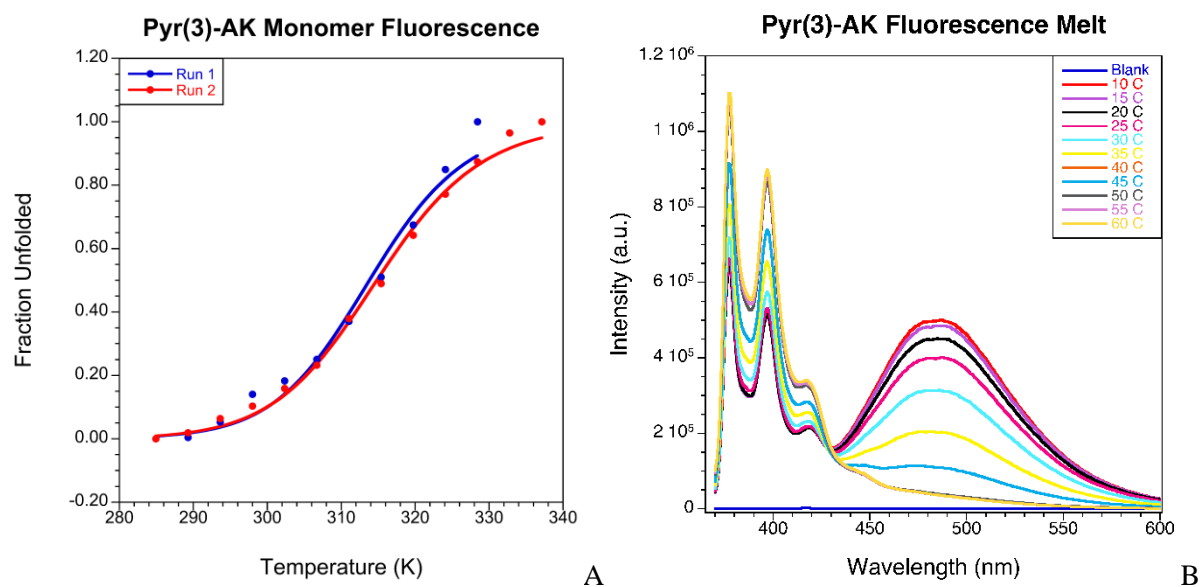


**Figure 3.25:** Fluorescence response of Pyr(3)-AK as a function of temperature. A.) Change in the normalized monomer integrated intensity, a proxy for the fraction of peptide in a folded state. B.) Raw spectra.

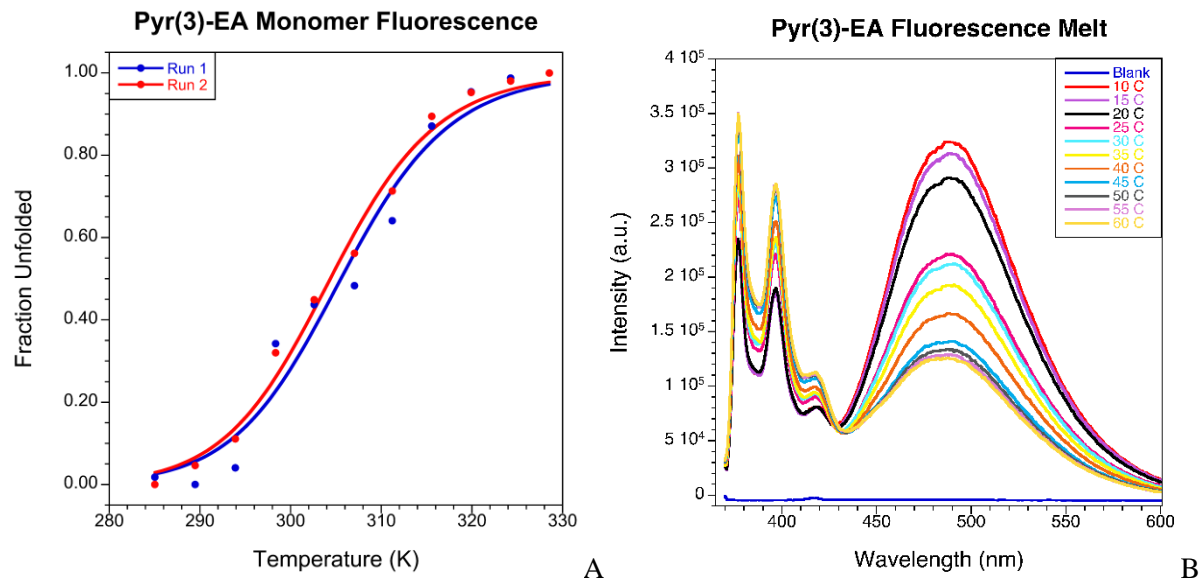


**Figure 3.26:** Fluorescence response of Pyr(3)-EA as a function of temperature. A.) Change in the normalized monomer integrated intensity, a proxy for the fraction of peptide in a folded state. B.) Raw spectra.

System	Average $T_m$ °C	Average $\Delta H$ (kcal/mol)
Ac-KK	N.A.	N.A.
Pyr(1)-KK	31.3	37.6
Pyr(3)-KK	39.2	48.6
Pyr(3)KA	37.7	42.0
Pyr(3)-AK	41.3	28.8
Pyr(3)-EA	31.8	31.1
Pyr(3)-KSarK	N.A.	N.A.
Pyr(3)-KSar <sub>3</sub> K	N.A.	N.A.

**Table 3.2: Combined thermal denaturation data via fluorescence:** Temperatures and unfolding enthalpies shown are averages of the two trials.



## Chapter 4: Discussion

### 4.1 Collagen spectral data analysis

Circular dichroism (CD) spectrometry was used to probe the higher-order structure of synthesized collagen systems. The data are consistent with triple helices for each of the synthesized peptides with the exception of the Pyr(3)-KSar<sub>3</sub>K system. Interestingly, the Pyr(3)-KSarK system is able to adopt a collagen *like* structure according to the CD results, however, its blue shift in the absorbance maximum suggests that it is not a typical triple helix. Literature data has indicated that in the case of an aza-glycine substituted system, distortion of the central hydrogen bond appears to have a great effect on the overall stability. In the azGly system synthesized by Chenoweth et al. increasing the number of hydrogen bond donors in the central position appeared to have the most stabilizing affect compared to increases in stability at the termini. Similarly, previous work has shown that distortions in the hydrogen bonding network in the central position of a triple helix has a greater destabilizing affect than distortions elsewhere.<sup>29</sup> Disruption at this site in the Pyr(3)-KSarK system should not yield a triple helix, yet a collagen like structure is observed. Nonetheless, the addition of pyrene onto the N-termini of triple helical systems did not appear to significantly disrupt formation of collagen like triple helical structures.

The Pyr(3)-EA system additionally displayed a CD spectrum that made the determination of triple helicity difficult due to the low intensities of the maximal and minimal absorbances in the spectrum. These results initially led us to suspect that monomeric collagen was being detected rather than the triple helical form. However, the system did display cooperative unwinding, although with a low melting temperature when subjected to a CD melting study, implying that the system was in fact structured (though not necessarily trimeric). This instability in the Pyr(3)-EA system could exist due to the repelling force of anionic glutamic acid groups in between the pyrene and collagen core with the pyrene systems themselves. The large aromatic cloud of pyrene has significant electron density that would seek to repel Glu sidechains and may destabilize the N-termini.

Additionally, in all cases where pyrene was incorporated, the spectra were distorted compared to the spectra obtained for Ac-KK (Figure 3.9). These distortions are most likely due to the attractive and repulsive forces of pyrene residues, and support the idea that addition of these residues does somewhat perturb the triple helix compared to control systems. The degree to which this distortion impacts the quaternary structure of collagen, however, is not determinable through the spectroscopic techniques utilized in this research.

#### **4.2 Discussion of thermal denaturation studies analyzed by CD spectrometry**

Once it was determined that quaternary structure suggestive of a triple helix was present, each collagen system was subjected to thermal denaturation experiments to determine the melting temperature  $T_m$ , as well as the enthalpy of unfolding. These values were obtained from the two-state equation described in chapter 3 section 2 of this thesis.<sup>39</sup> From thermal denaturation studies, it was determined that introduction of a pyrene fluorescent probe onto the N-termini of a collagen system increases the melting point in all tested cases other than the Pyr(3)-EA system and the Pyr(3)-KSarK system. These two, however, had other variables contributing to the low thermal stability, and most likely would be more stable than hypothetical Ac-EA and Ac-KSarK systems. The addition of a pyrenebutyric acid “Pyr(3)” moiety in the last coupling step in a peptide synthesis yielded an increase in melting point of approximately 9 °C in a Pyr(3)-KK system compared to the Ac-KK control. This increase of melting temperature was only 4 °C when pyreneacetic acid “Pyr(1)” was used as the N-terminal anchor (as in the Pyr(1)-KK). This modest increase in  $T_m$  value for the short-linker compound may reflect the energetic cost that is associated with disrupting the folding of the triple helix in order to accommodate interactions between pyrenes. By comparison, the Pyr(3)-KK system positions the pyrene anchor far enough away from the triple helical core that flexing of the linker allows for the formation of stronger associations between the pyrene anchors without strongly distorting the hydrogen bonding core of the triple helix.

To investigate the directionality of unfolding in a collagen model peptide system, systematic

replacement of lysine was conducted in the formation of the two collagen model peptides: Pyr(3)-AK and Pyr(3)-KA. Lysine was initially added to the peptide both to increase solubility of the collagen system in aqueous buffer as well as to prevent aggregation of separate triple helical systems into some higher-order structure. Lysine, however, can be seen to be destabilizing to the collagen system when comparing the melting points of Ac-KK with melting points of shorter (POG)<sub>7</sub> systems.<sup>1</sup> The destabilizing effects of lysine at either the N- or C-terminal position can, however, provide some insight into directionality of collagen unfolding. When observing the Pyr(3)-AK system, the melting temperature is approximately 26 °C higher than Pyr(3)-KK, and 34 °C higher than Ac-KK. Pyr(3)-KA, in contrast, is not significantly different than Pyr(3)-KK with average melting points within 0.2 degrees of each other. These results imply strongly that the Ala substitution at the N-terminus of the collagen core is much more stabilizing than the Ala substitution at the C-terminus. This is consistent with helical unfolding starting from the N-terminus. If unfolding began from the C-terminus, a difference in melting temperature would be expected for Lys-to-Ala substitution. Additionally, the results indicate that the cationic N-terminal Lys residue may be interacting in some way with the pyrene unit(s). Cation –  $\pi$  interactions are much stronger than  $\pi$  –  $\pi$  interactions. For example, in the gas phase a cation –  $\pi$  interaction between methylammonium and benzene is ~ -19 kcal/mol, while a gas phase stacking interaction between two benzenes is only roughly -2 kcal/mol.<sup>39</sup> As such, the electrostatic interactions between the  $\pi$  systems of the pyrene and the lysine side chains may actually be destabilizing.

### **4.3 Discussion of concentration dependent pyrene fluorescence and kinetics studies**

Utilization of fluorophores as tools to determine the folding state of peptide systems at low concentrations proved to be more difficult than planned. Thermal denaturation experiments performed at low concentrations of < 5  $\mu$ M gave little to no evidence of triple helical formation according to the excimer fluorescence (Figure 3.21). This necessitated study of concentration effects on the folding state of collagen. These studies, while illuminating, failed to define an obvious “critical aggregation concentration” for any of the studied systems. Instead, a linear relationship between integrated excimer

intensity vs. integrated monomer intensity was discovered, showing that in the concentration range in question, a greater percentage of the total make-up of the solution existed as a triple helical aggregate at higher concentrations than at lower concentrations. This makes sense in principle, as at higher concentration, there is a higher likelihood for individual monomers of pyrene-containing peptides to be near each other in solution. Additionally, as excimer emission requires only two pyrene moieties to be in contact in solution, and not necessarily the three that would exist in a triple helical system, the increase in excimer fluorescence should increase with concentration regardless of triple helical formation. The Pyr(3)-KSar<sub>3</sub>K control, however, does not obey a well-defined linear relationship in excimer intensity over this concentration range (Figure 3.19) and appears to reach a plateau in excimer intensity vs. monomer intensity by roughly 30  $\mu$ M. This could indicate that no significant additional excimer may be formed, and that all increases in E/M ratios in other systems after this point in concentration are due to the head-to-head aggregation of pre-formed triple helices.

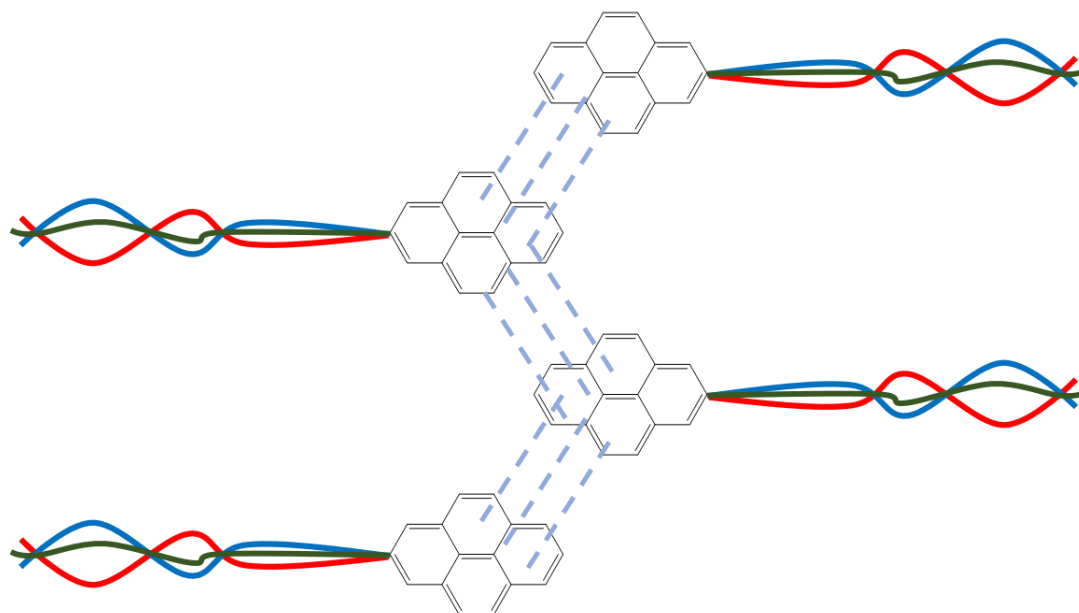


**Figure 4.1:** Head-to-Head aggregation of triple helices. Stacking interactions between adjacent helices may cause excimer not due to triple helical formation.

Folding kinetics of Pyr(3)-KA were studied to understand the affect of time on the folding/unfolding of collagen systems. Chenoweth et al. used CD to probe the reformation of helices over time after denaturation in their initial paper on aza-Gly.<sup>23</sup> Here, fluorescence was instead used to measure excimer intensity changes over time on a solution of  $\sim 30 \mu\text{M}$ . This solution was both pre-heated past a point of denaturation or pre-cooled to favor aggregation before fluorescence measurements were taken at room temperature over a time period of 180 minutes. These data allowed the determination of approximate rates of folding/unfolding for the Pyr(3)-KA system, but also allowed for the determination of the time at which half of the peptide population was folded for the systems,  $t_{1/2}$ . As the  $t_{1/2}$  was similar to the results of Chenoweth et al.<sup>23</sup> at 31.5 minutes compared to  $\sim 30$  minutes, with a rate constant of  $13.8 \text{ s}^{-1} \text{ M}^{-1.5}$  and  $10.3 \text{ s}^{-1} \text{ M}^{-1.5}$  for folding and unfolding respectively. The order of the reaction was found to be 1.5 according to fit given by equation (2). This may arise from using excimer intensity (which requires association of two species) as an indicator of the folding state. The incorporation of pyrene to the system does not appear to significantly alter the folding kinetics of the peptide when compared to literature, though this is a preliminary result. This information, did, however confirm that the equilibration period is slow for model systems.

#### **4.4 Discussion of thermal denaturation analyzed by fluorescence spectroscopy**

Each system was subjected to denaturation conditions using heat to determine the  $T_m$  and  $\Delta H$  of unfolding. The integrated intensities in the monomer and excimer regions over a temperature range from  $10 - 60 \text{ }^\circ\text{C}$  were recorded, and the normalized ratio of these values was calculated in order to determine an E/M ratio as a measure of the fraction folded. By these calculations, the  $T_m$  and  $\Delta H$  values for each system were determined. Several trends emerged.

First, the melting temperatures obtained by fluorescence spectroscopy appeared to follow a similar trend to the values obtained by circular dichroism. The Pyr(3)-EA system by this method was found to be comparable in melting temperature to the Pyr(1)-KK system. Akin to CD, the Pyr(3)-KK and Pyr(3)-KA systems had melting temperatures that were within approximately one degree of each other, further supporting the similarities between these collagenous systems. A stark difference, however, was in the Pyr(3)-AK system, which while having a higher melting temperature than that of the other systems, was much less stable than suggested by CD spectroscopy.

Second, there appears to be relatively little difference in the melting temperature values obtained by CD and that of those obtained by fluorescence, with the omission of the Pyr(3)-AK system. For all systems analyzed by fluorescence, the obtained melting temperatures were within approximately 1 °C from the values obtained by the traditional CD methodology. The slight variance in melting temperatures in the comparable systems is most likely due to the use of pyrene fluorescence as the factor being observed. This method is highly dependent on the degree of local fraying of the pyrene moiety rather than the bulk signal of the chiral (POG)<sub>7</sub> core as would occur in the use of CD. As stacking interactions necessitate the aromatic systems be within 3.4 – 3.8 angstroms, disruptions in the aromatic interactions do not require the helix unwind.<sup>30</sup> Due to this, it can be determined that the pyrene fluorescence gives insight into the degree of local fraying at the termini of a collagen system and is not necessarily measuring unfolding itself. The closeness of values between these fraying  $T_m$  values and the CD unfolding  $T_m$  values, however, does provide evidence that despite the specificity in what is being measured by fluorescence, the change in monomer fluorescence intensity can be used to approximate melting temperatures, even at concentrations that canonically would be out of the useful range of circular dichroism, as evidenced by the closeness in  $T_m$  values.

System	$T_m$ by CD (°C)	$T_m$ by Fluorescence (°C)	$\Delta T_m$ (°C)
Ac-KK	$30.9 \pm 1.3$	N.A.	N.A.
Pyr(1)-KK	$32.8 \pm 0.3$	31.3	- 2
Pyr(3)-KK	$38.7 \pm 0.3$	39.2	+ 1
Pyr(3)-KA	$38.4 \pm 0.6$	37.3	- 1
Pyr(3)-AK	$64.5 \pm 0.2$	41.3	- 23
Pyr(3)-EA	$30.6 \pm 0.3$	31.8	+ 1
Pyr(3)-KSarK	$25.7 \pm 0.3$	N.A.	N.A.
Pyr(3)-KSar <sub>3</sub> K	N.A.	N.A.	N.A.

**Table 4.1:** Difference between CD and Fluorescence  $T_m$  Values

The resulting enthalpy values obtained via fluorescence melting studies also illuminated an interesting trend. While melting temperatures of each system by the two different methods were similar, the enthalpy of unfolding values calculated from the fluorescence values were drastically different than those of CD. These data, found in Table 4.2, show that enthalpy values for each tagged system correlate well with the identity of the bracketing amino acids.

System	$\Delta H$ by CD (kcal/mol)	$\Delta H$ by Fluorescence (kcal/mol)	$\Delta \Delta H$ (kcal/mol)
Ac-KK	$32.4 \pm 0.9$	N.A.	N.A.
Pyr(1)-KK	$32.4 \pm 0.5$	37.6	+ 5
Pyr(3)-KK	$30.7 \pm 1.5$	48.6	+ 18
Pyr(3)-KA	$25.8 \pm 1.3$	42.0	+ 18

Pyr(3)-AK	45.2 ± 2.6	28.8	- 16
Pyr(3)-EA	31.7 ± 1.1	31.1	- 1
Pyr(3)-KSarK	41.6 ± 0.4	N.A.	N.A.
Pyr(3)-KSar <sub>3</sub> K	N.A.	N.A.	N.A.

**Table 4.2:** Difference between CD and Fluorescence  $\Delta H$  values

These values can give insight into the dynamics of the collagen systems at the termini compared to the system in bulk. For well-ordered helices, such as that of Pyr(3)-AK, the enthalpy of unfolding by CD is high due to the strength in the interactions of the three peptide strands. However, when fluorescence is used, the enthalpy of unfolding found is quite low. This difference can be thought of as a balance between the strength of the helix and the strength of the interacting pyrene moieties. For strongly interacting and well-ordered helices, there is less ability for the pyrene moieties to optimally approach in solution, thus giving rise to less strength in those interactions. This additionally provides an explanation for the difference in melting temperatures between the two methods for this system, as if the helix is indeed very ordered, then the fraying of the pyrenes on the termini of each peptide strand may require significantly less heat to disrupt than that of the underlying triple helix. For less-ordered helices, however, such as the Pyr(3)-KK system, less heat is needed to denature the collagen core and thus *more* heat is needed to cause separation between the optimally-interacting pyrenes. As lysine is destabilizing to collagen formation while alanine is less so, the degree to which presence of these amino acids at different positions impact the ability to form tight helices, and in turn stronger interacting pyrenes, can be observed.

An additional trend that is evident upon observation of the fluorescence spectra of the Pyr(3)-EA system in particular, is that the absolute intensity of excimer fluorescence remains high *even in the*



*absence of triple helices.* At 60 °C, the Pyr(3)-EA system is unfolded according to melting temperatures collected via both CD and fluorescence, yet even at this temperature, significant excimer remains. Additionally, the fluorescence spectra of the Pyr(3)-KK system have an anomalous absence of excimer even at low temperatures, even though its data can be fit to a sigmoidal melting curve. This may be a result of the character of unwound collagen monomers remaining in solution at higher temperatures as well as interactions between pyrene and charged systems in solution. Due to the one-residue stagger that is present in triple helical collagen, there is reason to believe that any “stacking” interaction that occurs in a pyrenated system is due to non-optimized interactions between pyrene groups. Pyrenes attached to monomeric collagen in solution may allow highly optimal excimer formation compared to triple helical collagen, as seen by the persistent excimer in systems such as Pyr(3)-EA. Additionally, this persistent excimer may be more evident in the Pyr(3)-EA system due to the lack of positive charge. Cation –  $\pi$  interactions are strong and electrostatically favorable. These free monomers in solution are more likely to associate via this electrostatic method in lysine containing systems, which may contribute to the odd lack of excimer profile in the Pyr(3)-KK system as cation –  $\pi$  interactions are not conducive to excimer formation, and the presence of free monomer, even at low temperatures, may distort results. In contrast, the Pyr(3)-EA system is the only one studied that does not contain a cation. Unlike the cationic systems, this persistent and ideal excimer should be able to aggregate in solution at high temperatures, thus contributing to the high absolute intensity in the excimer region in this system.

#### **4.5 Conclusions**

Addition of a pyrene tag on the N-terminus of a collagen model peptides allows for the study of local fraying at the site of the probe, at concentrations below those customarily used for CD spectroscopy. This fluorescent tag additionally imparts an increase in thermal stability, dependent on the identity of the adjacent amino acid, and the length of the linker between the pyrene and collagen core. Additionally, the resulting  $T_m$  values obtained by both CD and fluorescence spectroscopy appear to demonstrate the

potential for fluorescence to be used as a tool for determination of melting temperatures at concentrations inaccessible to CD. This tag thus allows for fundamental science research on the forces that act on collagen helices, including the role of enthalpy and entropy and how they affect the behavior of the probe itself.

## References

1. Bella, J.; Brodsky, B.; Berman, H. M. Hydration Structure of a Collagen Peptide. *Structure* **1995**, *3* (9), 893-906.
2. Shoulders, M.D.; Raines, R.T. Collagen Structure and Stability. *Annual Review of Biochemistry* **2009**, *78*, 929-958.
3. Martin, G.R.; Mergenhagen, S.E.; Prockop, D.J. Influence of Scurvy and Lathyrism (Odoratism) on Hydroxyproline Excretion. *Nature* **1961**, *191*, 1008-1009.
4. Brazel, D.; Oberbäumer, I.; Dieringer, H.; Babel, W.; Glanville, R.W.; Duetzmann, R.; Kühn, K. Completion of the Amino Acid Sequence of the  $\alpha 1$  Chain of Human Basement Membrane Collagen (type IV) reveals 21 Nontriplet Interruptions Located within the Collagenous Domain. *European Journal of Biochemistry* **1987**, *168*, 529-536.
5. Xiuxia, S.; Yalin, C; Quinquin, W.; Huanxiang, L.; Shaoru, W.; Jianxi, X. A Natural Interruption Displays Higher Global Stability and Local Conformational Flexibility than a Similar Gly Mutation Sequence in Collagen Mimic Peptides. *Biochemistry* **2015**, *54*, 6106-6113.
6. Boryskina, O.P.; Bolbukh, T.V.; Semenov, M.A.; Gasan, A.I.; Maleev, V.Y. Energies of Peptide-Peptide and Peptide-Water Hydrogen Bonds in Collagen: Evidences from Infrared Spectroscopy, Quartz Piezogravimetry, and Differential Scanning Calorimetry. *Journal of Molecular Structure* **2007**, *827*, 1-10.
7. Jenkins, C.L.; Vasbinder, M.M.; Miller, S.J.; Raines, R.T. Peptide Bond Isoesters: Ester or (E)-Alkene in the Backbone of the Collagen Triple Helix. *Organic Letters* **2005**, *7*, 2619-22.
8. Bächinger, H.P.; Bruckner, P.; Timpl, R.; Prockop, D.J.; Engel, J. Folding Mechanism of the Triple Helix in Type-III Collagen and Type-III pN-Collagen. *European Journal of Biochemistry* **1980**, *106*, 619-632.
9. Acevedo-Jake, A.M.; Jalan, A.A.; Hartgerink, J.D. Comparative NMR Analysis of Collagen Triple Helix Organization from N- to C-Termini. *Biomacromolecules* **2015**, *16*, 145-155.

10. Chattopadhyay, S.; Raines, R.T.; Collagen-Based Materials for Wound Healing. *Biopolymers* **2014**, *101*, 821-833.
11. Myllyharju, J.; Kivirikko, K.I.; Collagens and Collagen-related Diseases. *Annals of Medicine* **2001** *33*, 7-21.
12. Bretscher, L.E.; Jenkins, C.L.; Taylor, K.M.; DeRider, M.L.; Raines, R.T.; Conformational Stability of Collagen Relies on a Stereoelectronic Effect. *Journal of the American Chemical Society* **2001**, *123*, 777-778.
13. Hodges, J.A.; Raines, R.T. Stereoelectronic and Steric Effects in the Collagen Triple Helix: Toward a Code for Strand Association. *Journal of the American Chemical Society* **2005**, *127*, 15923-15932.
14. Yang, W.; Chan, V.C.; Kirkpatrick, A.; Ramshaw, J.A.M.; Brodsky, B. Gly-Pro-Arg Confers Stability Similar to Gly-Pro-Hyp in the Collagen Triple-Helix of Host-Guest Peptides. *Journal of Biological Chemistry* **1997**, *272*, 28837-28840.
15. Inouye, K.; Sakakibara, S.; Prockop, D.J. Effects of the Stereo-Configuration of the Hydroxyl Group in 4-hydroxyproline on the Triple-Helical Structures Formed by Homogeneous Peptides Resembling Collagen. *Biochimica et biophysica acta* **1976**, *420*, 133-141.
16. Kotch, F.W.; Guzei, I.A.; Raines, R.T. Stabilization of the Collagen Triple Helix by O-Methylation of Hydroxyproline Residues. *Journal of the American Chemical Society* **2008**, *130*, 2952-2953.
17. Shoulders, M.D.; Guzei, I.A.; Raines, R.T. 4-Chloroprolines: Synthesis, Conformational Analysis, and Effect on the Collagen Triple Helix. *Biopolymers* **2008**, *89*, 443-454.
18. Shoulders, M.D.; Hodges, J.A.; Raines, R.T. Reciprocity of Steric and Stereoelectronic Effects in the Collagen Triple Helix. *Journal of the American Chemical Society* **2006**, *128*, 8112-8113.
19. Cadamuro, S.A.; Reichold, R.; Kusebauch, U.; Musiol, H.J.; Renner, C. Conformational Properties of 4-Mercaptaproline and Related Derivatives. *Angewandte Chemie* **2008**, *47*, 2143-2146.

20. Vitagliano, L.; Berisio, R.; Mazzarella, L.; Zagari, A. Structural Basis of Collagen Stabilization Induced by Proline Hydroxylation. *Biopolymers* **2001**, *58*, 459-464.
21. Jenkins, C.L.; Bretscher, L.E.; Guzei, I.A.; Raines, R.T. Effect of 3-Hydroxyproline Residues on Collagen Stability. *Journal of the American Chemical Society* **2003**, *125*, 6422-6427.
22. Siebler, C.; Maryasin, B.; Kümin, M.; Erdmann, R.; Rigling, C.; Grünenfelder, C.; Oschenfeld, C.; Wennemers, H. Importance of Dipole Moments and Ambient Polarity for the Conformation of Xaa-Pro Moieties – a Combined Experimental and Theoretical study. *Royal Society of Chemistry* **2015**, *6*, 6725-6730.
23. Egli, J.; Siebler, C.; Kohler, M.; Zenobi, R.; Wennemers, H. Hydrophobic Moieties Bestow Fast-Folding and Hyperstability on Collagen Triple Helices. *Journal of the American Chemical Society* **2019**, *141*, 5607-5611.
24. Zhang, Y.; Malamakal, R.M.; Chenoweth, D.M. Aza-glycine Induces Collagen Hyperstability. *Journal of the American Chemical Society* **2015**, *137*, 12422-12425.
25. Zhang, Y.; Herling, M.; Chenoweth, D.M. General Solution for Stabilizing Triple Helical Collagen. *Journal of the American Chemical Society* **2016**, *138*, 9751-9754.
26. Kasznel, A.J.; Zhang, Y.; Hai, Y.; Chenoweth, D.M. Structural Basis for Aza-Glycine Stabilization of Collagen. *Journal of the American Chemical Society* **2017**, *139*, 9427-9430.
27. Chen, C.; Hsu, W.; Kao, T.; Horng, J. Self-Assembly of Short Collagen-Related Peptides into Fibrils via Cation- $\pi$  Interactions. *Biochemistry* **2011**, *50*, 2381-2383 .
28. Egli, J.; Erdmann, R.S.; Schmidt, P.J.; Wennemers, H.; Effect of N- and C- Terminal Functional Groups on the Stability of Collagen Triple Helices. *Chemical Communications* **2017**, *53*, 11036-11039.
29. Parmar, A.S.; Xu, F.; Pike, D.H.; Belure, S.V.; Hasan, N.F.; Drzewiecki, K.E.; Shreiber, D.I.; Nanda, V. Metal Stabilization of Collagen and de Novo Designed Mimetic Peptides. *Biochemistry* **2015**, *54*, 4987-4997.

30. Chen, Y.; Chen, C.; Horng, J. Thermodynamic and Kinetic Consequences of Substituting Glycine at Different Positions in a Pro-Hyp-Gly Repeat Collagen Model Peptide. *Peptide Science* **2010**, *96*, 60-68.
31. Martinez, C.; Iverson, B.L.; Rethinking the Term “pi-stacking”. *Chemical Science* **2012**, *3*, 2191-2201.
32. Janiak, C. A Critical Account on  $\pi$ -  $\pi$  Stacking in Metal Complexes with Aromatic Nitrogen Containing Ligands. *Dalton Transactions* **2000**, *21*, 3885-3896.
33. Cochran, A.; Skelton, N.; Starovasnik, M. Tryptophan Zippers: Stable, Monomeric  $\beta$ -Hairpins. *PNAS* **2001**, *98*, 5578-5583.
34. Casier, R; Duhamel, J. Pyrene Excimer Fluorescence as a Direct and Easy Experimental Means To Characterize the Length Scale and Internal Dynamics of Polypeptide Foldons. *Macromolecules* **2018**, *51*, 3450-3457.
35. Jones, G.; Vullev, V.I. Ground- and Excited-State Aggregation Properties of a Pyrene Derivative in Aqueous Media. *Journal of Physical Chemistry* **2001**, *105*, 6402-6406.
36. Feng, Q.; Wang, M.; Dong, B.; He, J.; Xu, C. Regulation of Arrangements of Pyrene Fluorophores via Solvates and Cocrystals for Fluorescence Modulation. *Crystal Growth and Design* **2013**, *13*, 4418-4427.
37. Sun, X.; Chai, Y.; Wang, Q.; Liu, H.; Wang, S.; Xiao, J. A Natural Interruption Displays Higher Global Stability and Local Conformational Flexibility than a Similar Gly Mutation Sequence in Collagen Mimic Peptides. *Biochemistry* **2015**, *54* 6106 – 6113 .
38. Greenfield, N. J. Analysis of the Kinetics of Folding of Proteins and Peptides Using Circular Dichroism. *Nature Protocols* **2006**, *1* (6), 2891 – 2899.
39. Vargas-Uribe, M.; Rodnin, M. V.; Ojemalm, K.; Holgado, A.; Kyrychenko, A.; Nilsson, I.; Posokhov, Y. O.; Makhatadze, G.; von Heijne, G.; Ladokhin, A. S. Thermodynamics of Membrane Insertion and Refolding of the Diphtheria Toxin T-Domain . *The Journal of Membrane Biology* **2015**, *248*, 383-394..

40. Anslyn, E.V.; Dougherty, D.A. *Modern Physical Organic Chemistry*; *University Science Books*: Mill Valley, California, **2006**; pg 181 – 184.

